

CONTENTS

Section	Page	
Preface	iii	1/A5
<u>Measurement of Exhaust Cloud Properties</u>		
CLOUD VOLUME STUDIES R. J. Bendura	1	1/A9
IN SITU EXHAUST CLOUD MEASUREMENTS Dewey Wornom	5	1/A13
MEASUREMENT OF PARTICULATES D. Woods	9	1/B3
ICE NUCLEI MEASUREMENTS FROM SOLID ROCKET MOTOR EFFLUENTS Edward E. Hindman, II	13	1/B7
GROUND-BASED MEASUREMENTS OF DM-2 ROCKET EXHAUST EFFLUENTS USING FIXED-FLOW SAMPLERS AND ELECTRETS Michael Susko	27	1/C7
<u>Prediction of Environmental Effects of the Exhaust Cloud</u>		
ACID RAIN: MESOSCALE MODEL Hsiao-ming Hsu	33	1/C13
ACID RAIN: MICROPHYSICAL MODEL A. N. Dingle	65	1/F5
SHUTTLE INADVERTENT WEATHER MODIFICATION EFFECTS G. Lala	83	1/G9
RESPONSE OF SELECTED PLANT AND INSECT SPECIES TO SIMULATED SRM EXHAUST MIXTURES AND TO EXHAUST COMPONENTS FROM SRM FUELS Walter W. Heck	85	1/G11
<u>Baseline Monitoring of the Environment</u>		
ECOLOGICAL BASELINE STUDIES Dave Vickers	101	2/B1
AIR QUALITY MONITOR AND ACID RAIN NETWORKS Hans Rudolph	117	2/C3

Environmental Impact Statement

ENVIRONMENTAL IMPACT STATEMENT FOR SHUTTLE OPERATIONS AT

VANDENBERG AIR FORCE BASE 125 2/C12

R. C. Wooten

JAN 24 1980

Item 836-H-10

NAS 1.55:2110

COMPLETED

NASA Conference Publication 2110

Proceedings of Shuttle Environmental Effects Program Review

ORIGINAL

A Conference held at
John F. Kennedy Space Center
Kennedy Space Center, Florida
March 21 and 22, 1978

NASA

132

NASA Conference Publication 2110

Proceedings of Shuttle Environmental Effects Program Review

Andrew E. Potter, *Editor*
Lyndon B. Johnson Space Center

A Conference sponsored by
John F. Kennedy Space Center
and held at Kennedy Space Center, Florida
March 21 and 22, 1978



National Aeronautics
and Space Administration

**Scientific and Technical
Information Office**

1980

Preface

Environmental effects of the Space Shuttle have been the subject of ongoing research by NASA since about 1972. The Final Environmental Impact Statement for the Shuttle Program (April 1978) summarized the environmental effects as of early to mid 1977. Since then, research in some areas of environmental effects has continued. This conference was held to review results from this program up to early 1978.

Blank Page

CONTENTS

Section	Page
Preface	iii
<u>Measurement of Exhaust Cloud Properties</u>	
CLOUD VOLUME STUDIES R. J. Bendura	1
IN SITU EXHAUST CLOUD MEASUREMENTS Dewey Wornom	5
MEASUREMENT OF PARTICULATES D. Woods	9
ICE NUCLEI MEASUREMENTS FROM SOLID ROCKET MOTOR EFFLUENTS Edward E. Hindman, II	13
GROUND-BASED MEASUREMENTS OF DM-2 ROCKET EXHAUST EFFLUENTS USING FIXED-FLOW SAMPLERS AND ELECTRETS Michael Susko	27
<u>Prediction of Environmental Effects of the Exhaust Cloud</u>	
ACID RAIN: MESOSCALE MODEL Hsiao-ming Hsu	33
ACID RAIN: MICROPHYSICAL MODEL A. N. Dingle	65
SHUTTLE INADVERTENT WEATHER MODIFICATION EFFECTS G. Lala	83
RESPONSE OF SELECTED PLANT AND INSECT SPECIES TO SIMULATED SRM EXHAUST MIXTURES AND TO EXHAUST COMPONENTS FROM SRM FUELS Walter W. Heck	85
<u>Baseline Monitoring of the Environment</u>	
ECOLOGICAL BASELINE STUDIES Dave Vickers	101
AIR QUALITY MONITOR AND ACID RAIN NETWORKS Hans Rudolph	117

Environmental Impact Statement

ENVIRONMENTAL IMPACT STATEMENT FOR SHUTTLE OPERATIONS AT VANDENBERG AIR FORCE BASE	125
R. C. Wooten	

CLOUD VOLUME STUDIES

By R. J. Bendura*

A time history of cloud growth for the Titan III launch at Cape Canaveral on September 5, 1977, was obtained by using optical data provided by three Askania trackers (position of the cloud) and three Hasselblad cameras (cloud volume). The trackers and the cameras (having 50-millimeter lenses and using 70-millimeter black-and-white film) were located several kilometers north (UCS-9), east (UCS-2), and south (JPL) of the two Titan launch pads so that the cloud could be photographed during its formation, its growth, and its rise. During the September 5 launch, weather conditions were good enough to enable tracking of the cloud for almost 40 minutes. At that time, the cloud was about 15 kilometers away from the nearest camera. The trajectory of the cloud enabled photographing the cloud with the Hasselblad camera from UCS-2 in nearly a downwind direction and from UCS-9 and JPL in a crosswind direction. The cloud was divided into elliptical increments with major and minor axes in the downwind and crosswind directions, respectively, to sum up the volume of the cloud at a particular time. Two quasi-independent measurements of ground cloud volume as a function of time were obtained; they are compared in figure 1. The data represented by the circles use the combination of the Hasselblad cameras of UCS-2 and of the JPL site. No data for the time period around 12 to about 28 minutes are available, however, because ambient clouds passing between the JPL camera and the exhaust cloud prevented the acquisition of any data. Data were acquired using the combination of cameras at the UCS-2 and UCS-9 sites, as represented by the squares. Based on the assumptions made and the quasi-independent camera technique applied, the optical data agree reasonably well, particularly during the early time periods when rapid growth is occurring; but the agreement is less good after 25 minutes. However, at this time, the cloud was 15 kilometers away from the nearest camera site and the cloud image was sufficiently small that a small error in defining the outline of the cloud due to ambient cloud interference or haze could result in a relatively large error in volume.

Aircraft time in the cloud, as measured by the rapid-response nephelometer onboard the aircraft, was also used for determining cloud volume. It was assumed that the cloud formed into a prolate spheroid with the downwind aircraft pass being along the major axis and the crosswind pass being along the minor axis. As shown in figure 1, the cloud volume measured in this manner compares favorably with the optical data after 12 minutes. Cloud volume from aircraft measurements for the entire operation is summarized in figure 2. The aircraft landed and was being refueled in the 1.5 to 3.0 hours after launch time period. The data suggest that the cloud volume may have peaked near 60 ± 10 cubic kilometers and that it remained relatively constant or

*NASA Langley Research Center.

began to decrease slightly soon after 3.5 hours. However, caution should be used in reaching any general conclusions since these measurements are reliable only within a factor of 3 or 4 and are subject to the detectability limits of the nephelometer. In addition, cloud volumes may behave differently for other meteorological conditions.

Cloud volume data from this mission are compared with optical data from prior missions in figure 3 and airborne data from prior missions in figure 4. No attempt has been made to correlate the data based on meteorological conditions.

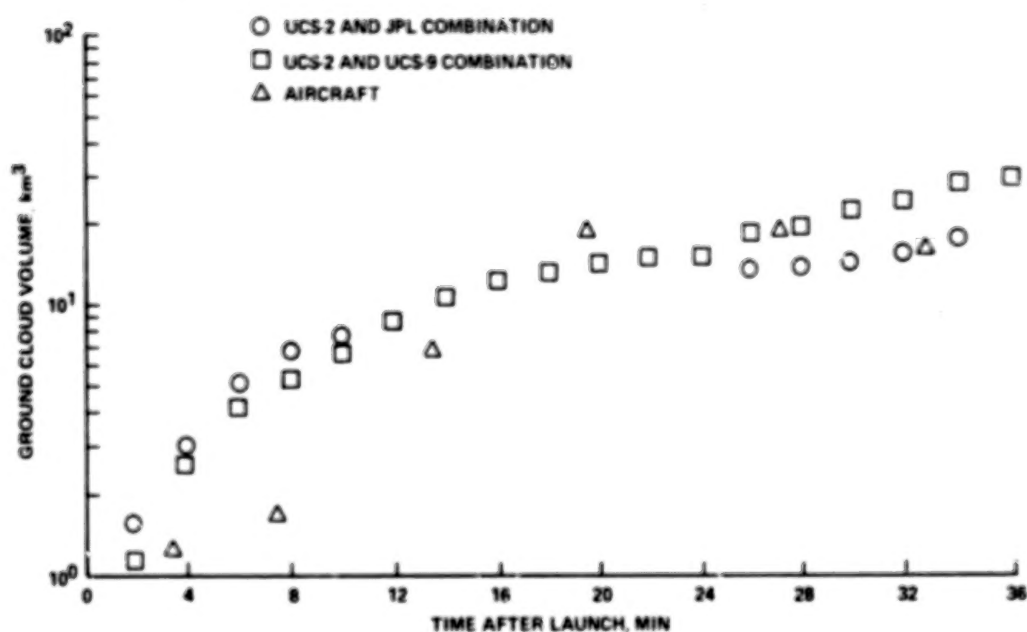


Figure 1.- Optical and airborne measurements of Titan III ground cloud volume as a function of time (September 5, 1977, Voyager I launch).

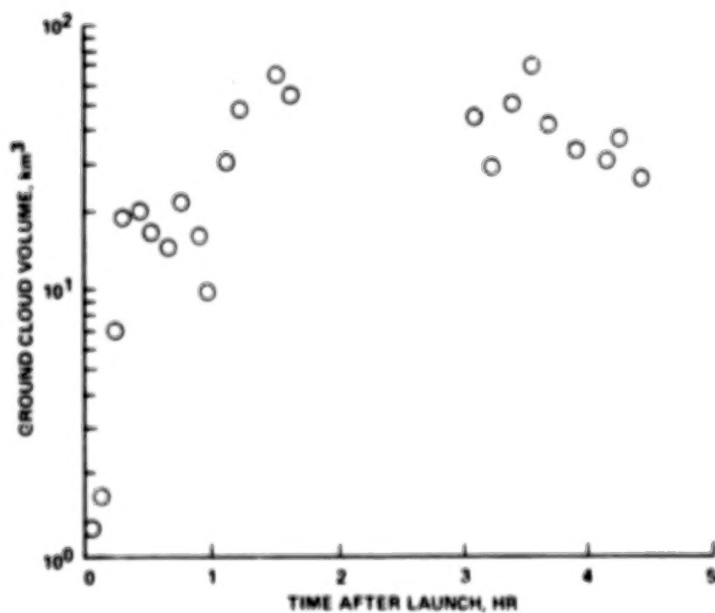


Figure 2.- Airborne measurements of the September 1977 Titan III exhaust cloud growth.

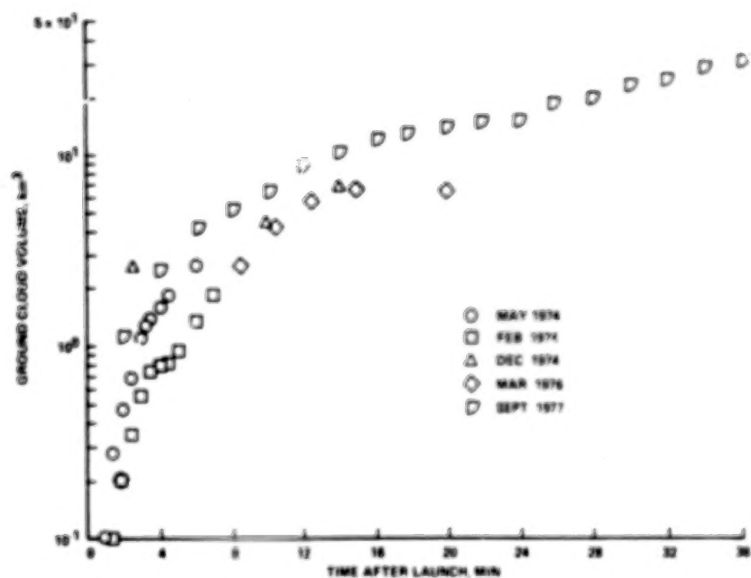


Figure 3.- Summary of exhaust cloud growth from optical measurements of five Titan III launches.

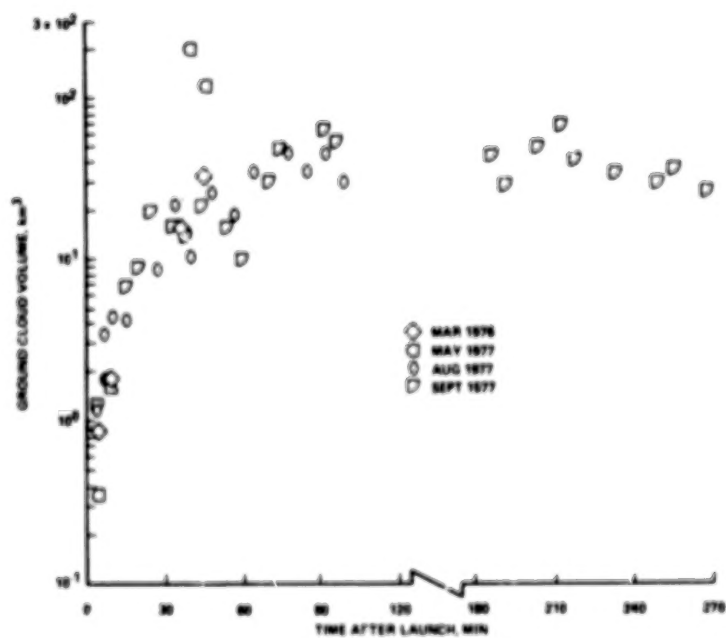


Figure 4.- Summary of exhaust cloud growth from airborne measurements of four Titan III launches.

IN SITU EXHAUST CLOUD MEASUREMENTS

By Dewey Wornom*

Airborne in situ exhaust cloud measurements were conducted after the full-scale monitoring activities in late 1974 and early 1975 to obtain better definitions of cloud particle size range, Cl_2 content, and HCl partitioning. Particle size distribution data (from 0.05 to 25 micrometers) and Cl_2 measurements were made during the May, August, and September 1977 Titan launches. HCl partitioning data will be obtained during the March 1978 launch or else in October 1978, the last Titan flight before the Space Shuttle is launched.¹ Basic effluent measurements of Shuttle launches for the scale factor are expected to be obtained in 1978.

Figure 1 plots the measurements of three basic effluents - HCl, NO_x , and particles - against minutes after launch. The bounds of measurements for earlier launches (1974 and 1975) are represented by the solid lines, and all the symbols representing followup measurements at these launches in 1977 are superimposed on those bounds. The measurements made in the followup launches in 1977 indicated that the HCl, NO_x , and particle concentrations did not exceed the earlier measurements.

The Cl_2 was measured at the August 1977 and September 1977 launches. Table I compares the maximum observed HCl concentration to the maximum Cl_2 concentration during the first six passes and gives the ratios of the Cl_2 to the HCl. The in situ Cl_2 measurements from the Voyager launch monitoring activities show that the maximum observed concentrations were approximately 50 parts per billion and well below 1 percent of the observed HCl concentrations.

*NASA Langley Research Center.

¹Since the Environmental Effects Project Review was held, the data from the March 1978 launch have been obtained; they will be the subject of a separate document.

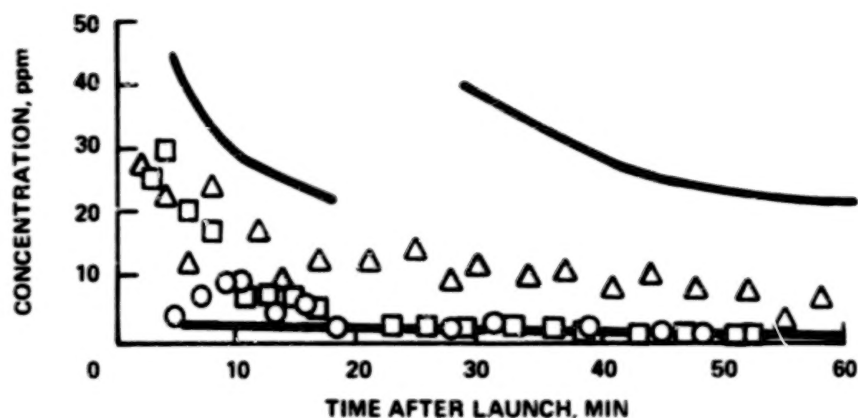
TABLE I.- COMPARISON OF MAXIMUM OBSERVED HCl
CONCENTRATION WITH MAXIMUM Cl₂ CONCENTRATION

Pass number	Maximum concentration		Ratio max. Cl ₂ to max. HCl
	HCl, ppm	Cl ₂ , ppb	
August 20, 1977, Titan launch			
1	26	(a)	(b)
2	30	42	1.4×10 ⁻³
3	23	70 (50) ^c	3×10 ⁻³ (2×10 ⁻³) ^c
4	18	82 (55)	4.5×10 ⁻³ (3×10 ⁻³)
5	7	60 (20)	8.5×10 ⁻³ (3×10 ⁻³)
6	7	66 (35)	9.4×10 ⁻³ (5×10 ⁻³)
September 5, 1977, Titan launch			
1	27	40	1.5×10 ⁻³
2	23	30	1.3×10 ⁻³
3	12	<10	<8×10 ⁻⁴
4	24	22	9×10 ⁻⁴
5	16	<10	<6×10 ⁻⁴
6	9.4	<10	<1.1×10 ⁻³

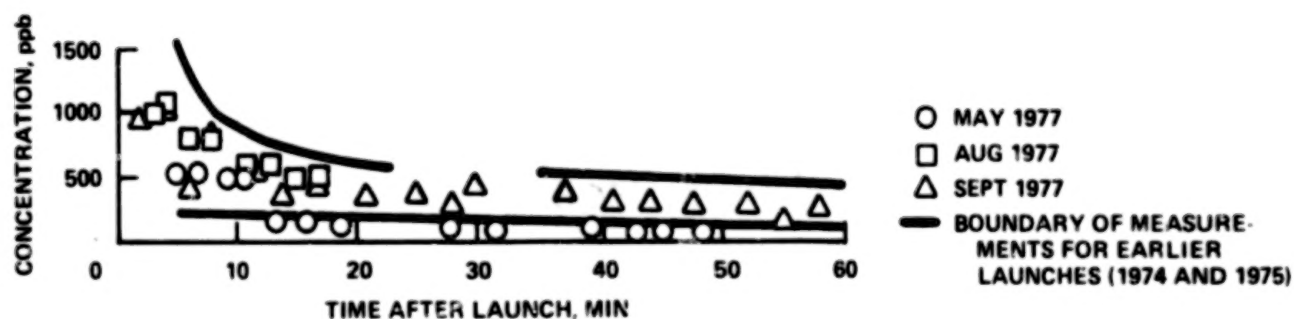
^aNot measured.

^bNot applicable.

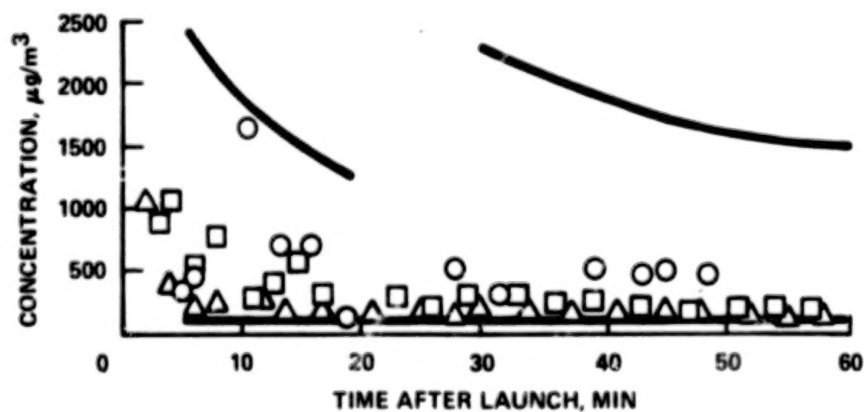
^cValues in parentheses are in situ measurements of Voyager launches.



(a) HCl.



(b) NO_x .



(c) Particles.

Figure 1.- Measurements of three basic effluents.

Blank Page

MEASUREMENT OF PARTICULATES

By D. Woods*

The size distributions of particles in the exhaust plumes from the Titan rockets launched in August and September 1977 were determined from in situ measurements made from a small sampling aircraft that flew through the plumes. Two different sampling instruments were employed, a quartz crystal microbalance (QCM) cascade impactor and a forward scattering spectrometer probe (FSSP).

The QCM was flown inside the forward baggage compartment of the aircraft. The particles were directed to the sensor through an inlet probe that was designed for isokinetic flow. These particles passed through a heated tube, where most of the liquid component was evaporated, before entering the QCM. The QCM, therefore, measured only the nonvolatile component of the aerosols in the plume covering an aerodynamic size ranging from 0.05 to 25 micrometers in diameter.

The FSSP was flown outside the aircraft under the nose section. This probe measures both the liquid droplets and the solid particles over a size range from 0.5 to 7.5 micrometers in diameter. The particles are counted and classified into 15 size intervals.

Figures 1 to 3 show the data for passes 2, 3, and 18, respectively, through the cloud from the August 1977 Titan launch. In each figure, curve A represents the size distribution (mass concentration as a function of particle diameter) obtained with the QCM; curve B represents the number concentrations (number of particles per cubic centimeter as a function of particle diameter) derived from curve A; and curve C represents the number concentrations as measured with the FSSP. The comparatively high concentrations measured by the FSSP indicate the presence of a large number of liquid droplets in the cloud. Figure 4 shows a similar set of plots for pass 1 from the September 1977 Titan plume. Finally, figure 5 compares May, August, and September 1977 in situ measurements of launch vehicle effluents (HCl, NO_x, and particles) with measurements from 1974 and 1975.

*NASA Langley Research Center.

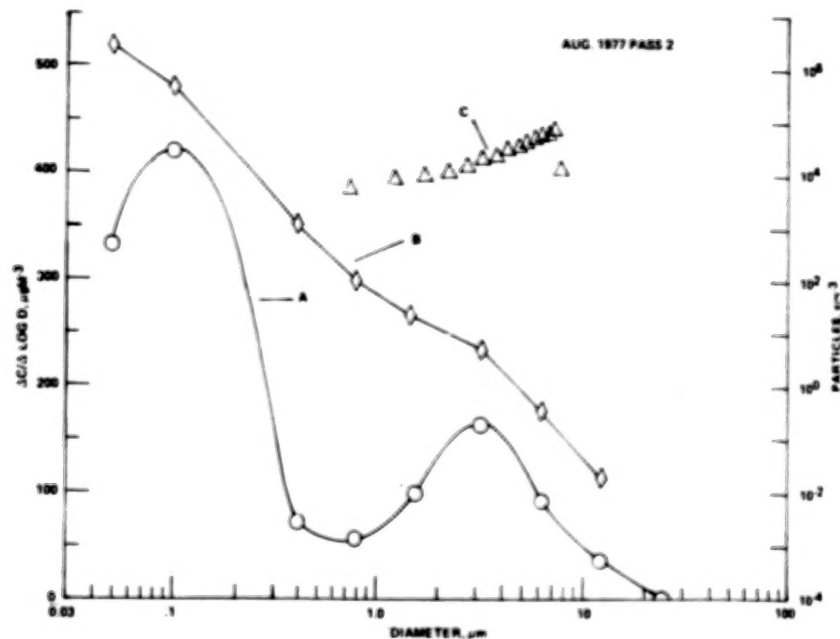


Figure 1.- Data for pass 2 from the August 1977 Titan launch.

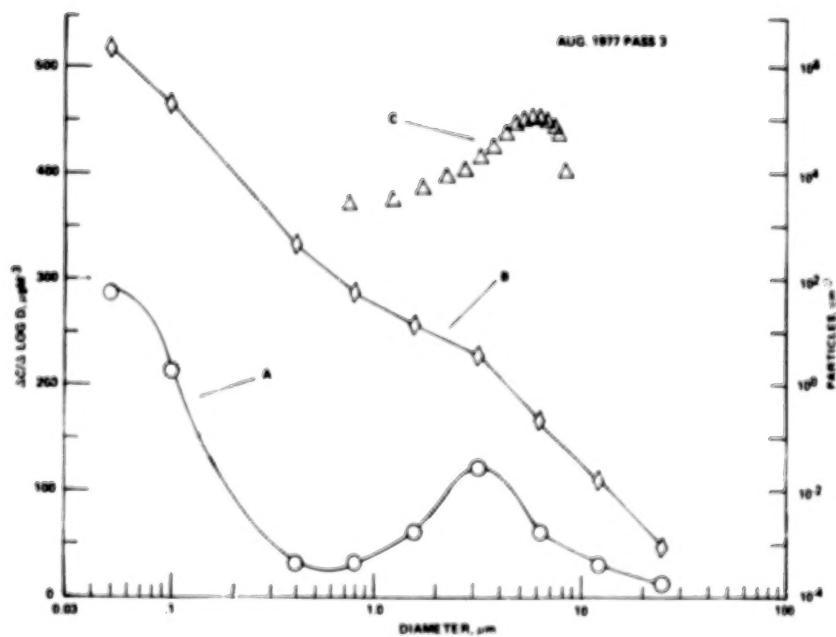


Figure 2.- Data for pass 3 from the August 1977 Titan launch.

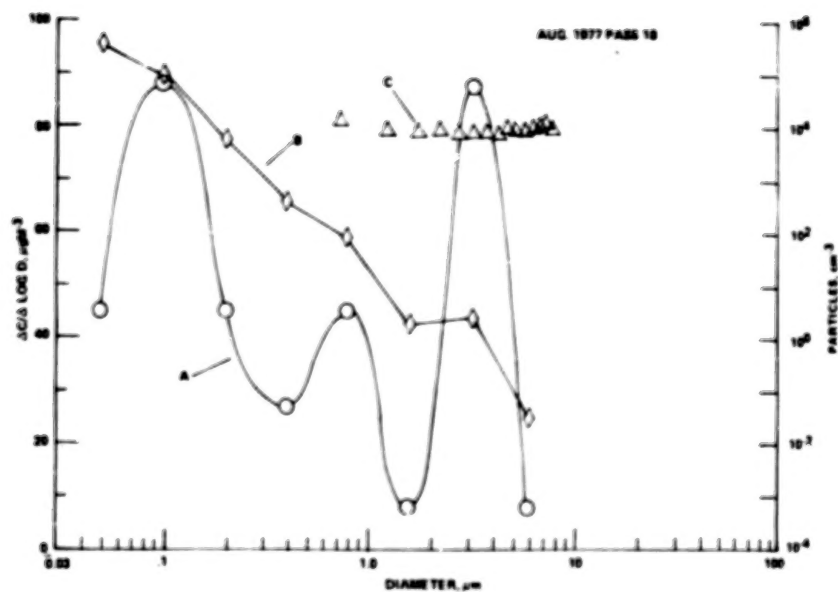


Figure 3.- Data for pass 18 from the August 1977 Titan launch.

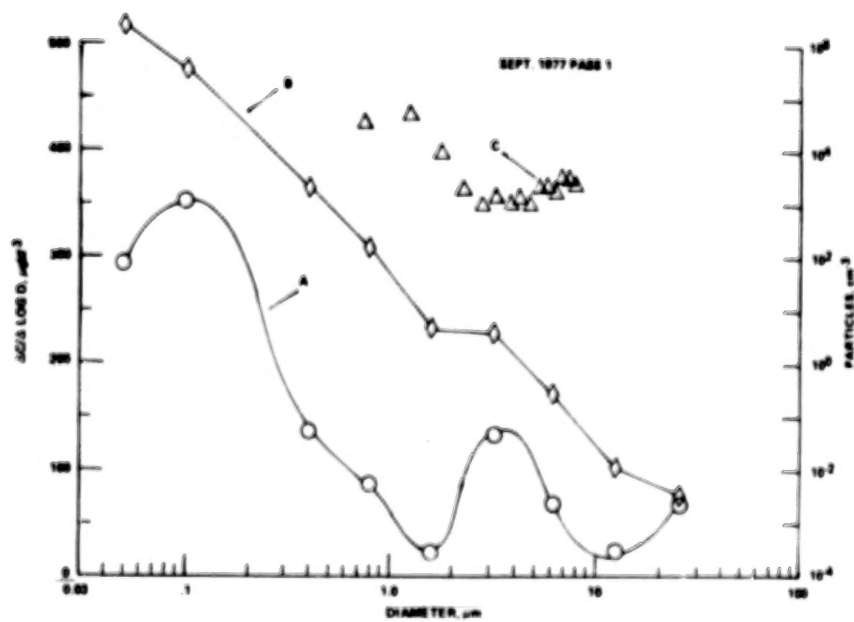


Figure 4.- Data for pass 1 from the September 1977 Titan launch.

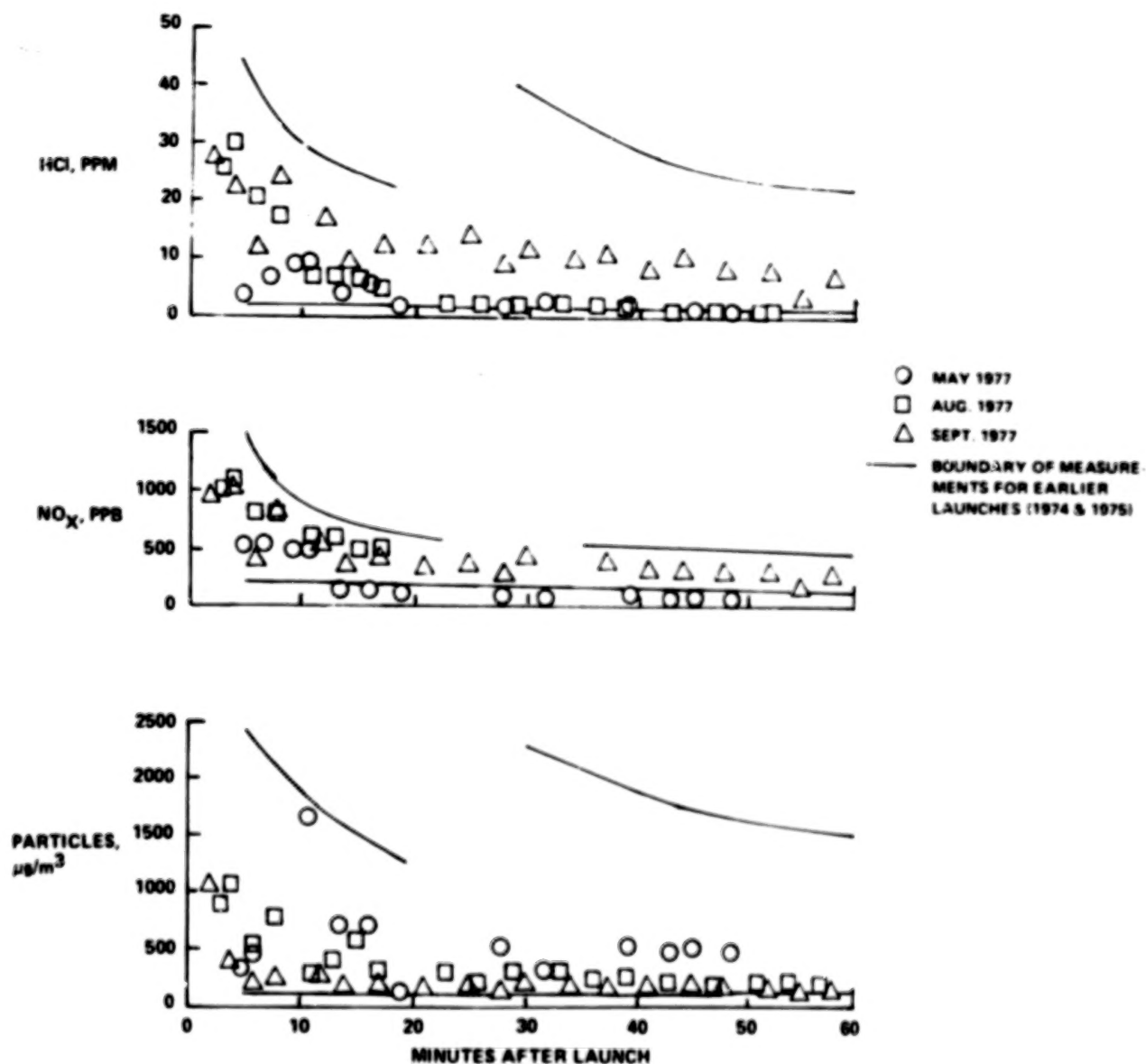


Figure 5.- Comparison of in situ measurements of launch vehicle effluents for 1974, 1975, and 1977 launches.

ICE NUCLEI MEASUREMENTS FROM SOLID ROCKET MOTOR EFFLUENTS

By Edward E. Hindman, II*

INTRODUCTION

In this paper, a study of ice-crystal-forming nuclei (IN) measured in solid rocket motor (SRM) exhaust products is described together with the involvement of the Naval Weapons Center (NWC) in these measurements. Preliminary results from laboratory investigations and flight preparations for the March 1978 Titan launch are discussed. The final section consists of a statement of future work necessary to provide adequate measurements of IN and cloud condensation nuclei (CCN) in the stabilized ground clouds from SRM's.

BACKGROUND

In the summer of 1976, Dr. W. G. Finnegan of the NWC received a call from the State University of New York at Albany (SUNYA), on behalf of the Institute of Man and Science at Rensselaerville, New York. Dr. Finnegan was asked to burn some propellant in NWC's 24-cubic-meter cloud chamber, which as nearly as possible simulates the properties of the supercooled clouds found in the atmosphere. Dr. F. K. Odencrantz, who performed the burns, measured 5×10^{10} IN/g of Al_2O_3 from the SRM propellant in the laboratory at $-20^\circ C$. This information was given to SUNYA.

The Space Shuttle will release 10^9 grams of propellant per launch; it may therefore release approximately 10^{19} IN per launch into the atmosphere. The hurricane modification program of the National Oceanic and Atmospheric Administration (NOAA) may release as many as 10^{19} IN per day. Thus, as a comparison, each Space Shuttle launch is potentially comparable to the world's largest intentional release of ice nuclei.

The National Aeronautics and Space Administration (NASA) called a meeting in the summer of 1977 at Estes Park, Colorado, of various atmospheric scientists knowledgeable in the art of nuclei counting. The consensus of that meeting was that measurements were needed to validate the magnitude of the effects of the propellant exhausts and to settle other questions that had arisen through the investigation performed by the Institute of Man and Science. The most critical parameters to be measured were the concentrations of ice nuclei and cloud condensation nuclei in stabilized ground clouds (SGC's) from the SRM's.

*Naval Weapons Center, China Lake, California.

In the fall of 1977, NASA launched a program, with the help of NOAA, NWC, and others, to instrument the NOAA C-130 aircraft at Miami to make measurements of the IN, the CCN, and the liquid particles in the SGC's from the Voyager/Titan III-C launches. Two flights were made, one in August 1977 and the other in September 1977.

In December 1977, the investigators involved met in Houston to report their preliminary findings. The final report of the investigations is being prepared by NWC; hence, the information here is subject to change. The contributions of NWC to the data collection and analysis included preliminary findings from IN and CCN measurements. Ice nuclei in the SGC's were measured using portable IN counters (INC's). The INC's consisted of a small chamber that contained a supercooled cloud similar to one that might exist in the atmosphere. If air that contains IN is injected into the cloud, ice crystals form and can be counted. An independent method of IN measurement, provided by NOAA and SUNYA, used filters to collect particles from the SGC. The filters were later exposed to a controlled, subcooled environment, where particles from the SGC that could serve as ice nuclei did so and were counted. The CCN measurements were made using a small cloud chamber of about 2 centimeters in diameter. That volume contains supersaturated air so that conditions during cloud formation in the atmosphere are simulated. When a sample of air containing CCN is introduced, droplets form and may be counted. The concentration of droplets is related to the concentration of CCN.

During a 5-hour flight, in which the SGC of the Titan launch of September 5, 1977, was observed, measurements were made using portable INC's, CCN counters, and filter devices. Air was captured in bags and taken to a laboratory at the end of the flight. Some 10 hours from launch, the air in the bags was sampled and found to contain active IN. The portable counters on-board the aircraft showed that ice nuclei were present in the cloud in amounts greater than found in the surrounding air, not contaminated by the cloud. The counters were not properly calibrated, and absolute counts were not possible. The filters exposed to the cloud were cut in half. The halves of the filters processed by NOAA personnel supported the data from the portable INC's, but the other half of the filters processed by SUNYA did not. The discrepancy between the results from the filters was not clarified. The CCN counters were saturated for the duration of the flight because the cloud was such an intense source of these nuclei. The consensus of the experts meeting in Houston in December was that the ice nuclei data were inconsistent and inadequate to improve on the analysis previously performed by the Institute of Man and Science.

The Voyager investigators decided on a course of action at that meeting. One item was to do basic laboratory studies of Al_2O_3 ice nuclei. Another item was to calibrate the portable INC's to be used in the airborne measurements following the March 1978 Titan launch at the NASA John F. Kennedy Space Center (KSC). The last item was to measure the concentrations of IN and the physical and chemical properties of the droplets in the SGC from the March launch.

LABORATORY MEASUREMENTS OF ICE NUCLEI FROM SHUTTLE PROPELLANT

Ice nuclei were measured from the effluent produced by burning Shuttle propellant (unpressurized) in the laboratory at Colorado State University (CSU) in Fort Collins, Colorado. Propellant was obtained from the Thiokol plant at Wasatch, Utah.

Objectives

A workshop at CSU was held on February 13 to 18, 1978. The objectives of the workshop were (1) to intercompare the portable INC's that were to be flown in the ground clouds; (2) to compare data from the portable INC's with data from the large, permanent isothermal cloud chamber (ICC) at CSU; (3) to acquire preliminary information on the IN activity of the Shuttle propellant; (4) to collect filter samples for IN and particle analysis similar to that done with the filters from the Voyager launches; and (5) to replicate ice crystals produced in the cloud chamber by nuclei from the propellant exhaust and to study them using a microprobe-equipped scanning electron microscope to determine nucleant composition.

Investigators and Their Instruments

The following investigators were present at CSU with their instruments.

1. Dr. F. Kirk Odencrantz from the NWC was present with a portable Mie INC.
2. Mr. Gerhard Langer from the National Center for Atmospheric Research (NCAR) was present with the NCAR portable INC that he had designed, a filter apparatus, and a portable CCN counter.
3. Dr. Farn Parungo from NOAA (Boulder, Colorado) took filter samples and made ice crystal replicas.
4. Mr. Paul Willis from NOAA (Miami, Florida) came with a portable Mie INC.
5. Dr. Dennis Garvey, director of the CSU facility, conducted the burning of the propellant, ran the ICC, and operated a Gardner condensation nucleus (CN) counter.
6. Dr. G. Gregory from the NASA Langley Research Center brought a portable HCl monitor.

Procedures

A schematic of the test setup in the Atmospheric Cloud Simulation and Aerosol Laboratory at CSU is shown in figure 1. Samples of the propellant, measuring 1 by 1 by 3 inches, were burned in the bottom of the wind tunnel (A). Because of the thrust developed during burning, it was necessary to immobilize the propellant in a small cage. The fan (B) drew air into the tunnel, mixing the exhaust products with the ambient air and diluting it by a known amount. A sample was taken from the top of the wind tunnel by means of a 4-liter syringe (C). A portion of the diluted sample was placed in a 770-liter aluminum storage tank (D), and the rest was put into the ICC (E). A measurement of the ice nuclei concentration was made in the isothermal chamber. Simultaneously, measurements of the concentration were made with the NCAR counter and the Mie counters, using air taken from the holding tank (D).

A supercooled water droplet cloud is formed in a 1-cubic-meter region inside the ICC. The exhaust material from the propellant is injected into the cloud. Ice crystals form and settle onto microscope slides. The slides are immediately placed on the cold stage of a microscope, and the ice crystals are counted. This counting procedure continues as long as crystals settle from the chamber. The crystals are counted on the cold stage and translated into numbers of crystals per liter. Finally, the number of crystals produced from the mass of propellant effluent in the cloud chamber is calculated.

The Mie and NCAR INC's are instruments in which ice crystals are grown in a cloud of supercooled water droplets. The chambers are about 2 feet high and 6 inches in diameter and are filled with a cloud of supercooled droplets. The crystals that are formed in the cloud chambers are drawn (because of the airflow) and settle to the bottom of the cloud chambers. In the Mie instrument, the crystals pass through a polarized light beam. Each crystal depolarizes the light and sends a signal of light to a photodetector. The signals detected by the photodetector are counted. In the NCAR instrument, the crystals pass through a capillary tube, one by one. Each crystal causes an acoustic wave, which is detected using a microphone. The "clicks" detected by the microphone are counted.

Results

Results from the experiments are preliminary. A final report is being prepared by NWC, and the results and conclusions reported here are subject to change.

Cross-calibration of portable INC's.— All the portable INC's measured ice nuclei concentrations from the Shuttle propellant that were above background concentrations; e.g., see the data from the NCAR INC (fig. 2). Counters operated at the same time produced measurements that often correlated; when one counter indicated low concentrations, the other two counters also indicated low concentrations of IN and vice versa (fig. 3). The differences between the numbers of IN measured by the three counters are due to the different response characteristics of the counters. These differences have not been resolved, and to do so would be a major research effort. The

important point is that the portable INC's can and do detect ice crystals produced by Shuttle propellant.

An unexpected phenomenon observed during the workshop was that ice nuclei concentrations first increased with time in the holding tank and then decreased (fig. 2). The IN concentrations should be high initially and then decay with time. When a few tenths of a gram of Shuttle propellant was wrapped with a Nichrome wire, dropped into the holding tank, and flashed off, the portable IN instruments determined the initial IN count to be quite low. Then, the IN counts started to increase with time and increased until finally they plateaued. Three days later, high concentrations of ice nuclei were still sampled out of the holding tank. This phenomenon indicates that HCl may be a factor in either the nucleation or the growth of ice crystals on the Al_2O_3 particles. The effect of HCl is not known; consequently, further work is needed.

Comparison of counters with the isothermal cloud chamber.- When the crystal concentrations were high, as measured by the NCAR counter, they were also high in the ICC and vice versa, as shown in figure 4. It appears from the results in figure 4 that there is a factor of about 1000 difference between the counts measured in the ICC and in the NCAR portable chamber. That is, the crystal concentrations in the ICC were a factor of about 1000 higher than the concentrations measured in the portable counter. Eight data points were collected from the NCAR counter and the ICC that cover a range of concentrations (fig. 4).

The NWC Mie counter produced one comparison point with the ICC (test 19). A difference in concentration of 10^3 between the portable counter and the ICC was observed (fig. 4). Similar results were obtained when the IN counts from the counter were compared with the counts from the NWC 24-cubic-meter cloud chamber. No data on the NOAA Mie counter were received for comparison purposes.

Preliminary ice nuclei activity.- No consistent set of ice nuclei activity figures were obtained, because of a lack of preparation time with the propellant. Nevertheless, the data obtained indicate that the results from the ICC (approximately 10^{11} IN/g of Al_2O_3) support the data obtained in the NWC 24-cubic-meter chamber (approximately 5×10^{10} IN/g of Al_2O_3). Both chambers were operated at -20° C. The most representative experiment run at the CSU workshop resulted in the production of 1.7×10^{11} IN/g of Al_2O_3 in the ICC (i.e., 5×10^{10} IN/g of propellant).

Filter samples.- Filter samples were collected at the workshop and reduced and analyzed at NCAR and at SUNYA. The results of the two analyses were consistent. Ice nuclei were detected in high concentrations on the filters; crystals grew all over the filters. The detection of ice nuclei on the filters supports the NOAA results from the filters exposed to the SGC's following the Voyager launches, but the result is inconsistent with the SUNYA results from the Voyager filters. The IN concentrations from the laboratory filters correlated with the IN concentrations from the NCAR counter.

Ice crystal replicas.- Ice crystal replicas that were collected in the bottom of the ICC showed particles containing aluminum in their centers when examined with the electron microscope. Dr. Parungo indicated that Al_2O_3 particles with traces of sulfur and calcium were responsible for the crystal formations.

CCN concentrations in propellant effluent.- Langer obtained such enormous concentrations of CCN from the Shuttle propellant that his instrument was saturated most of the time. This result is consistent with measurements in the ground clouds from the Voyager launches.

Preliminary Conclusions

All the portable INC's detected ice nuclei from the Shuttle propellant effluent; the results from the counters often correlated. The ice nuclei counts from the portable counters were a factor of about 1000 less than the counts from the laboratory ICC. The ice nucleus activity of the effluent (from unpressurized burns) was measured to be approximately 10^{11} IN/g of Al_2O_3 at -20°C as determined in the ICC. The laboratory results show ice nuclei activity at -15°C . Ice nuclei were detected in high concentrations on filters exposed to the effluent; this result was consistent with the results from the portable counters and the ICC. The concentrations of ice nuclei detected by the NCAR portable counter and by the filters correlated. The counts from the counter were higher than the counts from the filters. The ice crystals formed in the ICC were found with aluminum particles containing traces of sulfur and calcium in their centers; the crystals were probably nucleated by Al_2O_3 particles.

PROPOSED STEPS FOR LABORATORY WORK

The following steps for laboratory work are proposed.

1. Determine the cause of the differences in IN counts between the portable counters and the ICC.
2. Determine whether the ICC can be considered an "absolute" cloud chamber (compare results from seeding natural clouds and clouds in the ICC with Shuttle propellant effluent).
3. Determine the response of the ICC, portable counters, and filters to simulated SGC environments (various combinations of Al_2O_3 , HCl , CCN, and water-vapor concentrations).
4. Determine ice nuclei activity of the propellant effluent from pressurized burns (micro-SRM's).
5. Complete the comparison of the Mie portable counter and the ICC.

6. Determine the uniqueness and significance of the traces of sulfur and calcium in the Al_2O_3 IN.

ANTICIPATED FLIGHT MEASUREMENTS FROM THE TITAN III LAUNCH

The objectives of the Titan III flight (to occur after the program review) are to determine the concentrations of ice nuclei in the SGC using the portable counters investigated at CSU and to determine the physical and chemical properties of liquid particles in the SGC.

Investigators and Their Instruments

The following investigators participated in the experiment.

1. Dr. E. E. Hindman of NWC exposed pH paper and obtained ice nuclei concentrations with the Mie INC.
2. Mr. G. Langer of NCAR operated the NCAR INC counter, CCN counter, and filters.
3. Dr. L. Radke of the University of Washington, Chief Scientist aboard the B-23 aircraft (fig. 5), and his crew determined the sizes and the concentrations of liquid particles by means of the particle measuring system (PMS) probes and operated Formvar and foil impactor devices. Standard meteorological variables were measured aboard the aircraft. A side camera was aboard for obtaining photographs, and onboard-navigation data were used to determine, at any instant, the positions of the aircraft and the ground cloud. A condensation nucleus counter, an electrical aerosol analyzer (EAA), optical particle counters (OPC's), and a mass monitor were aboard for obtaining aerosol particle data. A grab sampling system with dilution capability was aboard to obtain air samples for IN, CCN, and aerosol particle measurements. The configuration of the instrumentation aboard the aircraft is shown in figure 6.

Procedures

The flight is planned to be coordinated between an NASA aircraft and the B-23. The two aircraft are to make alternate cloud penetrations. The cloud was to be monitored for a maximum of 7 hours.

Anticipated Results

Anticipated results are concentrations of IN, CCN, liquid droplets, and dry particles in time and space within the SGC as it drifts away from the launch site. The pH of the droplets will be determined. Cloud volume data will be obtained, and the meteorological conditions in the vicinity of the SGC will be recorded.

FUTURE WORK TO PROVIDE ADEQUATE MEASUREMENTS OF CLOUD- FORMING NUCLEI FROM SRM EFFLUENTS

Future work to provide adequate measurements of IN and CCN in SRM effluents includes the following.

1. Complete the proposed steps for laboratory work as previously outlined.
2. Monitor the SGC's produced by Titan and Shuttle launches at Vandenberg Air Force Base and by SRM firings at Thiokol, Utah. Opportunities to collect data other than at KSC will increase our limited knowledge of the behavior of Al_2O_3 ice nuclei in different environments.
3. Determine the effects of the Shuttle propellant effluents on precipitation from atmospheric supercooled clouds.

SUMMARY

Laboratory measurements show conclusively that the Shuttle propellant (burned unpressurized) is a source of ice nuclei; preliminary estimates of the magnitude of the source were obtained. Flight measurements of ice nuclei in Titan-produced stabilized ground clouds are inconclusive; the flight of the University of Washington B-23 aircraft is intended to provide definite measurements. Deficiencies in the laboratory and field measurements are identified. Future laboratory and field measurements are specified to eradicate the deficiencies. These investigations should provide adequate measurements of Shuttle-produced ice and cloud condensation nuclei.

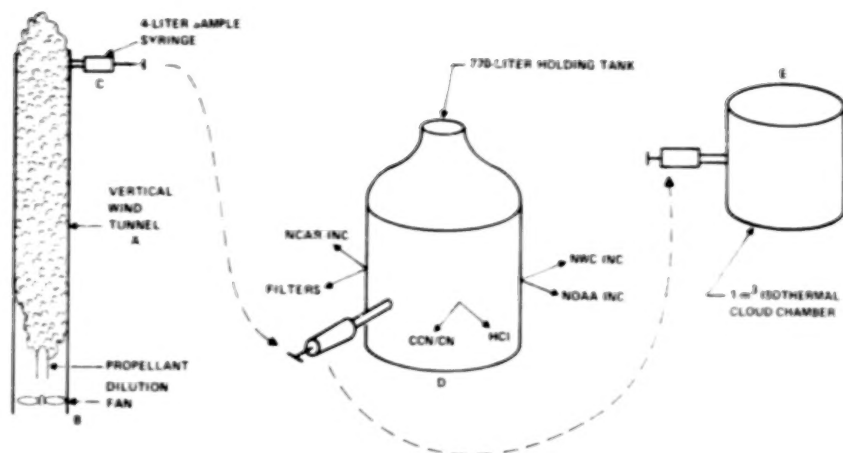


Figure 1.- Schematic of laboratory setup used to calibrate ice nuclei counters (INC's).

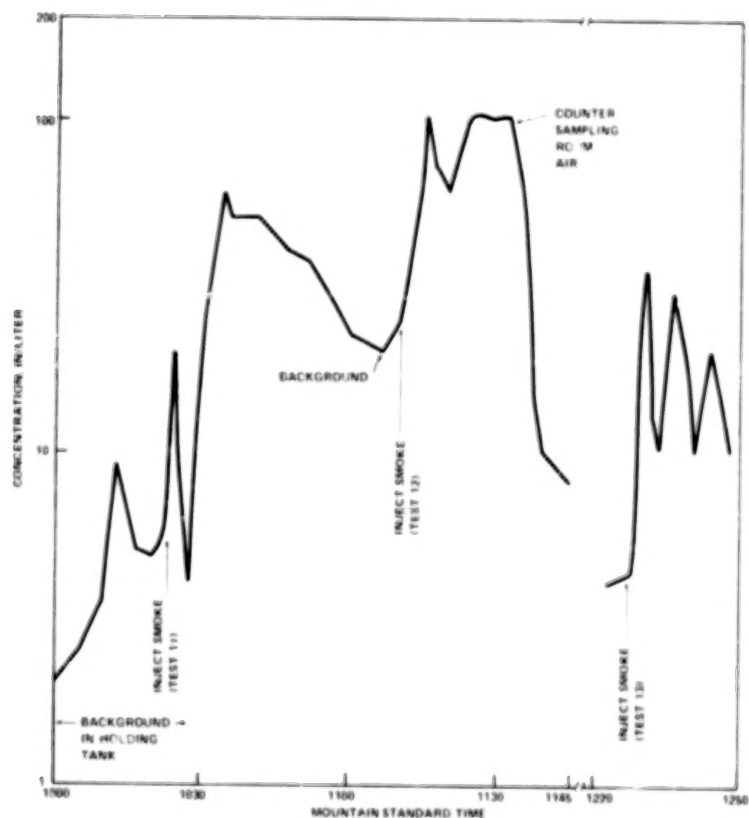


Figure 2.- Ice nuclei concentrations measured at -24°C with the NCAR counter on February 16, 1978. Note the curious increase-decrease-increase in IN concentration with time after injection of Shuttle propellant effluent on test 11.

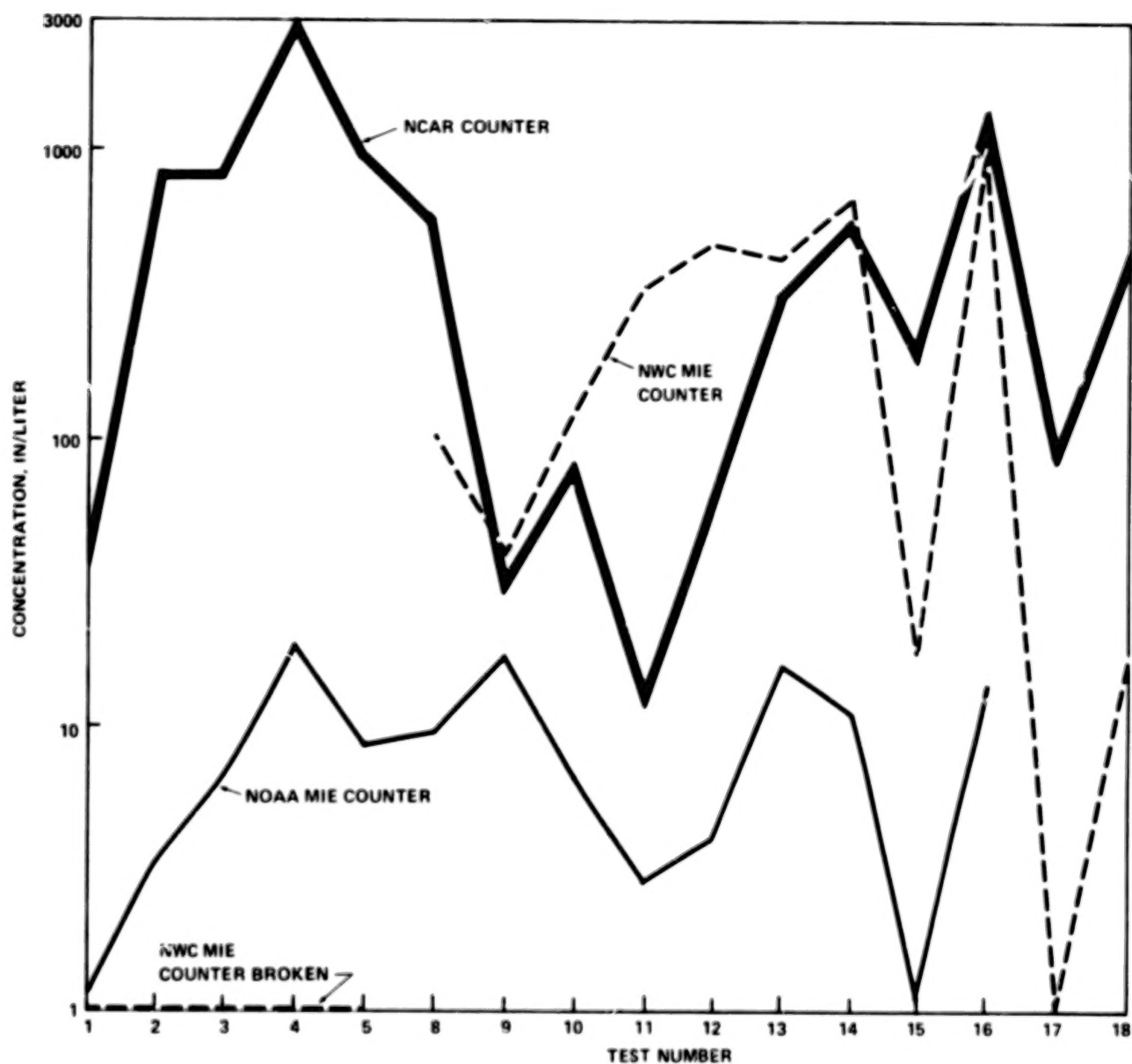


Figure 3.- Ice nuclei concentrations measured 2 minutes after injection of effluent from propellant burns into the holding tank. The values are instantaneous, not average.

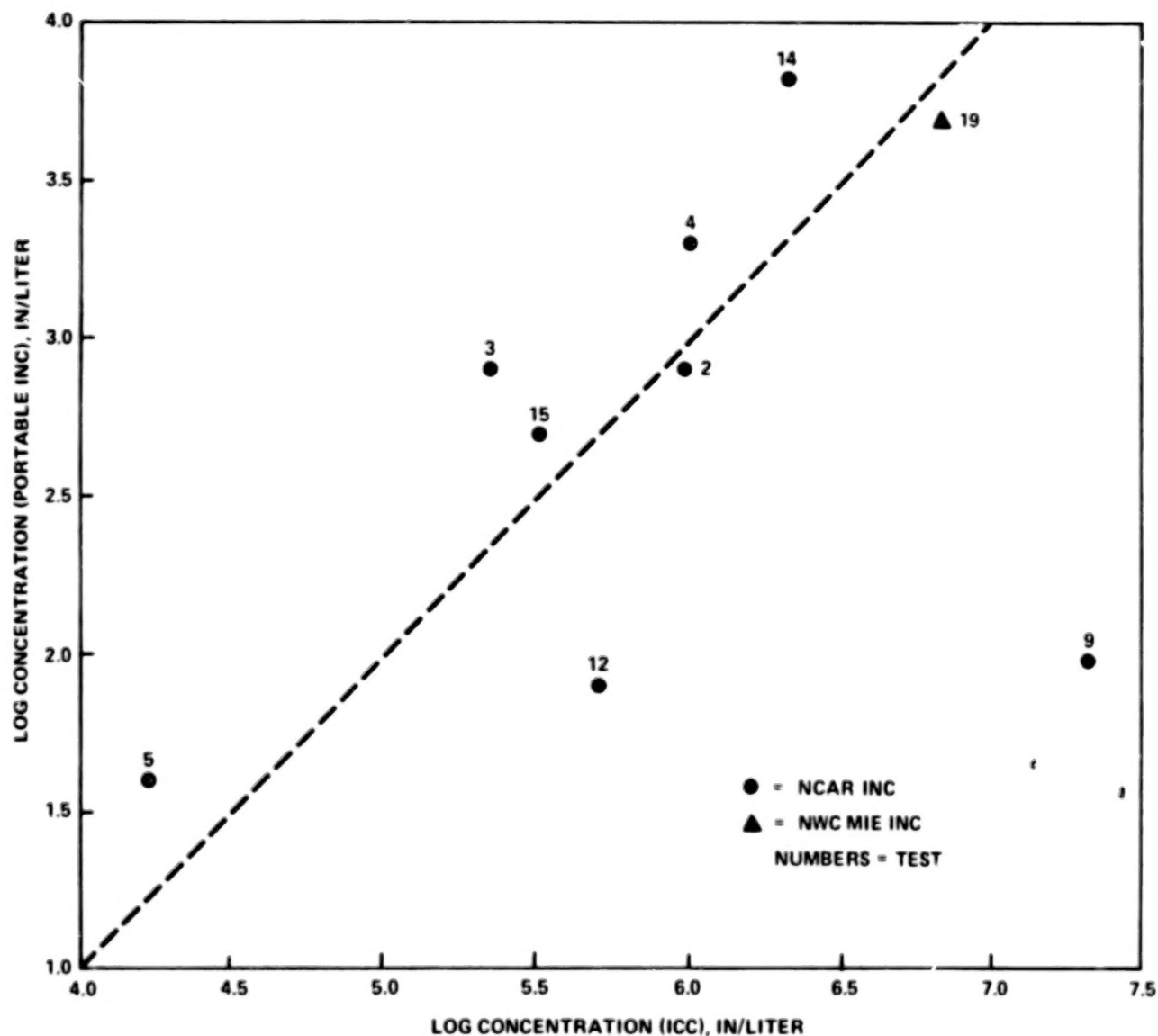
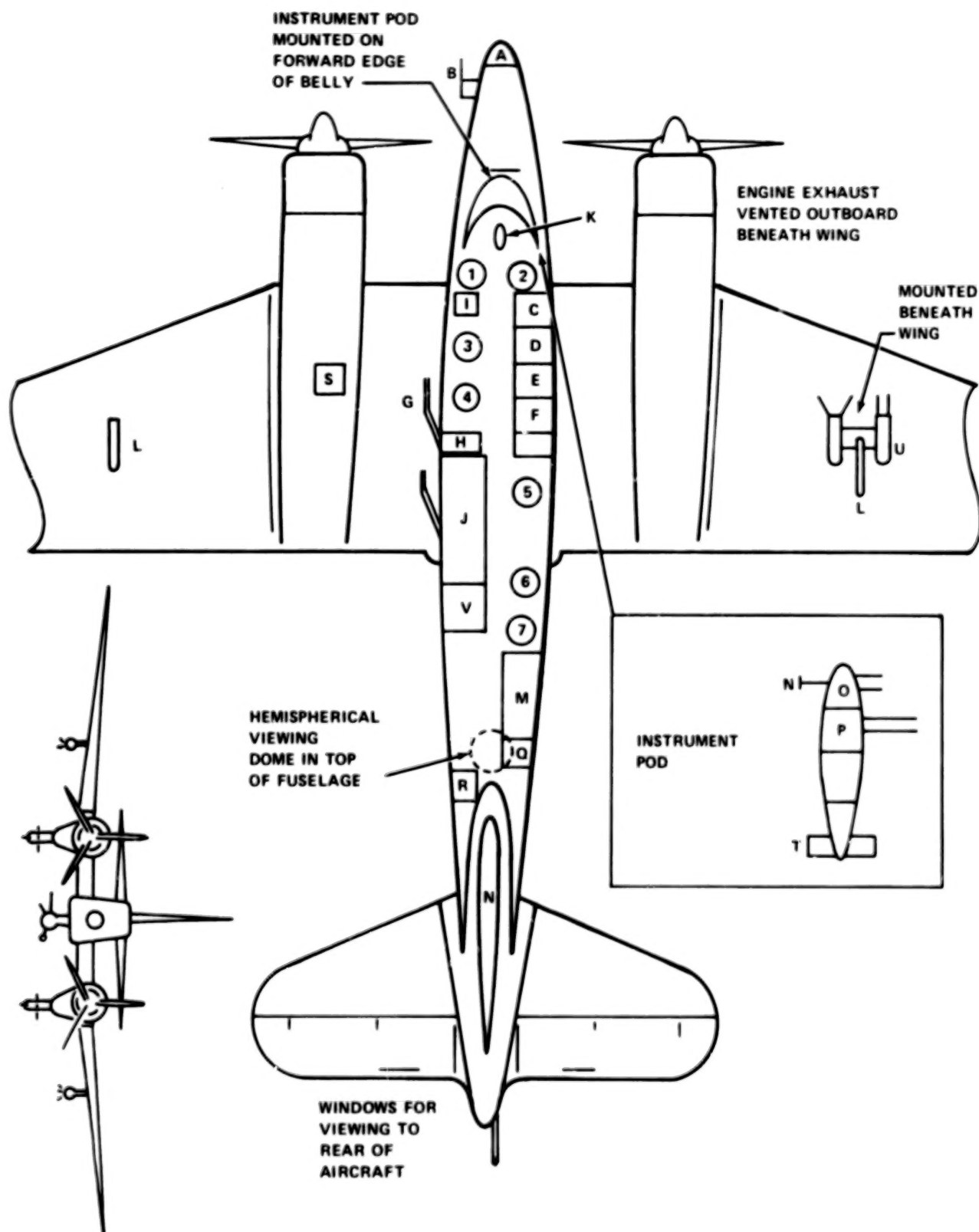


Figure 4.- Comparison of ice nuclei concentrations measured simultaneously with portable counters (NCAR and Mie) and the CSU isothermal cloud chamber (ICC). The dashed line is arbitrary and represents a difference between concentrations measured by the portable counters and the ICC of a factor of 1000.



(a) Detail.

Figure 5.- Plan view of instrumentation onboard the University of Washington Douglas B-23 aircraft.

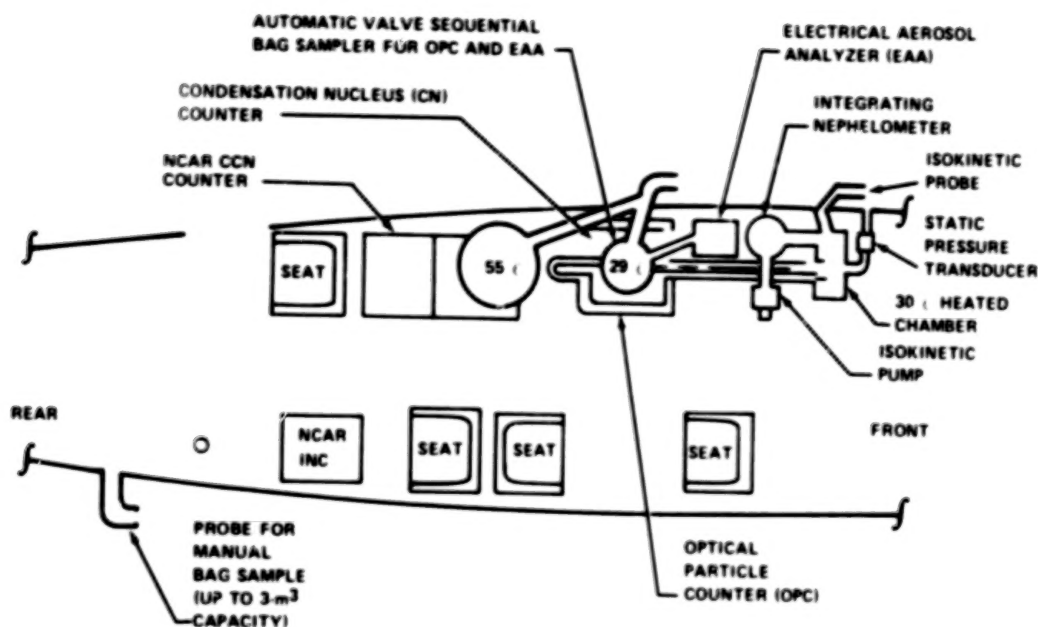
LEGEND

Locations of crew and research instruments on the University of Washington's Douglas B-23 aircraft:

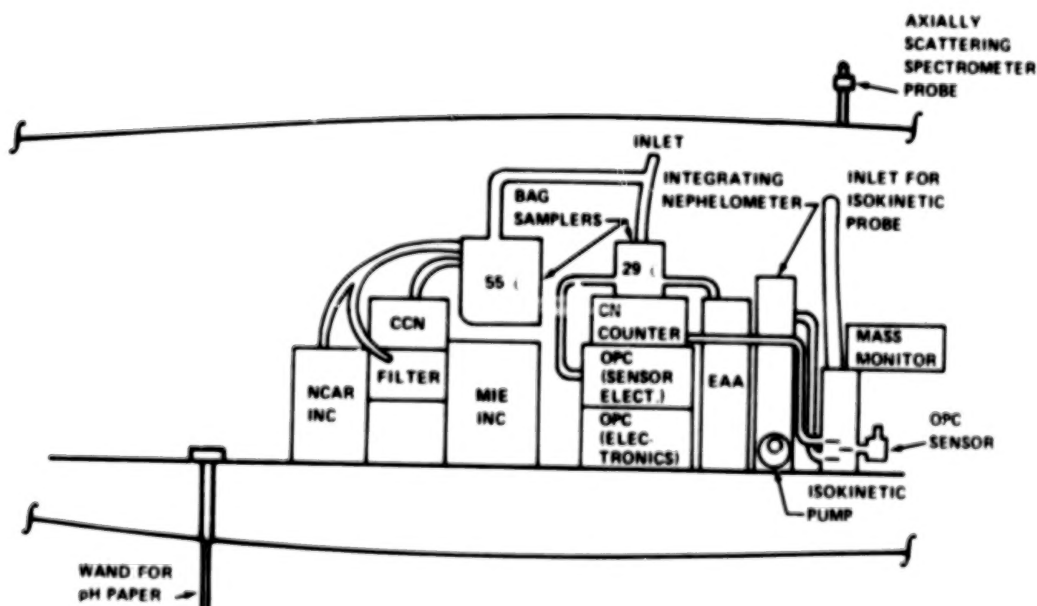
- 1-2 Pilot and copilot
- 3 Observer
- 4 Instrumentation engineer
- 5 Aerosol instrumentation monitor
- 6 Flight director
- 7 Gas instrumentation monitor
- A 5-cm gyro stabilized weather radar
- B Rosemount airspeed, pressure altitude and total temperature probes, MRI-turbulence probe and electronics, J-W liquid water probe, angle-of-attack sensor
- C Slaved position plotter for the vhf omnirange, distance-measuring equipment, research power panel (3 kW, 110 V, 60 Hz; 1.5 kW, 110 V, 400 Hz; 150 A, 28 Vdc)
- D Electronic controls for J-W liquid water indicator, reverse housing thermometer, electrical cloud particle counter and dew point thermometer, time-code generator and time display, WWV time standard receiver, TAS and T_{tot} analog computers, signal conditioning amplifiers, audio signal mixers, phase shift key time-share data multiplexers (63 channels), two-dimensional electric field and turbulence analog readouts, Doppler horizontal winds
- E Minicomputer (16-bit word; 16K-word capacity), computer interface to instrumentation, remote analog-to-digital converter, keyboard and printer
- F Hybrid analog-to-digital tape recorder (seven track; one-half inch) and high-speed six-channel analog strip chart recorder
- G Inlet for isokinetic aerosol sampling
- H Aircraft oxygen, digital readout of all flight parameters, dew point sensor, time-code reader and time display, heated aerosol plenum chamber, vertical velocity, millipore sequential filter system
- I Controls for metal foil impactor and continuous particle replicator
- J Aerosol analysis section, generally containing integrating nephelometer, sodium particle flame photometer, automatic CCN counter, vhf air-to-ground transceiver, electrical aerosol analyzer, optical particle counters, automatic condensation nucleus counter, automatic bag samplers (28- ℓ and 55- ℓ)
- K PMS axially scattering spectrometer (small droplet probe) vertically mounted
- L Bomb rack hard point suitable for small instrument pods
- M NCAR INC
- N Reverse flow static temperature probe
- O Automatic ice particle counter and metal foil hydrometer impactor
- P Continuous Formvar replicator
- Q Radar repeater, side-viewing automatic camera real-time display of PMS data
- R Radar altimeter, two-dimensional electric field mill electronics 20-channel telemetry transmitter
- S Instrument vacuum system consisting of four high-capacity vacuum pumps connected individually to the cabin
- T Anisokinetic large-volume aerosol sampler
- U PMS optical array precipitation spectrometer; PMS optical array colored droplet probe
- V Mie INC and filter holders

(b) Key.

Figure 5.- Concluded.



(a) Plan view.



(b) Side view.

Figure 6.- Configuration of University of Washington B-23 for March 1978 Titan III launch at KSC.

GROUND-BASED MEASUREMENTS OF DM-2 ROCKET EXHAUST EFFLUENTS USING FIXED-FLOW SAMPLERS AND ELECTRETS

By Michael Susko*

INTRODUCTION

Electret devices have been developed by the NASA George C. Marshall Space Flight Center (MSFC) to collect samples of rocket exhaust products for later analysis. The performance of the electrets was compared with that of Thiokol fixed-flow samplers during the static test firing of a solid rocket motor (SRM) demonstration model (DM-2) on January 19, 1978, at the Thiokol static rocket motor test site near Brigham City, Utah.

PROCEDURE

Thiokol fixed-flow air samplers were placed in six near-field and six far-field sites. The MSFC electrets were placed alongside each Thiokol air sampler. Four additional electret samplers were placed in other near- and far-field sites. The near-field location of the Thiokol air samplers and the MSFC electrets during the DM-2 static test is shown in figure 1; the far-field location, in figure 2.

The electret is fabricated by applying a field of 15 kilovolts to Teflon heated to approximately 200° C, near the melting point. When it cools, the Teflon has a permanent charge and is then defined as an electret. Rocket exhaust products are attracted to the surface of this type of electret. The material absorbed on the electret surface is analyzed later using X-ray spectroscopy.

MEASUREMENT OF ROCKET EFFLUENTS

The measurement of the rocket exhaust effluents by Thiokol air samplers and MSFC electrets indicated that the SRM had no significant effect on air quality in the area sampled. Thiokol had only one significant measurement. At Plant 78 (Site 12), Thiokol fixed-flow air samplers obtained a trace of contamination (0.094 mg/m³ (test); 0.0017 mg/m³ (background)) approximately 6.43 kilometers at a 330° heading from the static test stand. Of the total

*NASA George C. Marshall Space Flight Center.

weight, 0.0017 mg/m^3 was chlorine (0.0006 part per million), 0.0007 mg/m^3 was sulfur, 0.015 mg/m^3 was silicon, and 0.041 mg/m^3 was aluminum. Quantitative results obtained from X-ray spectroscopy analyses at Site 12 show that the electret had a background count of 1667 and a test count of 2409 after cloud passage, an increase of 742 counts. See table I for the Thiokol fixed-flow sampler results. The background pH (obtained by Thiokol at Plant 78) was basic (5.2) and increased to 7.5 in the test, an increase of 2.3 pH units more basic. One of the additional electrets (E-13) was closer to the static test site - approximately 585 meters at a heading of 325° . When the exhaust cloud passed directly over Site 13, the chlorine count from the X-ray spectroscopy analysis on this electret was 3576, an increase of 1909 counts (table II). Equating the counts of 742 to 0.0006 ppm and 1909 counts results in 0.0015 ppm . Again, no significant measurement of rocket exhaust effluents was found at the test site.

The SRM was oriented west to east and fired toward the east. The surface winds blew from the southeast, but the upper airflow was 25 m/sec from the southwest. At an altitude of approximately 6 kilometers, the windspeed increased to approximately 30 m/sec . A vertical profile of windspeed, wind direction, and air temperature used as inputs to the multilayer diffusion model for the DM-2 static test is given in figure 3.

CONCLUSIONS

The results show that the electrets can be used effectively for sampling rocket exhaust products. A special advantage of electrets is that they do not require power for operation. Consequently, they can be valuable for measuring rocket exhaust effluents in areas where other measuring devices may not be practical. An assessment of the effectiveness of the electret resulted in the following conclusions.

At Plant 78, 6.43 kilometers at a 330° heading from the static test site, Thiokol fixed-flow samplers obtained the only trace of contamination - 0.0017 mg/m^3 or 0.0006 ppm Cl . At this site, the Cl count from the dispersive X-ray spectroscopy analysis was 1667 (background) and 2409 (test), an increase of 742 counts.

An additional electret was placed at Site 13 (585 meters at a 325° heading from the static test firing). With no power available at this site, the electret was the only measurement device. The background count was 1667 and the test count was 3576, an increase of 1909 counts. Equating the 742 counts to 0.0006 ppm , the 1909 counts obtained at the closer test site converts to 0.0015 ppm . Again, no significant amount of rocket exhaust effluents was measured. In addition, simplicity in deployment of the electrets (no power necessary) makes the electret a valuable complementary device in detecting rocket gas effluents.

TABLE I.- QUANTITATIVE RESULTS OBTAINED FROM
X-RAY SPECTROSCOPY - SITE 12

[Air sampler 12, 6.43 kilometers at 330° heading from static test stand]

Energy, keV	Element	Total test counts ^a	Background counts
0.689	Fe	6 953	6 547
1.483	Al	74 888	73 595
1.748	Si	68 290	56 240
2.131	Au	1 449	783
2.328	S	4 061	4 692
2.626	Cl	2 409	1 667
3.334	Sn α	735	1 130
3.680	Sn β	84	--
5.436	Cr α	2 979	2 092
5.929	Cr β	428	--
5.418	Fe α	8 097	5 534
7.030	Fe β	908	106
7.502	Ni	483	--
8.0507	Cu α	2 279	2 105
8.930	Cu β	218	131

^a1000 seconds.

TABLE II.- QUANTITATIVE RESULTS OBTAINED FROM
X-RAY SPECTROSCOPY - SITE 13

[Electret 13, 585 meters at 325° heading from static test stand]

Energy, keV	Element	Total test counts ^a	Background counts
0.685	Fe	6 743	6 547
1.489	Al	72 063	73 595
1.741	Si	80 821	56 240
2.629	Cl	3 576	1 667
3.329	Sn _α	1 141	1 130
3.675	Sn _β	744	--
4.500	Ti	157	--
5.413	Cr _α	3 282	2 092
5.965	Cr _β	242	--
6.412	Fe _α	9 200	5 534
7.083	Fe _β	1 049	106
7.462	Ni	1 011	--
8.055	Cu _α	6 275	131
8.925	Cu _β	700	--

^a1000 seconds.



Figure 1.- Near-field location of Thiokol air samplers and MSFC electrets during DM-2 static test.

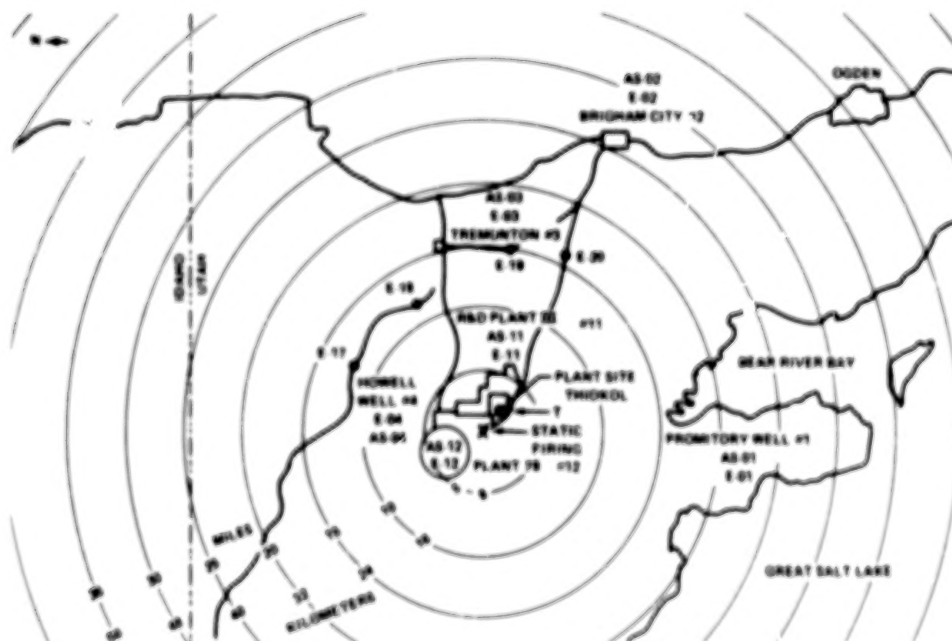


Figure 2.- Far-field location of Thiokol air samplers and MSFC electrets during DM-2 static test.

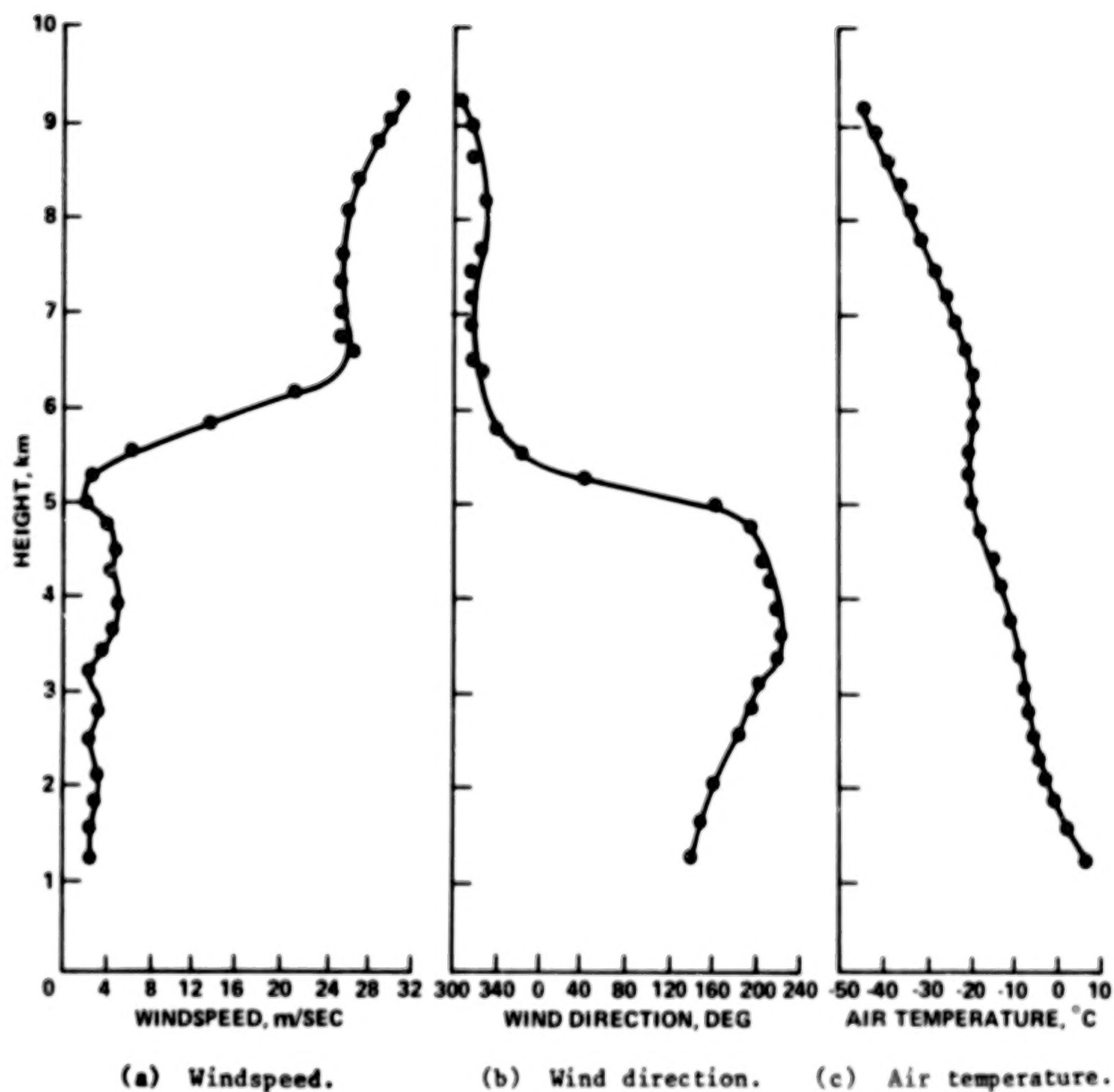


Figure 3.- Inputs to the MSFC multilayer diffusion model for DM-2 static test.

ACID RAIN: MESOSCALE MODEL

By Hsiao-ming Hsu*

INTRODUCTION

A mesoscale numerical model of the Florida peninsula has been formulated and applied to a dry, neutral atmosphere. The preliminary results of this model presented in this paper are very encouraging. To simulate synoptically undisturbed and disturbed situations in this area, several modifications have appeared desirable; thus, a new model quite different from the one just mentioned has evolved. A submesoscale model for the Cape Canaveral area will use the results from the mesoscale model as continuous inputs. The prospective use of the Control Data Corporation (CDC) STAR-100 computer at the NASA Langley Research Center for the submesoscale model is discussed.

PRELIMINARY RESULTS

The numerical model presented in reference 1 is tested under synoptically undisturbed conditions. Because this test is for demonstrating the simulation of only the basic dynamics in the mesoscale region and for detecting any programming error in the model, three assumptions are applied to simplify the calculation.

1. The atmosphere is assumed to be dry; i.e., the parameterization of cloud and precipitation physics is not yet included.

2. A constant potential temperature ($\theta = 298.16$ K) and a constant geostrophic windspeed ($V = 6$ m/sec) are assigned to the model as the initial conditions.

3. The daytime land surface temperature is represented by a single sine function that limits the maximum heating to 10 K at the end of the sixth hour of simulation. The water surface is assigned a constant temperature that is the same as the initial temperature of the land surface. (The time step is 5 minutes.)

Two cases, differing only in the direction of the prevailing geostrophic wind, are examined: a prevailing southwest wind and a prevailing southeast wind, both 6 m/sec at all levels initially.

*University of Michigan.

Prevailing Southwest Wind

Results from the simulation experiment of prevailing southwest wind are shown for the various levels and times in figures 1 to 3. The horizontal wind field at the 50-meter level shows only a slight change from the prevailing wind at the end of 2 hours (figs. 1(a) and 1(b)). By the third hour (fig. 1(c)), the low-level wind direction has turned noticeably at the shorelines and especially sharply along the east coast of the Florida peninsula. A definite low-level convergence zone is formed by the end of the fourth hour of simulation (fig. 1(d)). The sea-breeze convergence zone continues to develop and moves inland during the fifth (fig. 1(e)) and sixth (fig. 1(f)) hours.

The horizontal wind fields at 200-, 450-, 800-, and 1250-meter levels are shown at the end of the sixth hour in figure 2. The change of wind from 50 to 1250 meters reveals the vertical sea-breeze circulation along the east coast: the sea breeze gives onshore winds in the lower levels and offshore winds in the higher levels. The gradual veering of the wind from southeast or east near the surface to southwest aloft is clearly shown.

Figure 3 gives the computed horizontal distributions of vertical velocity at 1250 meters at the end of each hour of simulation. The velocity fields are mainly developed by the effects of advection over the gradually warmed peninsula. The convergence zone forms first along the west coast, whereas divergence prevails along the east coast. By the third hour, convergence is also noted along the east coast. Several distinct maximums of positive vertical velocity exist along the east coast at the sixth model hour. The maximum south of Lake Okeechobee, predicted by Pielke (ref. 2), has the greatest upward velocity. Two other maximums north of Lake Okeechobee, although weaker than the one just mentioned, are very close to the area of Cape Canaveral. Pielke has demonstrated that the predicted regions of positive vertical velocity agree qualitatively with radar and satellite observations of cloud and shower activity over southern Florida on undisturbed days. His study did not, however, extend north of Lake Okeechobee and so did not reveal the effects at Cape Canaveral. The maximums of positive upward motion in the author's results are expected to be closely related to cloud and shower activity, at least qualitatively. In this case, having the southwest wind in a synoptically undisturbed situation, disturbed weather contributed solely by the sea-breeze convergence appears both in the Cape Canaveral area and in southeastern Florida.

Prevailing Southeast Wind

The horizontal wind patterns for prevailing southeast wind at the 50-meter level are shown in figure 4 for the end of each model hour. Again, a slight turning is seen at the coastlines by the end of the second hour (fig. 4(b)). The convergence zone develops gradually along the west coast of Florida. At the sixth hour, the horizontal wind distributions at heights of 200, 450, 800, and 1250 meters indicate the sea-breeze circulation along the west coast (fig. 5). The vertical velocity fields at the 1250-meter level at the end of each model hour (fig. 6) show the evolution of the sea-breeze

convergence zone. Under the southeast wind regime, the area of Cape Canaveral is covered by a field of downward vertical velocity after the second hour (fig. 6(b)), but a band of upward motion that occurs inland during the fifth and sixth hours (figs. 6(e) and 6(f), respectively) indicates possible weather disturbance. Along the western shore of Florida, however, the vertical velocity fields are more strongly developed.

For both cases, the motion fields appear to be somewhat exaggerated after 5 hours of simulation. This result is a product of the highly idealized assumption that the atmosphere is adiabatic (constant potential temperature $\theta = 298.16$ K) initially. The computations are stopped at the end of the sixth hour.

Discussion

Analogous features are shown under the two different prevailing wind directions. They are not caused by different dynamics but by the orientation of the Florida peninsula with respect to the wind. On synoptically undisturbed days, the local weather is dominated by the sea breeze. For the Cape Canaveral area, locally disturbed weather can be expected to appear under a general southwest flow. Under a general southeast flow, disturbances at the Cape are not expected, but they might develop inland and downwind from the Cape. This conclusion agrees qualitatively with Neumann's report that the probability of having afternoon thunderstorms under southeast winds is low but that the probability of having them under southwest winds in the summer months at the Cape is more than 50 percent (ref. 3).

Comparison of the author's results with those of Pielke (ref. 2) reveals that the strength of upward motion is weaker in the author's simulation than in Pielke's before the end of the fifth hour. Because the author's horizontal grid spacing is about three times longer than Pielke's, the extremes shown by Pielke's model are necessarily greater than those shown by the author's. At the same time, the author's model is flexible in that the grid spacing can be adjusted in both the horizontal and vertical directions. The question of increased resolution of the model in turn raises the question of the limits of computer capacity. The author proposes, as a second stage of model development, the introduction of a cloud-scale model (grid spacing 2 by 2 by 0.5 kilometers) the initial and boundary conditions of which will be derived from the mesoscale model.

Although it is clear that the modeled mesoscale dynamic processes do predict the sea-breeze regimes along the Florida coasts, it is also clear that important modifications must be introduced to achieve more complete simulations. These are presented and discussed in the following section.

RECENT DEVELOPMENTS

To generate more complete mesoscale information over the region of the Florida peninsula, the following additional considerations are introduced.

Parameterization of Convective Cloud and Precipitation

The study of parameterization described in the section entitled "Future Work" leads to the conclusion that Kuo's method (ref. 4) is the best approach for meeting the requirements of fidelity with simplicity. This parameterization is recommended partly by its more rigorous derivation and partly by its potential for further development. It will, for example, enable the use of a convective cloud model to obtain values for the cloud temperature and specific humidity.

The parameterization allows for two kinds of moisture sources for a convective cloud (fig. 7). One is the net convergence of moisture between cloud base and cloud top

$$- \int_{z_b}^z \left[\frac{\partial}{\partial x}(\rho qu) + \frac{\partial}{\partial y}(\rho qv) + \frac{\partial}{\partial z}(\rho qw) \right] dz$$

and the other is the evaporation between the surface and cloud base

$$\rho_{z_b} C_D V_{z_b} (q_g - q_{z_b})$$

Then, the total moisture available to the air column in the convective cloud is

$$M = - \int_{z_b}^z \left[\frac{\partial}{\partial x}(\rho qu) + \frac{\partial}{\partial y}(\rho qv) + \frac{\partial}{\partial z}(\rho qw) \right] dz + \rho_{z_b} C_D V_{z_b} (q_g - q_{z_b}) \quad (1)$$

where z_t and z_b are the heights of cloud top and cloud base, respectively; u and v are the x - and y -component velocities; w is vertical velocity; q is the specific humidity; ρ is density; C_D is the drag coefficient; V is the horizontal windspeed; and g denotes the surface.

The total moisture available M may fuel the convective cloud by becoming entrained through the cloud sides, by pumping moisture through the cloud base,

or by evaporating part of M in the environment. Two kinds of sink from a convective cloud are parameterized: the evaporation from cloud sides and the precipitation received at the surface. The evaporation both in the environment and from cloud sides represents moisture input to the air column βM . The precipitation received at the surface represents the removal of moisture $(1 - \beta)M$ from the air column. The processes within the dashed box in figure 7 are the subgrid processes in the author's mesoscale model and are not evaluated explicitly.

The source term for the potential temperature θ can be expressed by

$$S_{\theta 2} = \frac{L}{\pi} C \quad (2)$$

where L is the latent heat of evaporation and C is the precipitation rate produced by a convective cloud. The value π is the scaled pressure

$$\pi = c_p \left(\frac{p}{p_0} \right)^{\frac{R}{c_p}} \quad (3)$$

where c_p is the specific heat at constant pressure, R is the gas constant for dry air, p is the pressure, and $p_0 = 1000$ millibars is a reference pressure.

The vertically integrated precipitation rate gives the total amount of precipitation.

$$\int_{z_b}^{z_t} \rho C \, dz = (1 - \beta)M \quad (4)$$

The precipitation rate produced by a convective cloud may be written as

$$\rho C = (1 - \beta)M \left(\frac{N(z)}{z_t - z_b} \right) \quad (5)$$

if the vertical distribution function $N(z)$ of θ satisfies

$$\int_{z_b}^{z_t} N(z) dz = z_t - z_b \quad (6)$$

Supposing that $N(z)$ is represented as a function of the difference of potential temperatures between the cloud interior and its environment,

$$N(z) = \frac{(\theta_c - \theta)}{\langle \theta_c - \theta \rangle} \quad (7)$$

where

$$\langle \theta_c - \theta \rangle = \frac{1}{(z_t - z_b)} \int_{z_b}^{z_t} (\theta_c - \theta) dz \quad (8)$$

Then,

$$C = \frac{(1 - \beta)M}{\rho(z_t - z_b)} \frac{(\theta_c - \theta)}{\langle \theta_c - \theta \rangle} \quad (9)$$

where the subscript c denotes cloud.

Substituting equation (9) into equation (2) gives

$$S_{\theta 2} = \frac{L(1 - \beta)M}{\pi \rho(z_t - z_b)} \frac{(\theta_c - \theta)}{\langle \theta_c - \theta \rangle} \quad (10)$$

for the source term for θ . Similarly, the source term for q is

$$S_{q2} = - \frac{(1 - \beta)M}{\rho(z_t - z_b)} \frac{(\theta_c - \theta)}{(\theta_c - \theta)} \quad (11)$$

The coefficient β representing the fraction of M remaining in the air column is a very important and crucial factor. The whole evaporation process is controlled by β . It has been assumed to have the following form (ref. 5).

$$\beta = \begin{cases} \left[\frac{1 - (\overline{q/q_s})}{1 - (\overline{q/q_s})^*} \right]^n, & \text{when } (\overline{q/q_s}) \geq (\overline{q/q_s})^* \\ 1, & \text{when } (\overline{q/q_s}) < (\overline{q/q_s})^* \end{cases} \quad (12)$$

where the subscript $*$ represents a critical value to be specified and the superscript n is a constant.

The cloud variables that have the subscript c are determined by the saturated adiabat between cloud base and cloud top. It is intended that these values will eventually be computed by using a convective cloud model.

Diagnostic Vertical Velocity Equation

It is intended to represent all diurnal, seasonal, and synoptic characteristics of the region of interest. A shallow model clearly does not meet this requirement. To account for deep convection, the model is extended to 16 kilometers vertically in 18 levels (table I). The assumption of constant density can no longer be used and must be replaced by the complete continuity equation for a compressible fluid. Finally, a modified Richardson's equation is used to calculate the vertical velocity diagnostically.

The principle of mass conservation gives the continuity equation in three dimensions.

$$\nabla \cdot \vec{V} = - \frac{1}{\rho} \frac{d\rho}{dt} \quad (13)$$

where

$$\nabla = \frac{\partial}{\partial x} \vec{i} + \frac{\partial}{\partial y} \vec{j} + \frac{\partial}{\partial z} \vec{k}$$

$$\vec{V} = u\vec{i} + v\vec{j} + w\vec{k}$$

and

$$\frac{d}{dt} = \frac{\partial}{\partial t} + \vec{V} \cdot \nabla$$

Taking the logarithm of the equation of state and the definitions of π and θ yields

$$\ln p = \ln \rho + \ln R + \ln T \quad (14)$$

$$\ln \pi = \ln c_p + R/c_p \ln p - R/c_p \ln p_0 \quad (15)$$

$$\ln \theta = \ln T - \ln \pi + \ln c_p \quad (16)$$

where T is the temperature. Differentiating equations (14), (15), and (16) and making substitutions, one obtains

$$\frac{1}{\rho} \frac{d\rho}{dt} = \frac{c_v}{R} \frac{1}{\pi} \frac{d\pi}{dt} - \frac{1}{\theta} \frac{d\theta}{dt} \quad (17)$$

where c_v is the specific heat at constant volume. Substitution of equation (17) into equation (13) gives

$$\nabla \cdot \vec{V} = - \frac{c_v}{R} \frac{1}{\pi} \frac{d\pi}{dt} + \frac{1}{\theta} \frac{d\theta}{dt} \quad (18)$$

Multiplying p/π on each side of equation (18), taking $\vec{V} \cdot \nabla \pi$ in $d\pi/dt$ from the right-hand side of equation (18) to the left-hand side, and rearranging terms, one has

$$\nabla \cdot \left(\frac{p}{\pi} \vec{V} \right) = - \frac{c_v}{R} \frac{p}{2} \frac{\partial \pi}{\partial t} + \frac{p}{\pi \theta} \frac{d\theta}{dt} \quad (19)$$

The time derivative of the hydrostatic equation

$$\frac{\partial}{\partial t} \left(\frac{\partial \pi}{\partial z} \right) = \frac{\partial}{\partial t} \left(- \frac{g}{\theta_v} \right) \quad (20)$$

is integrated from any level z to the model top H to determine $\partial \pi / \partial t$.

$$\frac{\partial \pi}{\partial t} = A + B \quad (21)$$

where

$$A = \frac{\partial \pi}{\partial t} \Big|_H \quad (22)$$

$$B = g \int_z^H \frac{\partial}{\partial t} \left(\frac{1}{\theta_v} \right) dz' \quad (23)$$

and

$$\theta_v = (1 + 0.609q)\theta$$

Both $\partial/\partial t(1/\theta_v)$ and $d\theta/dt$ can be evaluated explicitly from the equations of potential temperature and specific humidity in the model. Then, equation (19) becomes

$$\nabla \cdot \left(\frac{p}{\pi} \vec{V} \right) = - \frac{c_v}{R} \frac{p}{\pi^2} (A + B) + \frac{p}{\pi \theta} \frac{d\theta}{dt} \quad (24)$$

after substituting equation (21) into equation (19).

Integrating equation (24) from the surface to any height z and applying the surface boundary condition for w , $w = 0$ at $z = 0$, one has

$$w = - \frac{\pi}{p} \int_0^z \left[\frac{\partial}{\partial x} \left(\frac{p}{\pi} u \right) + \frac{\partial}{\partial y} \left(\frac{p}{\pi} v \right) \right] dz$$

$$- \frac{\pi}{p} \int_0^z \left[\frac{c_v}{R} \frac{p}{\pi^2} (A + B) - \frac{p}{\pi \theta} \frac{d\theta}{dt} \right] dz \quad (25)$$

This equation gives the values of the vertical velocity at any point and is called the "modified" Richardson's equation.

If the top boundary condition for w , $w = 0$ at $z = H$, is further applied, the pressure tendency will be given as follows.

$$\left. \frac{\partial \pi}{\partial t} \right|_H = A$$

$$= \frac{-\int_0^H \left[\frac{\partial}{\partial x} \left(\frac{p}{\pi} u \right) + \frac{\partial}{\partial y} \left(\frac{p}{\pi} v \right) + \frac{c_v}{R} \frac{p}{\pi^2} B - \frac{p}{\pi \theta} \frac{d\theta}{dt} \right] dz}{\frac{c_v}{R} \int_0^H \frac{p}{\pi^2} dz} \quad (26)$$

The pressure is adjusted by the predicted value from equation (26) at the model top, and the rest of the π -field is calculated from the hydrostatic equation.

Lateral and Upper Boundary Conditions

The Neumann-type lateral boundary condition gives some noise along the boundaries. It can be found in figures 3 and 6. The amplitude of this noise is small, but the noise will be amplified in a stably stratified atmosphere and become fast-moving internal gravity waves. These waves can seriously contaminate the model results. Perkey and Kreitzberg (ref. 6) developed a method to control this problem; this method has been adapted to the present model.

For both lateral and upper boundaries, the variables u , v , θ , and q (represented by D) on the boundary region will be determined by weighting their local tendencies.

$$\frac{\partial D}{\partial t}(I) = W_1(I) \left. \frac{\partial D}{\partial t}(I) \right|_m + \left[1 - W_1(I) \right] \left. \frac{\partial D}{\partial t}(I) \right|_k \quad (27)$$

where the subscripts m and l represent mesoscale and large scale, respectively. The weighting functions for $\partial D/\partial t$ are as follows.

$$\left. \begin{aligned} W_1(B) &= 0.0 \\ W_1(B \pm 1) &= 0.3 \\ W_1(B \pm 2) &= 0.7 \\ W_1(B \pm 3) &= 0.9 \\ W_1(B \pm 4) &= 1.0 \end{aligned} \right\} \quad (28)$$

where B denotes the grid point at the boundary, $B \pm 1$ is the grid point next to B (one grid space in from the boundary), etc.

The vertical velocity w is also determined by means of a weighting procedure as follows.

$$W(I) = W_2(I)w(I) \Big|_m \quad (29)$$

The weighting functions for w are as follows.

$$\left. \begin{aligned} W_2(B) &= 0.00 \\ W_2(B \pm 1) &= 0.25 \\ W_2(B \pm 2) &= 0.50 \\ W_2(B \pm 3) &= 0.75 \\ W_2(B \pm 4) &= 1.00 \end{aligned} \right\} \quad (30)$$

These weighting functions may be adjusted, depending upon test results.

Boundary-Layer Parameterization

To understand the full diurnal variation of mesoscale weather is one of the author's goals. Deardorff's equation (ref. 7) may be used to model the daytime growth of the height of the planetary boundary layer (PBL). The equation is not, however, capable of simulating the variation of the height of the PBL after sunset and before sunrise next morning. To predict the height of the PBL at night, the formulation developed by Smeda (ref. 8) will be used.

$$\frac{\partial H_*}{\partial t} = - \left(u|_{H_*} \frac{\partial H_*}{\partial x} + v|_{H_*} \frac{\partial H_*}{\partial y} \right) + 0.06 \frac{u_*^2}{H_* f} \left[1 - \left(\frac{2.3 H_* f}{u_*} \right)^3 \right] \quad (31)$$

where $f = 2\Omega \sin \phi$, Ω is the Earth rotation rate, ϕ is the latitude, H_* is the height of the PBL, and u_* is the frictional velocity. The vertical profile of the eddy exchange coefficients remains the same as before.

FUTURE WORK

Improvements of the Mesoscale Model

The mesoscale model is now quite well developed and will be used to provide basic predictive information for the Florida peninsula. As is evident in the model derivations, it has been necessary to idealize and/or parameterize numerous component parts of the problem. It is anticipated that development of techniques and procedures for handling these component parts will continue and that improvements of the model will be made possible by these developments. This is a continuing process which will provide improvement but cannot be expected to achieve perfection in the model.

Development of a Submesoscale Model

To simulate the processes of the solid rocket motor exhaust product removal and the patterns of deposition that they produce in the area of Cape Canaveral after Space Shuttle launches, a submesoscale numerical model is being developed. The model domain is in three dimensions, 90 by 90 by 15 kilometers. The approximate location is shown in figure 8. Processes will be depicted in terms of the behavior of the meteorological variables and model parameters at some 65 596 grid points (a spacing of 2 by 2 by 0.5 kilometers). The basic equations are derived from the theory of atmospheric dynamics and thermodynamics, cloud and precipitation physics, boundary-layer dynamics, and air pollution chemistry. Initial and boundary conditions will be obtained continuously from the output of the mesoscale model.

The requirements of this model in terms of computer capacity and speed are very great. Consequently, a comparative study of the available and soon-to-be available computer facilities has been undertaken.

COMPARATIVE STUDY OF COMPUTER FACILITIES

A brief comparative study of the prominent advanced computer systems that are or may become available has been made. The systems considered are the CDC-6600, the CDC-7600, the Amdahl-470V/6, the CRAY-1, and the STAR-100.

Central processing unit (CPU) rates and memory storage capacities are tabulated and compared in terms of performance ratios in table II. The internal core memory is augmented by virtual memory of unlimited capacity in the Amdahl and the STAR systems. This may be a necessary feature for the submesoscale model.

Clearly, the STAR-100 system is comparable to the CRAY-1 in terms of the CPU rates. The variation of these rates for a given unit is a function of the kind and extent of the computations and tends upward for the array computers as the number of grid points increases. For the STAR-100, in particular, the CPU performance ratio with respect to the CDC-6600 varies as shown in table III.

It is, of course, not valid to extrapolate the trend shown. The anticipated model space of 65 596 grid points will clearly require use of the virtual memory capability of the STAR. At present, no means exists for estimating how the size of the model will affect the overall speed of simulation.

Advantages of the Amdahl-470V/6 at the University of Michigan and of the CRAY-1/CDC-7600 at the National Center for Atmospheric Research (NCAR) are that both have sophisticated graphics facilities and that the CRAY has both scalar and vector registers. It is not yet clear to what extent these features might simplify the procedures and facilitate the presentation of simulation results.

One consideration of significance in selecting the computer facility to be used is that of competing demands for computer times. The NCAR is currently inviting requests for time on the CRAY, and there is little doubt that the atmospheric modeling community will respond. If the STAR is made available on comparable financial terms to the present project, the much more restricted competition for its use will probably make it the more attractive alternative.

REFERENCES

1. Dingle, A. N.: Rain Scavenging of Solid Rocket Exhaust Clouds. NASA CR-2928, 1978.
2. Pielke, R. A.: A Three-Dimensional Numerical Model of the Sea Breezes Over South Florida. Monthly Weather Rev., vol. 102, 1974, pp. 115-139.
3. Neumann, C. J.: Frequency and Duration of Thunderstorms at Cape Kennedy, Part II. WBTM-SOS-6, 1970.
4. Kuo, H.-L.: Further Studies of the Parameterization of the Influence of Cumulus Convection on Large-Scale Flow. J. Atmos. Sci., vol. 31, 1974, pp. 1232-1240.
5. Anthes, R. A.: A Cumulus Parameterization Scheme Utilizing a One-Dimensional Cloud Model. Monthly Weather Rev., vol. 105, 1977, pp. 270-286.
6. Perkey, D. J.; and Kreitzberg, C. W.: A Time-Dependent Lateral Boundary Scheme for Limited-Area Primitive Equation Models. Monthly Weather Rev., vol. 104, 1976, pp. 744-755.
7. Deardorff, J. W.: Three-Dimensional Numerical Study of the Height and Mean Structure of a Heated Planetary Boundary Layer. Boundary Layer Meteorol., vol. 7, 1974, pp. 81-106.
8. Smeda, M. S.: Incorporation of Planetary Boundary Layer Processes Into Numerical Forecasting Models. Rep. DM-23, Univ. of Stockholm, 1977.

TABLE I.- VERTICAL GRID FOR DEEP CONVECTION MODEL
HEIGHT OF VERTICAL LEVEL

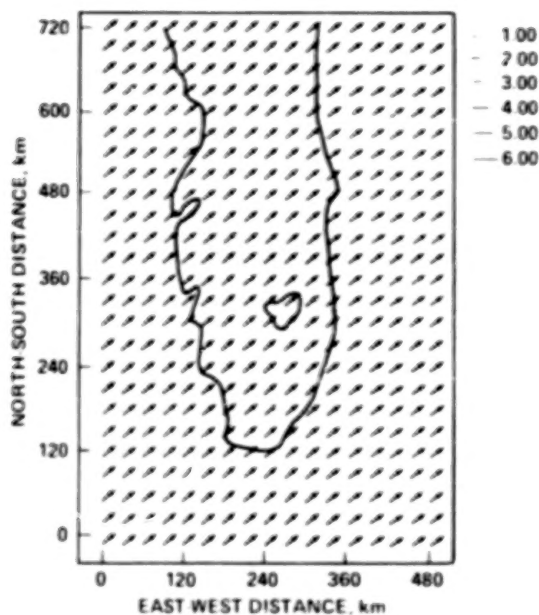
Level no.	Height, km
18	16.00
17	14.00
16	12.00
15	10.00
14	8.50
13	7.00
12	6.00
11	5.00
10	4.05
9	3.20
8	2.45
7	1.80
6	1.25
5	.80
4	.45
3	.20
2	.05
1	0

TABLE II.- COMPARATIVE CPU RATES AND STORAGE CAPACITIES

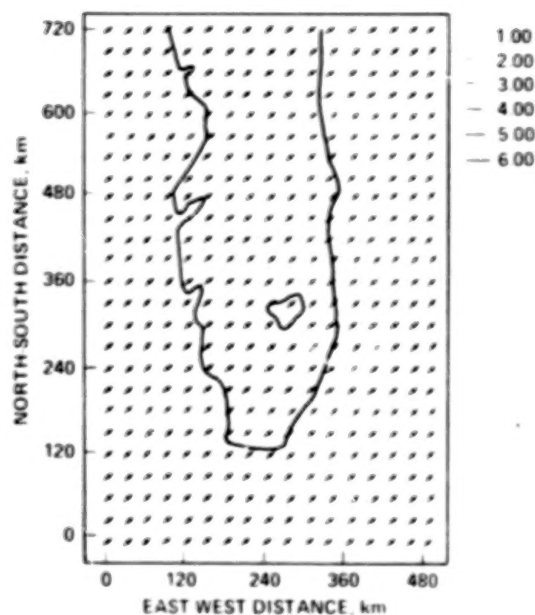
^a Amdahl-470V/6	^b CDC-6600	^b CDC STAR-100	^c CDC-7600	^c CRAY-1
CPU performance ratio				
1.0 to 1.33	0.37	2.59 to 24.89	1.85	3.7 to 14.8
2.7 to 3.6	1.0	7.00 to 67.2	5.0	10.0 to 40.0
0.39 to 0.51	0.14	1.00 to 9.6	0.71	1.43 to 5.71
0.04 to 0.05	0.01	0.10 to 1.0	0.07	0.11 to 0.42
0.54 to 0.72	0.2	1.4 to 13.44	1.0	2.0 to 8.0
0.27 to 0.36	0.1	0.7 to 6.72	0.5	1.0 to 4.0
0.03 to 0.09	0.03	0.175 to 1.68	0.13	0.25 to 1.0
CPU word storage capacity				
1 048 576 plus VM ^d	131 000	512 000 plus VM ^d	512 000	1 048 576

^aUniversity of Michigan.^bNASA Langley Research Center.^cNational Center for Atmospheric Research.^dVirtual memory.TABLE III.- CPU PERFORMANCE RATIOS FOR STAR-100/CDC-6600
IN RELATION TO NUMBER OF GRID POINTS

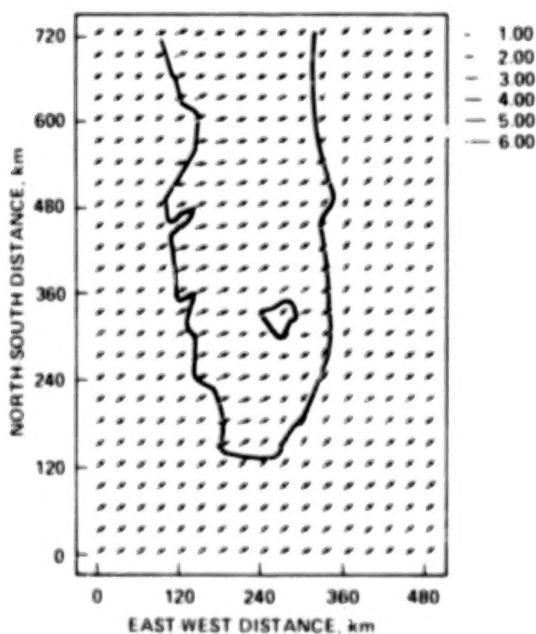
No. of grid points	CPU performance ratio STAR-100/CDC-6600
168	13.5
280	12.3
336	20.3
504	24.4
2800	67.2



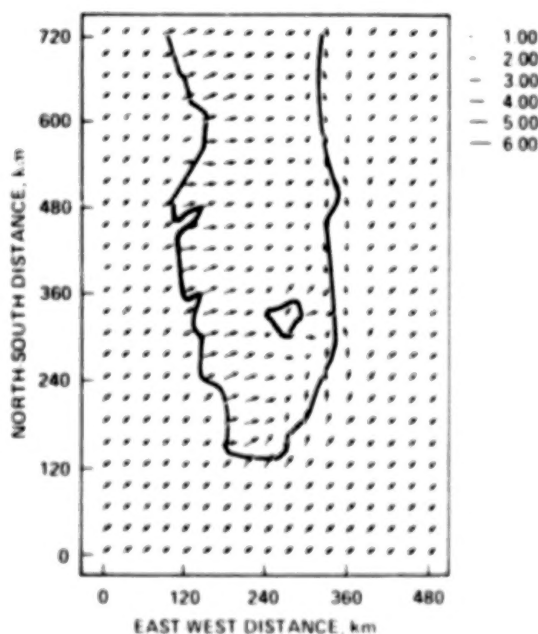
(a) After first hour.



(b) After second hour.

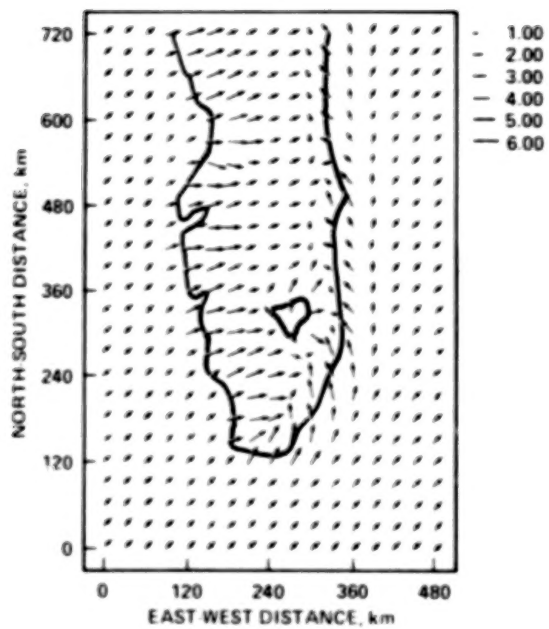


(c) After third hour.

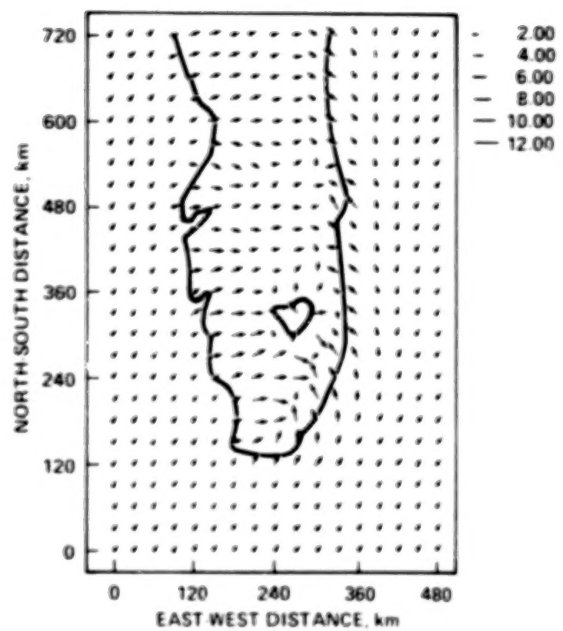


(d) After fourth hour.

Figure 1.- Horizontal wind field for various elapsed times at 50-meter level. Velocity vectors are in meters per second. (Conditions are as follows: undisturbed, neutral, and dry air; initial windspeed of 6 m/sec from southwest at all levels.)

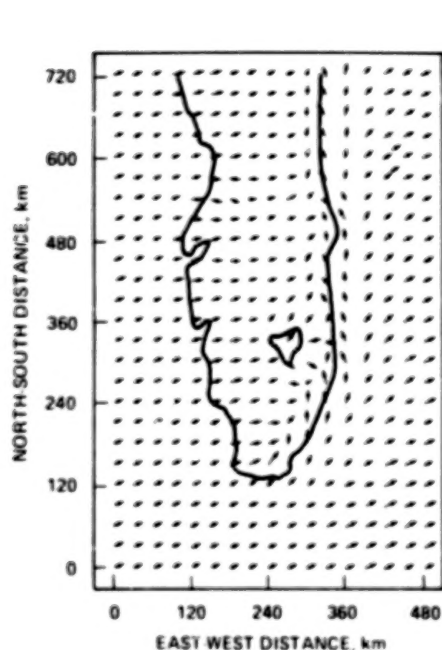


(e) After fifth hour.

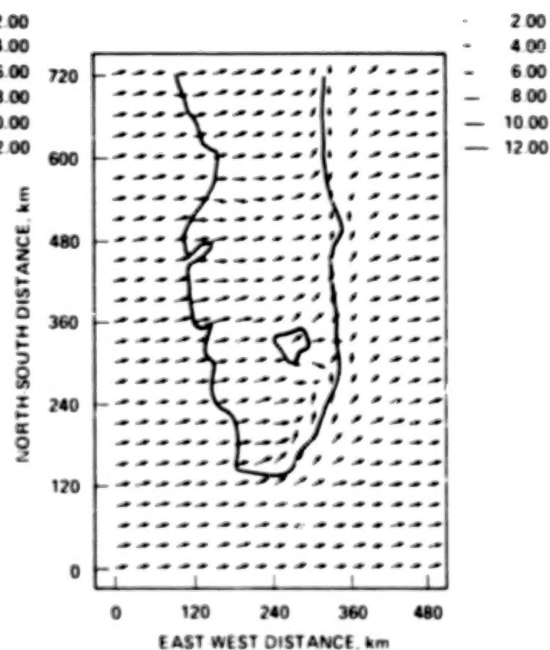


(f) After sixth hour.

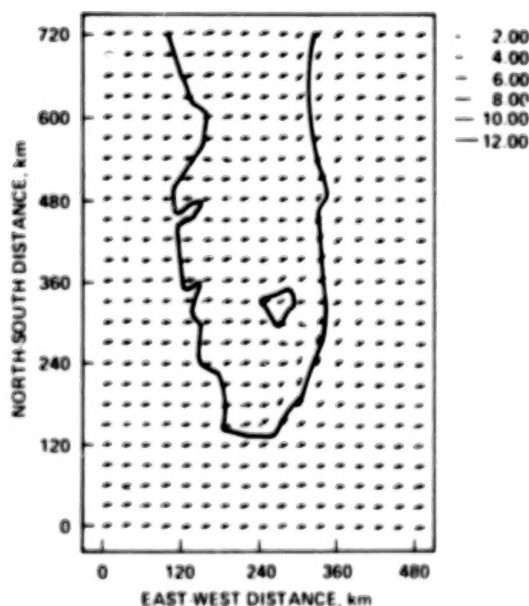
Figure 1.- Concluded.



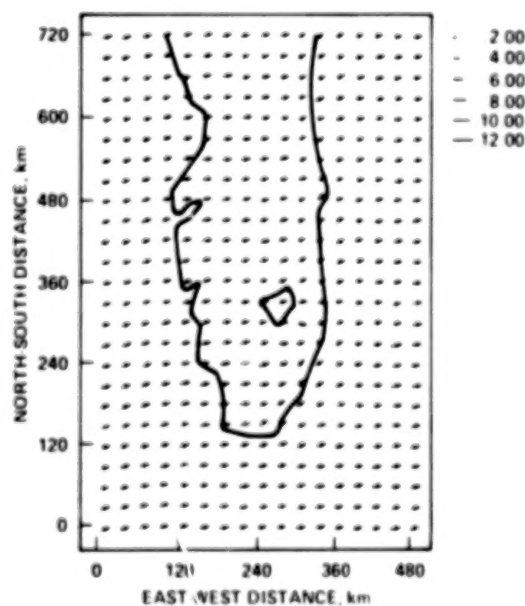
(a) At 200-meter level.



(b) At 450-meter level.

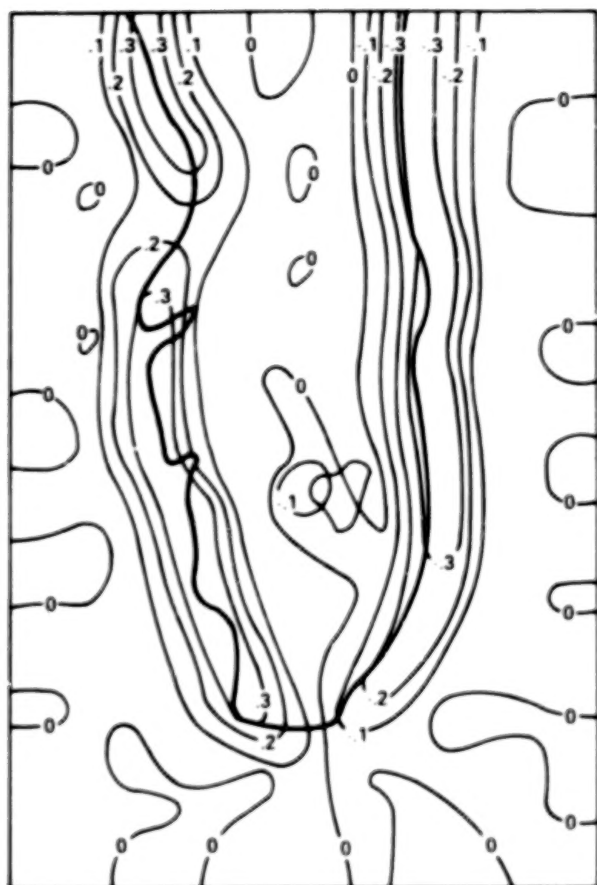


(c) At 800-meter level.



(d) At 1250-meter level.

Figure 2.- Horizontal wind field at various altitudes after sixth hour. Velocity vectors are in meters per second. (Conditions are the same as for fig. 1.)

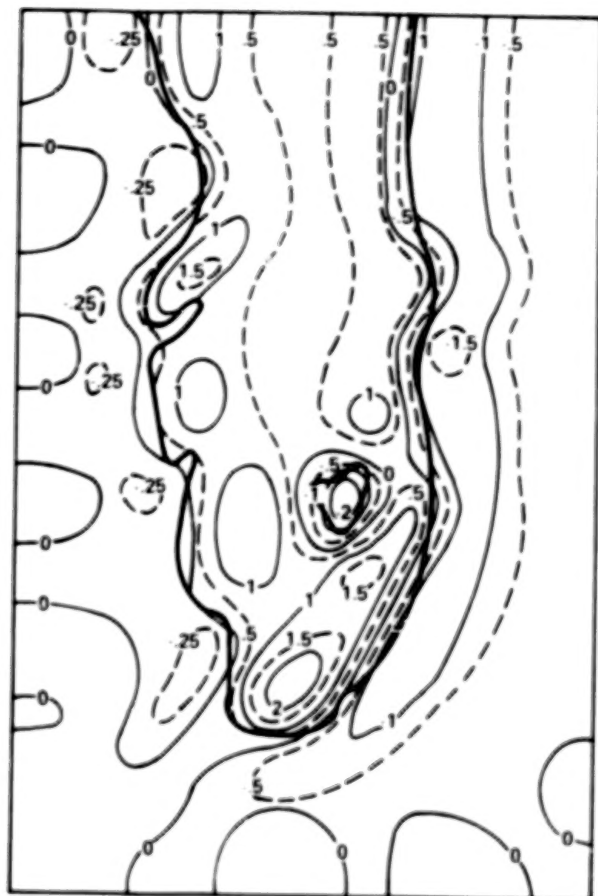


(a) After first hour.



(b) After second hour.

Figure 3.- Distribution of vertical wind velocity (centimeters per second) for various elapsed times at 1250-meter level. (Conditions are the same as for fig. 1.)

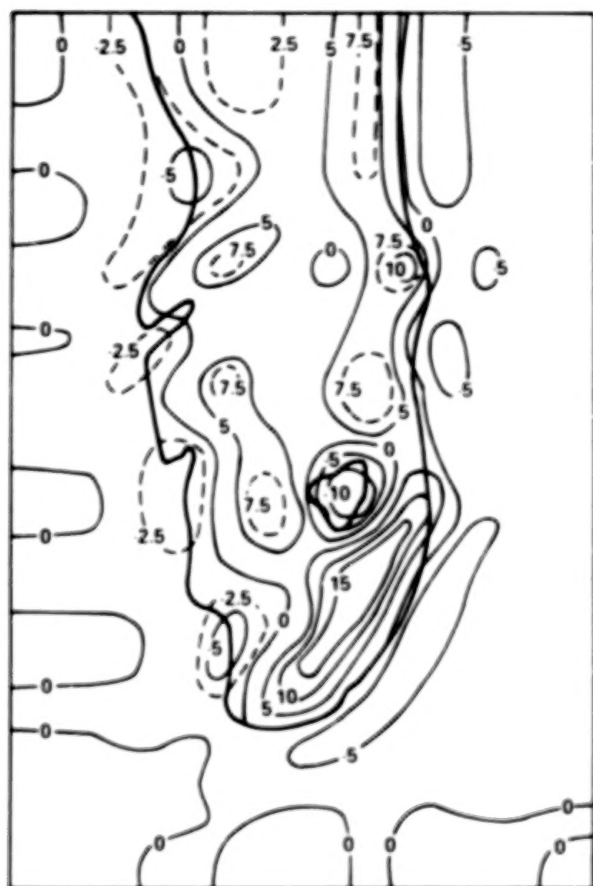


(c) After third hour.



(d) After fourth hour.

Figure 3.- Continued.

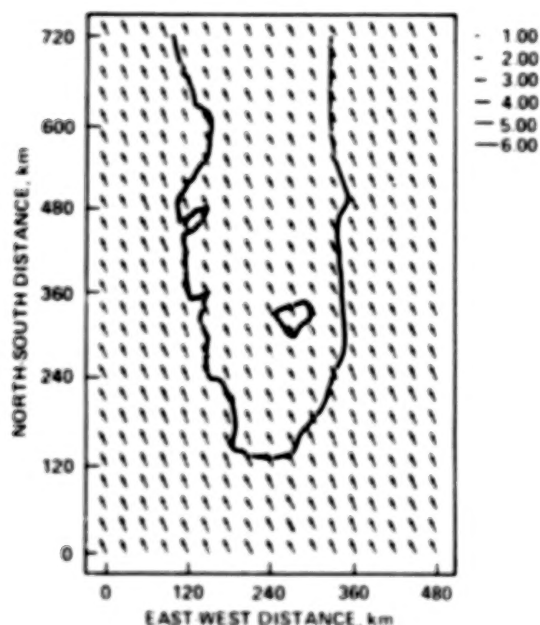


(e) After fifth hour.

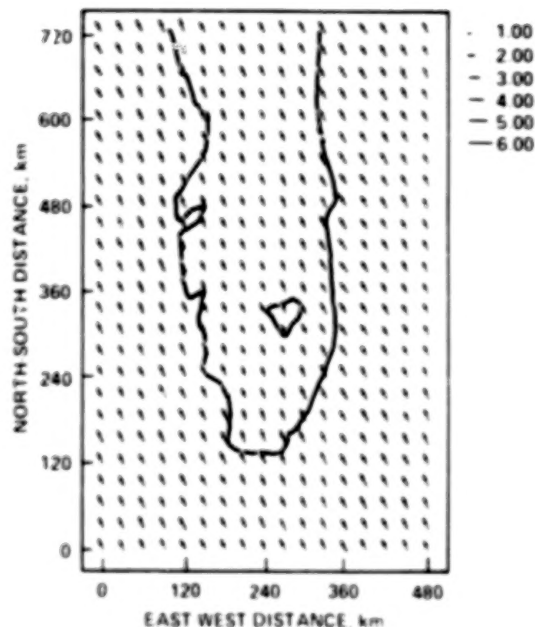


(f) After sixth hour.

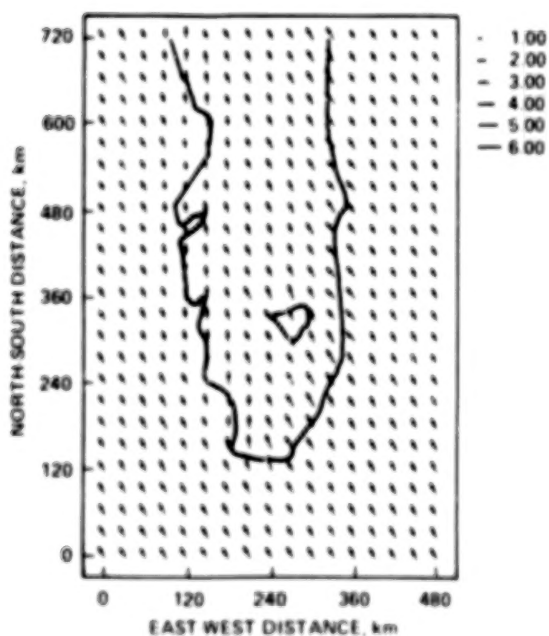
Figure 3.- Concluded.



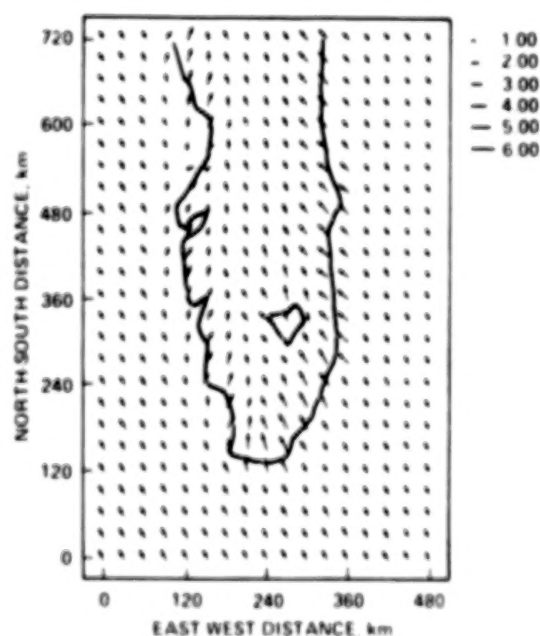
(a) After first hour.



(b) After second hour.

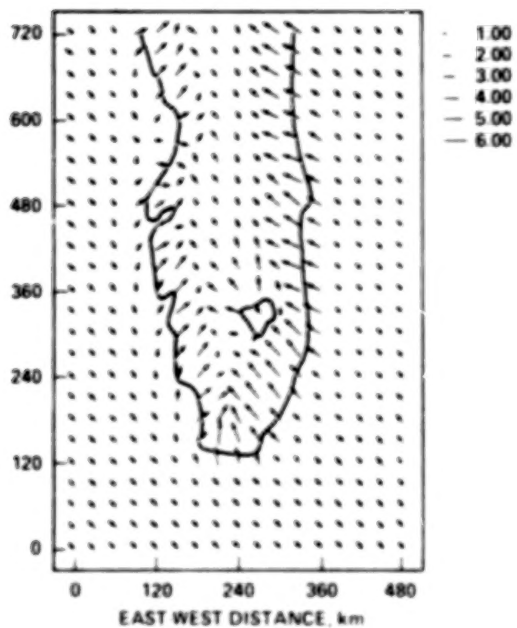


(c) After third hour.

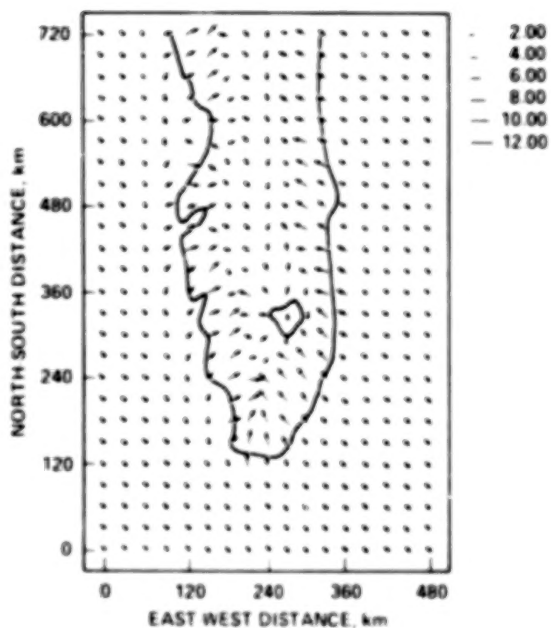


(d) After fourth hour.

Figure 4.- Horizontal wind field for various elapsed times at 50-meter level. Velocity vectors are in meters per second. (Conditions are as follows: undisturbed, neutral, and dry air; initial windspeed of 6 m/sec from southeast at all levels.)

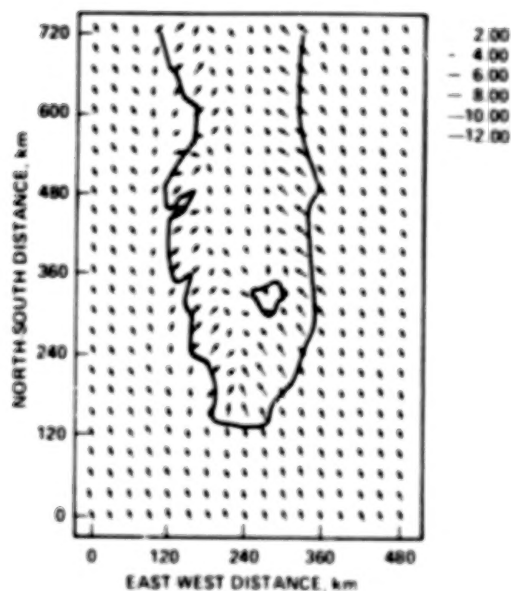


(e) After fifth hour.

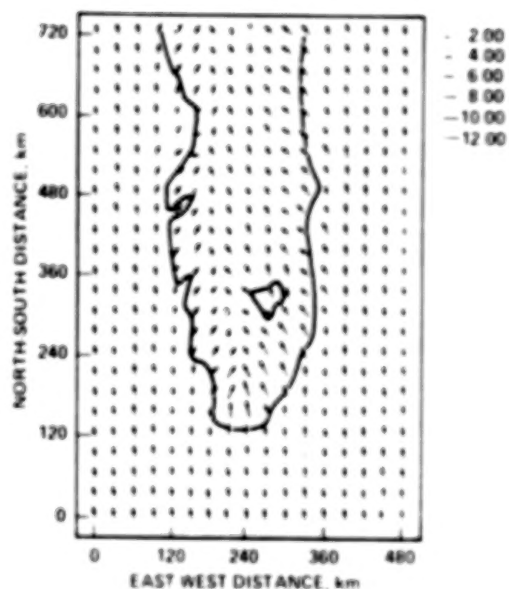


(f) After sixth hour.

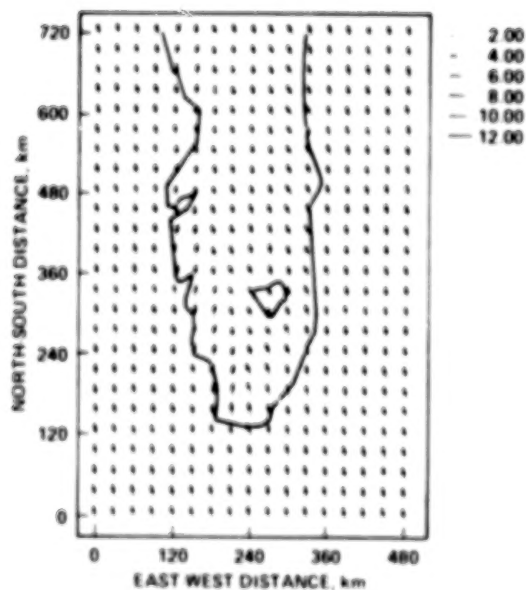
Figure 4.- Concluded.



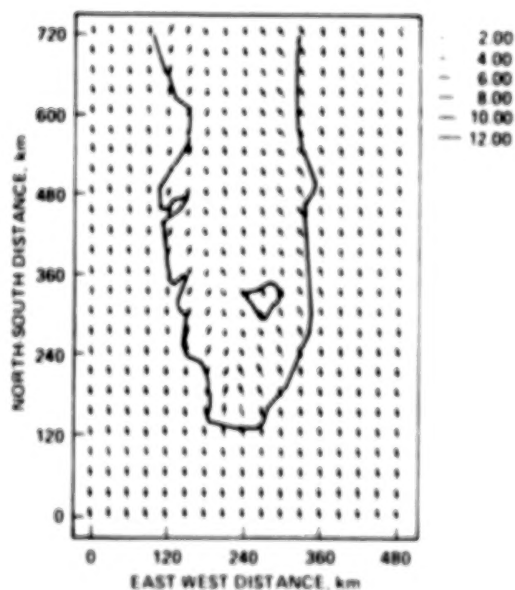
(a) At 200-meter level.



(b) At 450-meter level.



(c) At 800-meter level.



(d) At 1250-meter level.

Figure 5.- Horizontal wind field at various altitudes after sixth hour. Velocity vectors are in meters per second. (Conditions are the same as for fig. 4.)

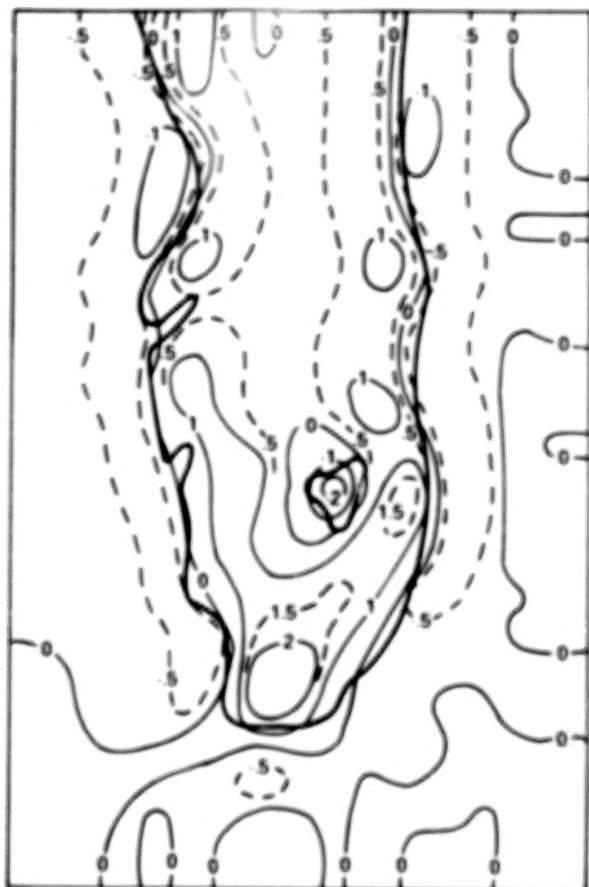


(a) After first hour.

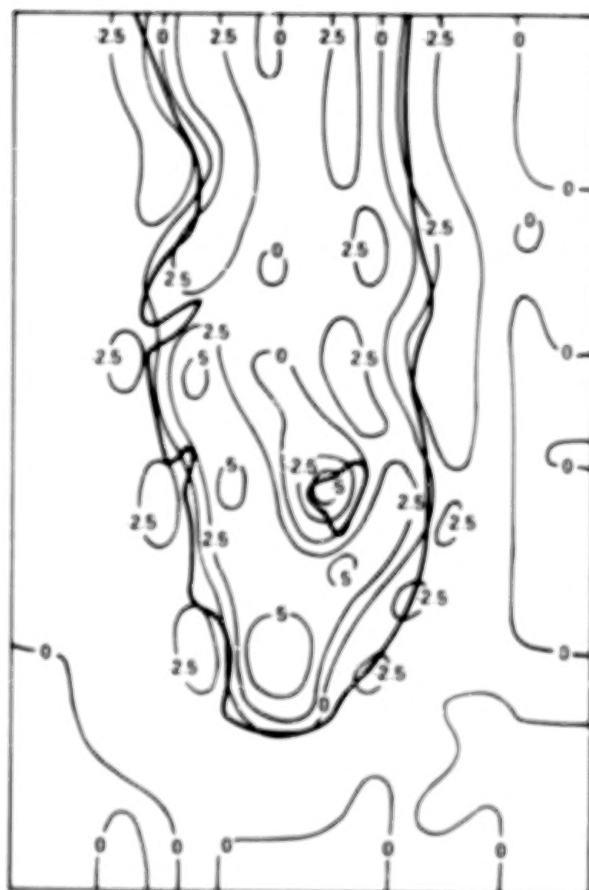


(b) After second hour.

Figure 6.- Distribution of vertical wind velocity (centimeters per second) for various elapsed times at 1250-meter level. (Conditions are the same as for fig. 4.)

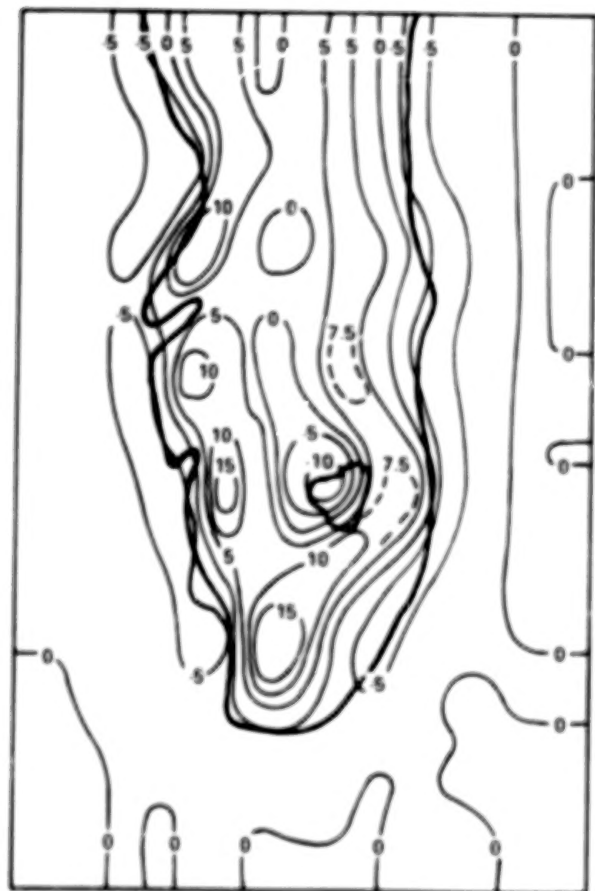


(c) After third hour.

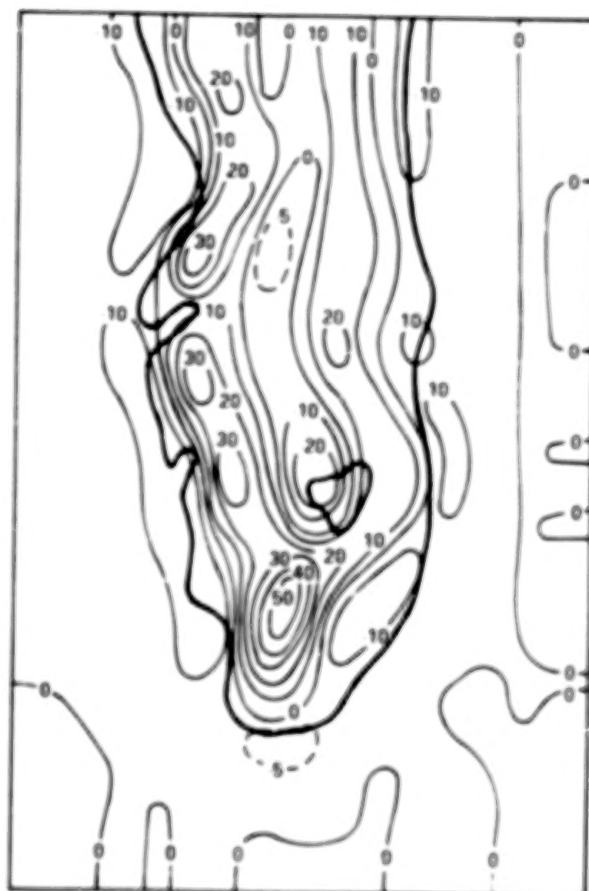


(d) After fourth hour.

Figure 6.- Continued.



(e) After fifth hour.



(f) After sixth hour.

Figure 6.- Concluded.

BLANK PAGE

BLANK PAGE

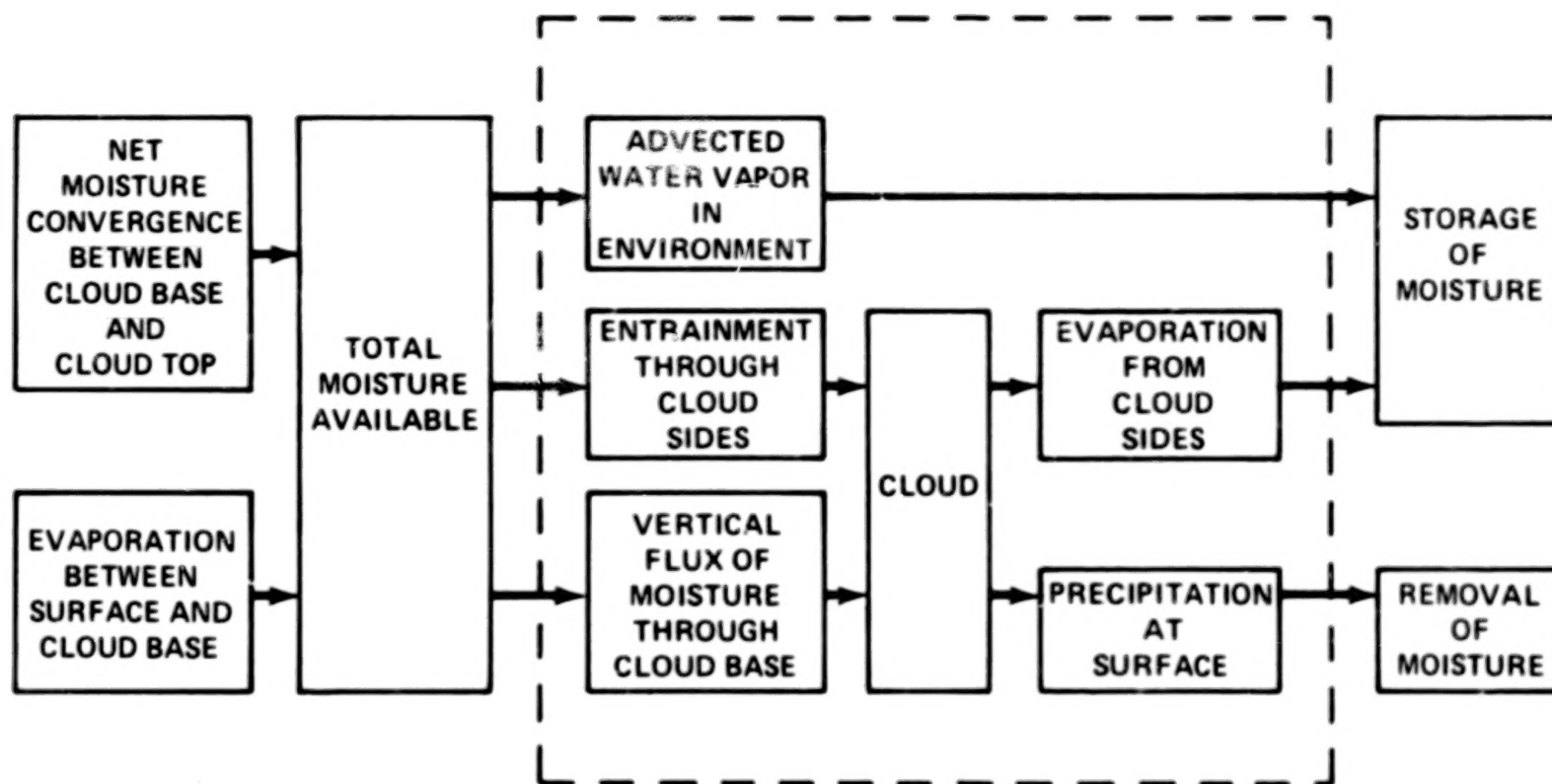


Figure 7.- Parameterization scheme for convective cloud and precipitation in the mesoscale model.

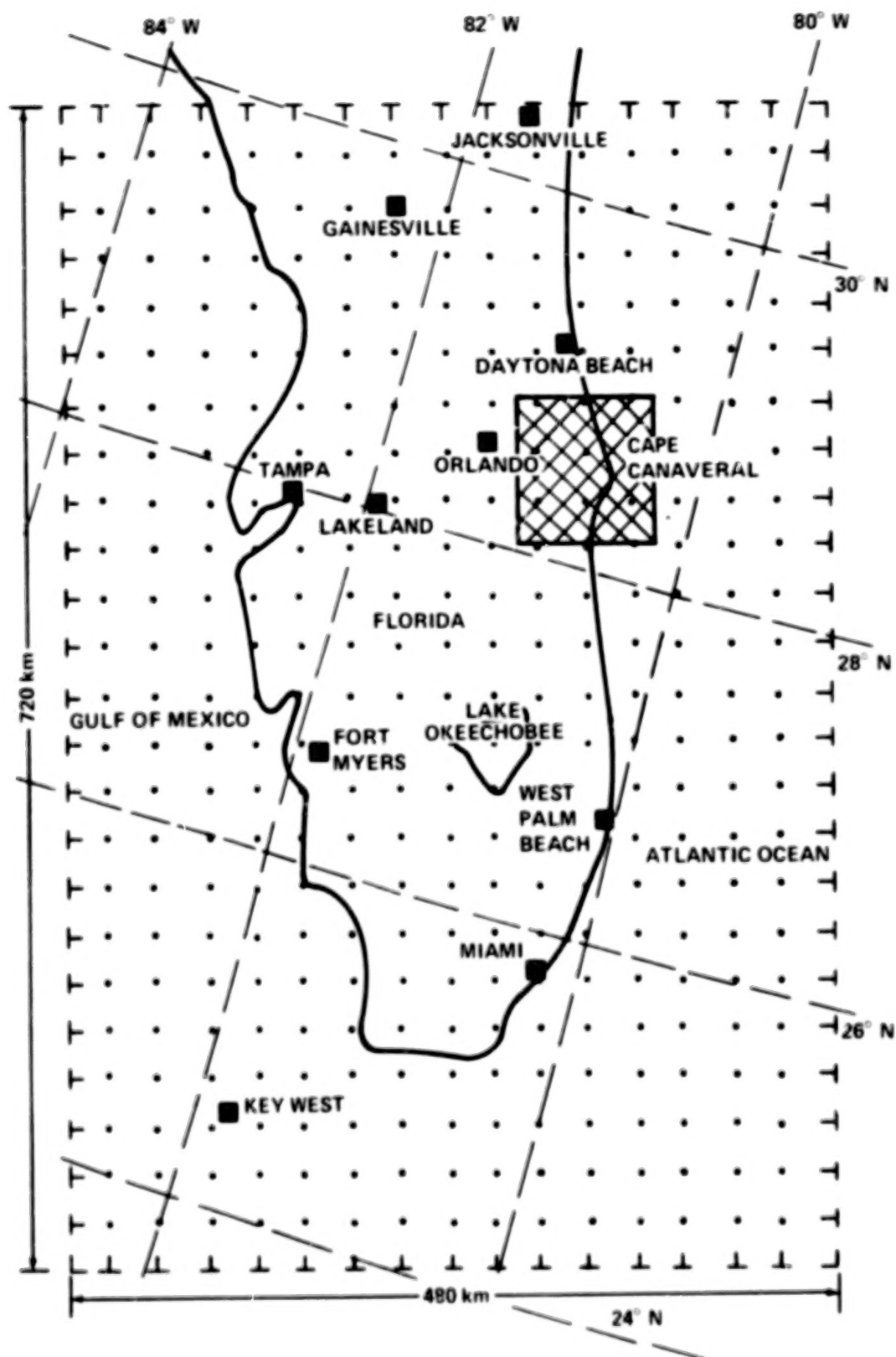


Figure 8.- Map showing the area to be covered by the submesoscale model.

Blank Page

ACID RAIN: MICROPHYSICAL MODEL

By A. N. Dingle*

BASIC EQUATIONS

When HCl and H₂O vapors are present together, they jointly determine the equilibrium vapor pressure of each component over an HCl_{aq} droplet. It is assumed that the two vapors may be treated as if they diffuse independently. Thus, the change of mass of a solution droplet may be expressed as

$$dm_r = dm_1 + dm_2 \quad (1)$$

where the subscripts indicate the respective components; i.e., H₂O and HCl. Then, analogously with equation (1),

$$\frac{dm_1}{dt} = \frac{4\pi r D_1 F v_1 V}{R_1} \left(\frac{e_{a1}}{T_a} - \frac{e_{r1}}{T_r} \right) \quad (2)$$

and

$$\frac{dm_2}{dt} = \frac{4\pi r D_2 F v_2 V}{R_2} \left(\frac{e_{a2}}{T_a} - \frac{e_{r2}}{T_r} \right) \quad (3)$$

The energy balance of the droplet may be expressed by

$$Q_T = Q_L + Q_K + Q_R - Q_r + Q_M + Q_F + Q_D \quad (4)$$

*University of Michigan.

where Q_T , the internal energy increase, is defined as

$$Q_T = m_r c_r \frac{dT_r}{dt}$$

Q_L , the latent energy release, is defined as

$$Q_L = Q_{L_1} + Q_{L_2}$$

$$Q_{L_1} = L_1 (dm_1/dt)$$

$$Q_{L_2} = L_2 (dm_2/dt)$$

Q_K , the conductive heat transfer from drop, is defined as

$$Q_K = -4\pi r K F_K V (T_r - T_a)$$

Q_R , the radiative transfer from drop, is defined as

$$Q_R = -16\pi r^2 \sigma_R E T_a^3 (T_r - T_a)$$

Q_r , the surface increase energy, is defined as

$$Q_r = 4\pi r^2 \left\{ \frac{2\sigma}{3} \left[\frac{1}{m_1} \frac{dm_r}{dt} + \frac{\mu}{\rho_r} \frac{\partial \rho_r}{\partial u} \left(\frac{1}{m_1} \frac{dm_1}{dt} - \frac{1}{m_2} \frac{dm_2}{dt} \right) \right] \right. \\ \left. - \mu \frac{\partial r}{\partial u} \left(\frac{1}{m_1} \frac{dm_1}{dt} - \frac{1}{m_2} \frac{dm_2}{dt} \right) + \frac{dT_r}{dt} \left(\frac{\partial \sigma}{\partial T} - \frac{2\sigma}{3} \frac{1}{\rho_r} \frac{\partial \rho_r}{\partial T} \right) \right\}$$

Q_M , mixing, is defined as

$$Q_M = -c_r (T_r - T_a) \frac{dm_r}{dt}$$

Q_F , frictional conversion, is defined as

$$Q_F = \frac{2r^2 m_r g^2}{9\nu_f} (\rho_r - \rho_a)$$

and Q_D , the heat of dilution, is defined as

$$Q_D = \frac{\nu}{m_r} \frac{dh}{d\nu} \frac{dm_r}{dt}$$

A detailed discussion of the energy terms is given in reference 1 and need not be repeated here. A study of the relative magnitudes of these terms for different sizes of droplets of 4.0 molal HCl_{aq} in a 1-m/sec updraft (table I) shows that only Q_F is definitely negligible in the cloud droplet size range. This allows simplification of equation (4) to

$$Q_T = Q_L + Q_K + Q_R - Q_r + Q_M + Q_D \quad (5)$$

By means of the definitive expressions, the droplet temperature elevation may be written as

$$(T_r - T_a) = \left\{ \frac{(Q_L + Q_D - Q_T - Q_r)}{\left[4\pi r (K_F K_V + 4r\sigma_R E T_a^3) + c_r \frac{dm_r}{dt} \right]} \right\} \quad (6)$$

In addition, for each time step, the mass conservation accounts are kept. Assuming that there is no dilution of the air parcel by turbulent mixing with environmental air,

$$\frac{dx_1}{dt} = - \sum_i n_i \left(\frac{dm_1}{dt} \right)_i \quad (7)$$

$$\frac{dx_2}{dt} = - \sum_i n_i \left(\frac{dm_2}{dt} \right)_i \quad (8)$$

The environmental temperature and pressure changes from one time step to another are given by

$$\frac{dp}{dt} = -w_a \left(g + \frac{dw}{dt} \right) \quad (9)$$

and

$$\frac{dT_a}{dt} = - \frac{\left[L_1 \frac{dx_1}{dt} + L_2 \frac{dx_2}{dt} + \left(g + \frac{dw}{dt} \right) \frac{dz}{dt} (1 + x_1 + x_2) \right]}{c_p + x_1 c_{p1} + x_2 c_{p2} + \sum_i (m_r c_r)_i n_i} \quad (10)$$

where the summation in the denominator represents the heat capacity of the liquid carried with the rising air parcel. Equations (2), (3), and (6) for each droplet size category and equations (7), (8), (9), and (10) constitute the explicit model for two volatile components.

NUMERICAL INTEGRATION TECHNIQUES

The numerical technique used for the integration of the microphysical equations is Hamming's modified predictor-corrector method started by a Rungë-Kutta procedure. This method has been described in reference 1 and is given in reference 2. At present, there are $2n + 2$ first-order ordinary differential equations to be solved simultaneously, where n is the number of droplet size classes. In terms of the variables used in reference 2, y'_1 through y'_n are the derivatives with respect to time of the mass of water in a droplet in a specific size class:

$$y'_1 \Big|_1^n = \frac{dm_1}{dt} \Big|_1$$

$$= \frac{4\pi r D_1 F_{v1} V}{R_1} \left(\frac{e_{a1}}{T_a} - \frac{e_{r1}}{T_r} \right)$$

y'_{n+1} through y'_{2n} are the derivatives with respect to time of the HCl mass of a droplet in a specific size class:

$$y'_1 \Big|_{n+1}^{2n} = \frac{dm_2}{dt} \Big|_1$$

$$= \frac{4\pi r D_2 F_{v2} V}{R_2} \left(\frac{e_{a2}}{T_a} - \frac{e_{r2}}{T_r} \right)$$

y'_{2n+1} is the derivative with respect to time of cloud air temperature:

$$y'_{2n+1} = \frac{dT_a}{dt} = \frac{L_1 \frac{dx_1}{dt} + L_2 \frac{dx_2}{dt} + \left(g + \frac{dw}{dt}\right) \frac{dz}{dt} (1 + x_1 + x_2)}{c_p + x_1 c_{p1} + x_2 c_{p2} + \sum (m_r c_r)_i n_i} \quad (11)$$

where n_i in the denominator on the right-hand side of equation (11) refers not to the number of size classes but to the number of droplets in size class i and where y'_{2n+2} is the derivative with respect to time of the cloud air pressure:

$$y'_{2n+2} = \frac{dp}{dt} = - \left(\rho_a g \frac{dz}{dt} + \rho_a \frac{dz}{dt} \frac{d^2 z}{dt^2} \right)$$

The droplet distribution is initialized by assuming a starting pressure or height ($y_{2n+2}(0)$), temperature ($y_{2n+1}(0)$), relative humidity, and vapor pressure of HCl of the center of the cloud. The small droplets are assumed to be in equilibrium with the environment and the large droplets near equilibrium. Under these assumptions, the mass of H_2O ($y_1(0) + y_n(0)$) and mass of HCl ($y_{n+1}(0) + y_{2n}(0)$) on each droplet are determined. Integration of the microphysical equations now begins.

One of the benefits of the Hamming method is the fact that the local truncation error (LTE) is calculated at each increment of integration or time step and can be used to modify this time step. If the sum of the LTE's for each equation exceeds a given tolerance limit specified by the user, a new time step that is one-half the length of the previous time step is selected and the integration is restarted at the last accepted integrated values. This halving of the time step continues until the new values are within the error limit or until the number of halvings exceeds a specified limit. If the sum of LTE's is between the tolerance limit and one-fiftieth of the given tolerance limit, the calculated values are accepted and integration continues. Finally, if the sum of the LTE's is less than one-fiftieth of the given tolerance limit, the

calculated values are accepted, the time step is doubled, and the integration continues. With this time step adjustment, the integration is more accurate and efficient than if a fixed time step were used.

A computational instability was encountered during the integration of the microphysical equations. Some droplets were found to fluctuate wildly about their equilibrium values. The vapor pressures of HCl and H₂O in the environment may not equal the equilibrium vapor pressures at the droplet surface which are a function of temperature, molality, and radius. The existence of a vapor gradient allows the molality of HCl or H₂O (or both) independently of each other. The consequent condensation/evaporation of vapors may overcompensate the change in molality necessary for the droplet to reach equilibrium with the environment. The overcompensation of molality causes the vapor gradient to change sign, and during the next step, growth is in the opposite direction. To correct for the resultant instability or oscillation of the droplets about their equilibrium, the following scheme was developed.

Consider, for the moment, one diffusing vapor. The vapor difference at the droplet surface is some value B:

$$B = e_a - e_r$$

If the droplet goes to equilibrium, B goes to zero. The change of vapor difference for a droplet that goes to equilibrium during the time step is

$$B = - \left[(e_a - e_r)^{(t+\Delta t)} - (e_a - e_r)^{(t)} \right]$$

Grouping terms, one obtains

$$\left. \begin{aligned} B &= - \left[\frac{d}{dt} (e_a) \Delta t - (e_r^{(t+\Delta t)} - e_r^{(t)}) \right] \\ \Delta e &= B + d/dt (e_a) \Delta t \end{aligned} \right\} \quad (12)$$

The vapor gradient is not allowed to collapse far beyond zero in a time step. Therefore, the change in vapor pressure Δe defines the maximum allowable change in vapor pressure. The maximum change in vapor pressure can then be used to find the maximum allowable change in droplet molality during a time step. The derivation of the maximum change in molality follows.

The vapor pressure to a droplet can be expressed as a function of droplet molality, temperature, and radius.

$$e = f(\mu, T, r)$$

Differentiating, one finds that

$$de = \frac{\partial e}{\partial \mu} d\mu + \frac{\partial e}{\partial T} dT + \frac{\partial e}{\partial r} dr \quad (13)$$

Having the equations for the vapor pressure of each component over a flat solution as a function of T and μ (ref. 1), it is an easy matter to differentiate and find that

$$\left. \frac{\partial e}{\partial \mu} \right|_{T, r} = A \quad (14a)$$

and

$$\left. \frac{\partial e}{\partial T} \right|_{\mu, r} = F \quad (14b)$$

Now, for a droplet of radius r , the vapor pressure at the surface is

$$\begin{aligned} e_r &= e_{r=\infty} \exp\left(\frac{2\sigma}{\rho r R_v T}\right) \\ &= e_{r=\infty}^k \end{aligned}$$

Then,

$$\begin{aligned}\left. \frac{\partial e}{\partial r} \right|_{T,u} &= e_r \left(\frac{-2\sigma}{\rho r^2 R_v T} \right) \\ &= -e_r \frac{k}{r}\end{aligned}$$

Transforming $dr \rightarrow dm$, one obtains

$$\begin{aligned}\left. \frac{\partial e}{\partial r} \right|_{T,u} dr &= -e_r \frac{k}{r} \frac{dm}{4\pi \rho r^2} \\ &= G dm\end{aligned}\tag{14c}$$

Substituting equations (14a), (14b), and (14c) into equation (13) yields

$$de = A du + F dT + G dm$$

and in finite difference form,

$$\begin{aligned}\Delta e &= A \Delta u + F \Delta T + G \Delta m \\ &= B + \frac{de}{dt} \Delta T\end{aligned}\tag{15}$$

From the definition of molality, one finds that

$$\Delta u = -\frac{u}{m_1} \Delta m_1 + \frac{u}{m_2} \Delta m_2$$

where m_1 is the solvent and m_2 is the solute.

The relative growth rate (dm_2/dm_1) can be determined from the growth equations (2) and (3):

$$\frac{dm_2}{dm_1} = \frac{\left(\frac{dm_2}{dt}\right)}{\left(\frac{dm_1}{dt}\right)}$$

Then,

$$\Delta u = v \left(\frac{1}{m_1} + \frac{1}{m_2} \frac{dm_2}{dm_1} \right) \Delta m_1 \quad (16)$$

Substituting equation (16) into equation (15) and solving for Δu ,

$$\Delta u = \frac{B + \frac{d}{dt} (e_a) \Delta t - F \Delta T}{A + \frac{G}{v \left(-\frac{1}{m_1} + \frac{1}{m_2} \frac{dm_2}{dm_1} \right)}} \quad (17)$$

where $d(e_a)/dt$ and dT_a/dt are estimated by backward differencing. Then,

$$F \Delta T = F \frac{dT_a}{dt} \Delta t$$

The maximum allowable change of molality determined from equation (17), Δu_1 , applies to the solvent. Similar calculations for the solute result in another value, Δu_2 . With the smaller value of the two, the maximum allowable values of Δm_1 and Δm_2 can be found in equation (16). This method is approximate.

However, one would not want to prevent the droplet from crossing the equilibrium line when the natural process is to do so. If the growth of the droplets becomes unstable, it will fluctuate wildly across the equilibrium line. Therefore, a domain about the equilibrium line is defined. If the droplet tends to grow and/or evaporate quickly outside that domain, it is assumed that there is a numerical instability. For the current computation, if the change of mass of either component computed by the numerical integration is less than three times the maximum allowable change estimated above, the integrated value is assumed correct. In practice, the factor of 3 is quite arbitrary; however, it is found that the ratio of calculated Δm to the estimated maximum allowable Δm is either $\ll 1$ or $\gg 10$. If the droplet growth is constrained in this manner, after the first few seconds on integration, only the two smallest size classes need adjustment and the model is stable.

RESULTS

To assess the situation in which droplet growth should be most favored, the microphysical model has been used to simulate the case of a ground cloud (GC) without dilution by entrainment and without precipitation. The updraft speeds used (table II) were chosen to approximate the observed behavior of several Titan ground clouds (ref. 3) as shown in figure 1. Thus, in this case, the GC reaches a height of 1000 meters at $t = 250$ seconds and stops rising after $t = 500$ seconds at a level of 1500 meters.

The initial GC temperature (at $t = 90$ seconds) is set at 25°C , and the initial HCl vapor pressure is 3.8 dyn/cm^2 , corresponding to a concentration of 4 p/m at the 950-millibar level. The dry particle distribution was taken from the suggestion of Lala (ref. 4). It is a bimodal distribution of the following form.

$$\frac{dN}{d \log r} = \sum_{i=1}^2 \frac{N_i \ln 10}{\sqrt{2\pi} \ln^2 \sigma_{gi}} \exp \left[- \frac{(\ln r - \ln r_{gi})^2}{2 \ln^2 \sigma_{gi}} \right]$$

The various parameters suggested by Lala (ref. 4) are as follows.

$$N_2 = N_1 / 8000$$

$$\sum_{r=0.01}^{10} N = 1.5 \times 10^4 \text{ particles/cm}^3$$

$$\sigma_{g1} = \sigma_{g2}$$

$$= 2.0 \text{ micrometers}$$

$$r_{g1} = 0.05 \text{ micrometer}$$

$$r_{g2} = 1.0 \text{ micrometer}$$

The distribution is plotted in figure 2.

The course of the relative humidity H for the period 90 seconds $\leq t \leq 720$ seconds is shown in figure 3 for initial humidity values of 80, 90, and 100 percent. The effect of rapid initial droplet growth in the 100-percent case is to reduce the initial humidity quickly to a minimum of 98 percent at $t = 99$ seconds and then, with continued rising and cooling of the cloud, to approach the nearly constant value of 99.7 percent after 200 seconds. The asymptotic humidity value decreases by about 0.1-percent steps to the 90- and 80-percent cases.

Figure 4 shows the course of the HCl vapor pressure. It is reduced to 10^{-3} dyn/cm² at about $t = 300$ seconds for the 100-percent case, about 100 seconds later for the 90-percent case, and not until $t \approx 500$ seconds for the 80-percent case. The droplet molalities decrease to 0.1 at $t = 225, 300,$ and 500 seconds for the 100-, 90-, and 80-percent cases, respectively (fig. 5).

The droplet-size spectra after 720 seconds are shown in figure 6. The outstanding feature of this set of results is the enhancement of the growth of the largest droplets as the initial humidity is lowered. The curves are truncated at 7 micrometers, although the largest drops formed exceed 20 micrometers in radius. These are, however, very few in number. The bifurcation in the 100-percent relative humidity size distribution curve is an artifact produced in this case by the mechanics of calculating dN/dr . The equivalent cloud liquid water content figures at 720 seconds are, respectively, 2.8, 2.1, and 1.6 g/m³ with mean droplet radii of 3.8, 3.75, and 3.4 micrometers.

An additional result of this study is that the droplet molalities are nearly constant across the size distribution at each value of t , a fact which will be helpful in parameterizing the microphysical processes for the submesoscale dynamic model. A summary of results at $t = 720$ seconds is given in table III.

REFERENCES

1. Dingle, A. N.: Rain Scavenging of Solid Rocket Exhaust Clouds. NASA CR-2928, 1978.
2. System/360 Scientific Subroutine Package (360A-CM-03X) Version 3 Programmer's Manual. International Business Machines Corp., Technical Publications Dept. H20-0205-3 (White Plains, N.Y.), 1970, p. 545.
3. Stephens, J. B.; and Stewart, R.: Rocket Exhaust Effluent Modeling for Tropospheric Air Quality and Environmental Assessments: Preliminary Report for NASA Space Shuttle Tropospheric Environmental Effects Meeting, Langley Research Center (Hampton, Va. 24026), Feb. 1975.
4. Lala, G. G.: First draft for Position Paper on the Potential of Inadvertent Weather Modification of the Florida Peninsula Resulting From Neutralization of Space Shuttle Solid Rocket Booster Exhaust Clouds, by E. Ballay, L. Bosart, E. Droessler, J. Jiusto, G. G. Lala, V. Mohnen, V. Schaefer, and P. Squires. Prepared for NASA Langley Research Center by Institute of Man and Science (Rensselaerville, N.Y.), Feb. 1978.

TABLE I.- ESTIMATES OF THE ENERGY TERMS

[In relation to Q_T for the HCl/H₂O system at $\mu = 4$]

Energy term	$r = 0.1 \mu\text{m}$	$r = 1.0 \mu\text{m}$	$r = 10 \mu\text{m}$
Q_L/Q_T ($\approx Q_R/Q_T$)	1.46×10^4	4.28×10^4	1.95×10^3
Q_R/Q_T ($E = 1$)	.92	9.7	3.7
Q_T/Q_T	8.9	2.6	.012
Q_μ/Q_T	.006	1.05	.24
Q_F/Q_T	8×10^{-15}	1.2×10^{-12}	1.2×10^{-10}
Q_p/Q_T	94	276	13

TABLE II.- UPDRAFT SPEEDS AND HEIGHTS FOR
STABILIZED GROUND CLOUD

Time, sec	Updraft speed, m/sec	Height, m
90 to 250	4	360 to 1000
250 to 500	2	1000 to 1500
500 to 720	0	1500

TABLE III.- VARIABLES AT TIME = 720 SECONDS

Variable	Initial Humidity, percent		
	80	90	100
Temperature, K	290.99	292.45	293.73
Relative humidity, percent . . .	99.59	99.65	99.70
HCl vapor pressure, dyn/cm ² . . .	0.001	0.001	0.001
Droplet molality	0.09	0.07	0.05
Liquid water content, g/m ³ . . .	1.56	2.14	2.80
Mean radius, μm	3.40	3.74	3.79
Standard deviation, μm	0.45	0.62	0.31
Largest droplet, μm	19.56	20.91	17.04

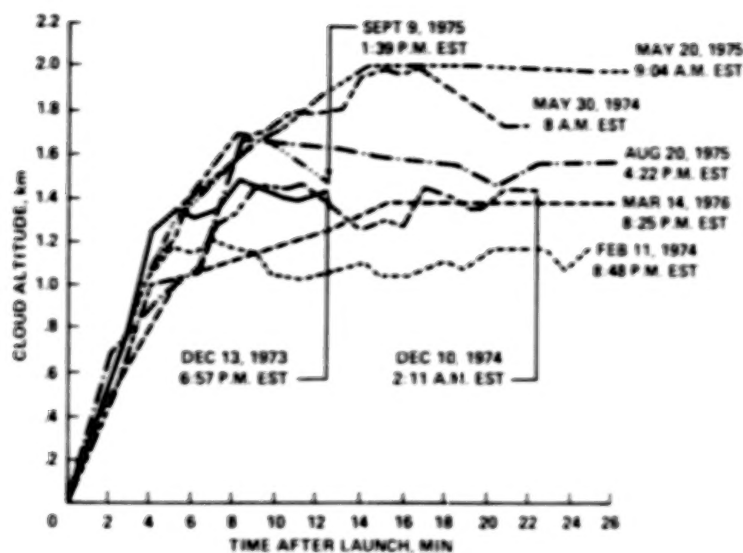


Figure 1.- Cloud rise and stabilization heights in eight Titan III launches.

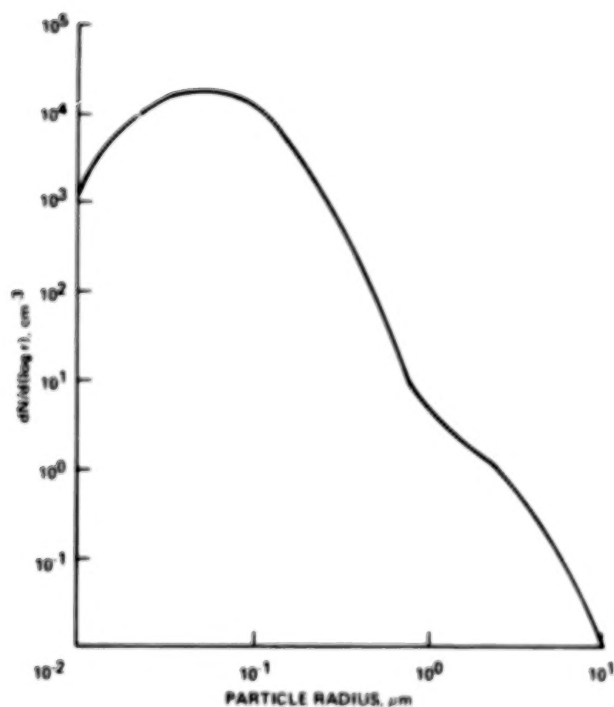


Figure 2.- Particle size distribution of Al₂O₃ in the ground cloud (after ref. 4).

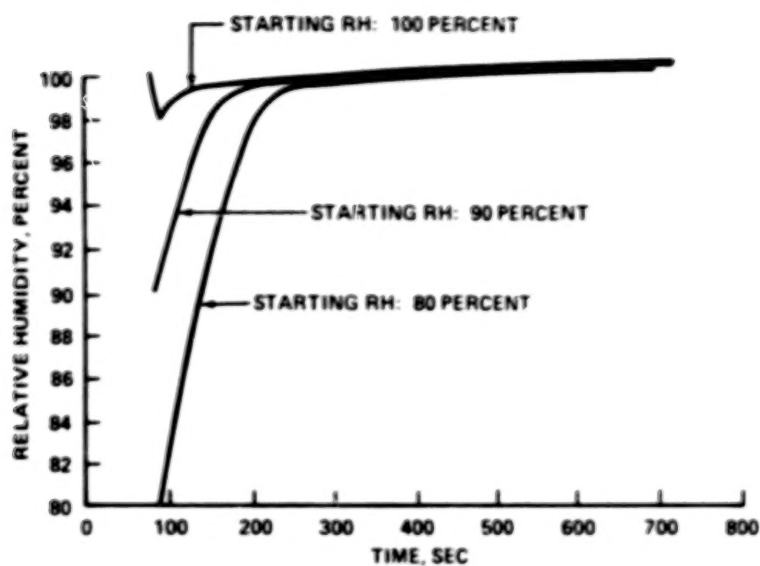


Figure 3.- Course of the relative humidity from $t = 90$ seconds to $t = 720$ seconds for initial humidity values of 80, 90, and 100 percent.

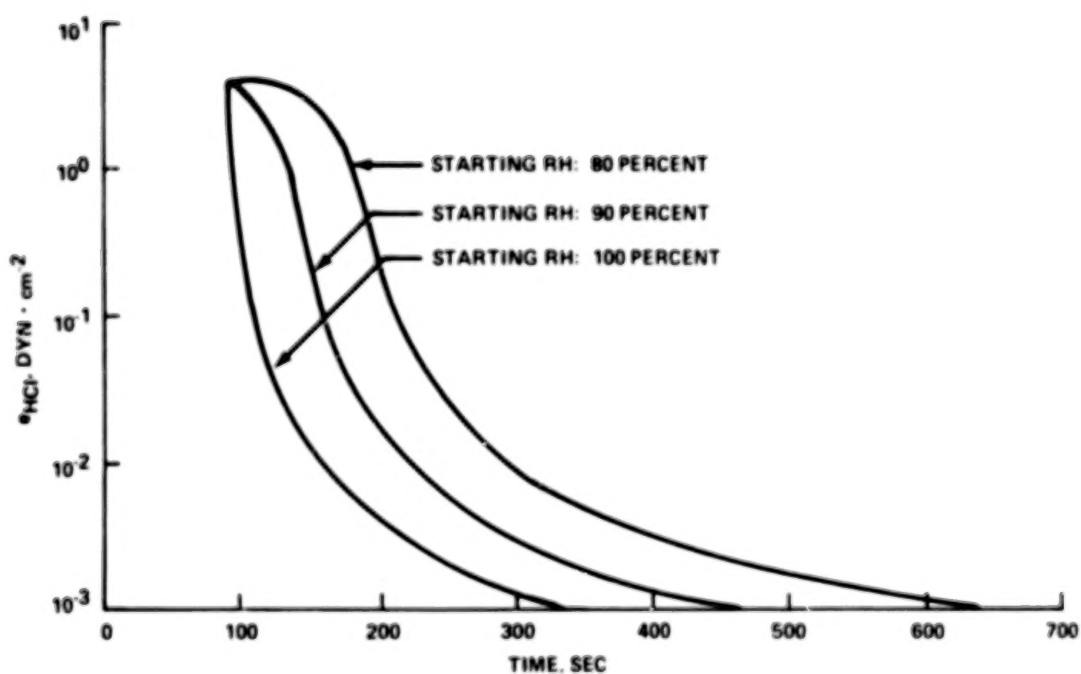


Figure 4.- Course of the HCl vapor pressure.

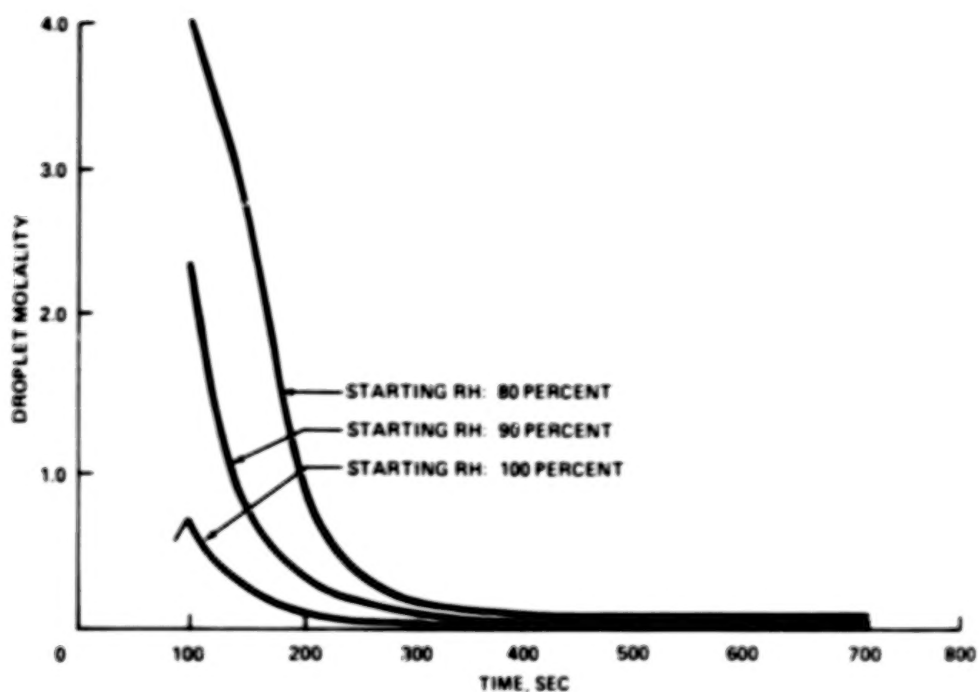


Figure 5.- Change of droplet molality with time.

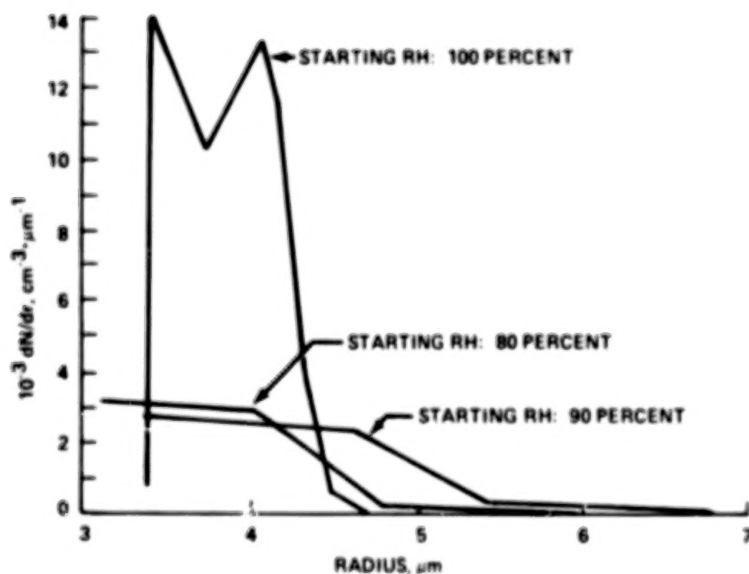


Figure 6.- Droplet-size spectra after 720 seconds (truncated at $r = 7$ micrometers).

SHUTTLE INADVERTENT WEATHER MODIFICATION EFFECTS

By G. Lala*

ABSTRACT

A group of meteorologists at the State University of New York at Albany have analyzed the inadvertent weather modification aspects of the Space Shuttle exhaust cloud. Two studies were involved: a study of weather modification by normal launch clouds and a study of weather modification assuming that the HCl in the cloud was neutralized. In some respects, the conclusions of these two studies are not much different. The area in which weather modification might be expected is precipitation - both the warm rain process and the cold rain process. Some influence on these precipitation mechanisms for as long as perhaps 3 days might be expected. Neutralization of the cloud makes the weather modification a little more likely; the times seem to be expanded by about 1 day when neutralization occurs. It is difficult to make a definite prediction because it is not known exactly what the cloud would be like. Until good cloud measurements are available, it will be difficult to ascertain the effects. The question of how the modification is defined is very important. Weather modification in this context refers to the region occupied by the exhaust cloud. If weather modifications are measured with a rain gage network and the climatic data on rain gages are studied, no indication of weather modification would be seen.

*State University of New York at Albany.

Blank Page

RESPONSE OF SELECTED PLANT AND INSECT SPECIES TO SIMULATED SRM EXHAUST MIXTURES AND TO EXHAUST COMPONENTS FROM SRM FUELS

By Walter W. Heck*

INTRODUCTION

This research was developed to determine possible biologic effects of exhaust products from solid rocket motor (SRM) burns associated with the Space Shuttle. The major components of the exhaust that might have an adverse effect on vegetation are HCl and Al_2O_3 . It is possible that Cl_2 and NO_2 may be sufficiently important to deserve study.

The basic objective of this research is to determine dose-response curves for native and cultivated plants and selected insects exposed to simulated exhaust and component chemicals from SRM exhaust. Specific objectives are (1) to develop a system for dispensing and monitoring component chemicals of SRM exhaust (HCl and Al_2O_3); (2) to develop a system for exposing test plants to simulated SRM exhaust (controlled fuel burns); (3) to determine dose-response curves for single and multiple acute exposures of selected plant species to HCl, Al_2O_3 , mixtures of the two, and simulated exhaust; (4) to work closely with the NASA John F. Kennedy Space Center and the staff of the Florida Technological University in Orlando, Florida, in the development of native and cultivated plant species for use in exposures and for possible later use in vegetation monitoring systems; (5) to determine the effects of HCl, Al_2O_3 , and mixtures of the two on the honeybee, the corn earworm, and the common lacewing; and (6) to determine the effects of simulated exhaust on the honeybee.

Personnel involved in the study included the following senior staff members.

1. Dr. John T. Ambrose, entomologist and bee specialist of North Carolina State University (NCSU), who is serving as a consultant and organized the study on the honeybee, the corn earworm, and the common lacewing
2. Dr. A. S. Heagle, plant pathologist with the U.S. Department of Agriculture, who is primarily responsible for the field program and is the project officer for the precipitation project that started in February 1978
3. Dr. W. M. Knott, ecologist and plant physiologist with NCSU, who was primarily responsible for the work on the effects of the gases and particulates on vegetation

*U.S. Department of Agriculture.

4. Dr. E. P. Stahel, chemical engineer with NCSU, who was the principal consultant in the development of the facilities presently in use

Four graduate students worked on this project.

1. Louise A. Romanow, working toward a Master of Science degree in entomology, who was responsible for the insect studies

2. Alan G. Sawyer, working toward a Master of Science degree in chemical engineering, who was primarily responsible for working with Dr. Stahel in the original development of the facilities

3. James D. Tyson, working toward a Master of Science degree in chemical engineering, who studied the chemical characterization of the test chambers

4. Madeleine Engel, working toward a Master of Science degree in plant pathology, who characterized the uptake and localization of chlorine in plant tissues

FACILITIES DEVELOPMENT

The primary objective of the facilities development phase of the project was to develop systems for dispensing and monitoring HCl and the Al_2O_3 particulates and for dispensing and monitoring the exhaust products from a solid propellant burn. The three facilities include the HCl exposure system, the Al_2O_3 particle system, and the exhaust system. Figure 1 is a schematic of the four greenhouse chambers used for HCl and particulate exposures, and figure 2 shows details of a single chamber. Charcoal filtration of the air occurs upstream of the inlet manifold. The gases are injected into each chamber's inlet duct. The impeller stirs the air within the reactor; the impeller permits variation of airflow into the chamber without changing the rate of air movement within the chamber. High-intensity lamps are used over each chamber because the plants have a minimum light intensity threshold for response to pollutants; the plants are insensitive in the dark. With the high-intensity lamps, research in the greenhouse can continue all 12 months of the year. The gas is exhausted through the outlet manifold and through a charcoal filter before being exhausted outside the greenhouse. The chambers are 42 inches in diameter and 48 inches high. These have been tested using ozone and sulfur dioxide along with a continuous monitoring system.

Figure 3 depicts the particulate system. A small, motor-driven variable-speed syringe pump drives this system. The Al_2O_3 is placed in the Teflon cylinder and slowly pushed into the airstream using a Teflon-tipped plunger. The system has been modified since this schematic was prepared to include a Teflon holder filled with Al_2O_3 that is pushed into the airstream. This device permits better mixing and the breakup of the particulate. Efforts have been made with the NASA Langley Research Center and the NASA George C. Marshall Space Flight Center to define the aluminum oxide particulates used. Two sizes of particulates are used: an alpha particle of

about 2 micrometers diameter and a gamma alumina that is less than 0.5 micrometer in size. Under the microscope, the large-sized particulates look similar, with the small often adhering to the larger.

The burn system consists of a control system (fig. 4) and an exposure system (fig. 5). The control system has an airflow rate comparable to that through the exposure chambers, but the air contains no propellant exhaust. The exposure chambers will have various propellant exhaust concentrations in the air passing through them.

The control system consists of a variable-flow blower connected to a closed-top field chamber. The variable-flow blower is equipped with a control converting alternating current (ac) to direct current (dc). The control is connected to a dc motor to regulate the dc motor speed from 125 to 2500 rpm. The dc motor is connected to a high-volume, direct-drive blower with a wheel diameter of 10-5/8 inches. The variable-flow blower system has a maximum airflow of approximately 2000 cfm. However, an airflow of 1350 cfm will be the maximum needed for the controlled-burn system. The closed-top field chamber is 8 feet high and 10 feet in diameter, and the pressure drop through it is assumed to be negligible because it acts as a constant-volume reservoir. The connecting line between blower and chamber and the exhaust line are 1-foot-diameter plastic lines.

The polybutadieneacrylonitrile (PBAN) propellant controlled-burn system has a constant-flow blower producing 3000 cfm. The blower is equipped with a 2-horsepower ac motor (single phase) connected to a radial blade blower. The constant-flow blower is connected to the burn chamber by a 3-foot galvanized tin duct (10-3/4 by 14-5/8 inches). The galvanized duct is painted with epoxy resin on the inside to prevent corrosion.

The burn chamber is a 3-foot cube constructed of galvanized tin and painted with epoxy resin on the inside to prevent corrosion. The blower duct is centered on one side of the burn chamber. Two epoxy-painted galvanized baffles, located immediately inside the burn chamber, are equally spaced in the inlet duct to disperse the airflow through the burn chamber. The baffles are oriented 45° upward and 45° downward from an imaginary horizontal plane passing through the center of the blower duct. On the side opposite the blower duct inlet, a 2-foot-diameter hole is centered with a 6-inch epoxy-painted galvanized sleeve protruding from the burn chamber. On one of the sides adjacent to the blower duct inlet, a 30-inch-square epoxy-painted galvanized door is hinged to the burn chamber for replenishing the system with PBAN propellant. Inside the burn chamber, three 1/4-inch-thick copper plates (24 by 24 inches) rest on epoxy-painted angle irons that provide equal spacing between the plates and perfect symmetry about the center of the burn chamber. The three copper plates are grooved to accommodate 30 feet of propellant strand - 10 feet per plate. Therefore, each plate is grooved 1/8 inch deep by 7/16 inch wide in a geometry that gives a length of 10 feet. The temperature rise around the burn chamber is about 2° C for a 30-foot strand of 7/16-inch-square propellant, based on a value of 1596.4 calories evolved per gram of PBAN propellant burned. Each strand of propellant is coated with a restrictor formulation to ensure a uniform burn front.

From the galvanized sleeve of the burn chamber, 3 feet of 2-foot-diameter plastic line extends to a 3-foot-diameter tetrahedron. The tetrahedron is constructed of epoxy-painted galvanized tin with a constant angle of 109.5° between the 2-foot-diameter inlet plastic line and the three 1-foot-diameter outlet plastic lines. The tetrahedron is assumed to achieve equal splitting of the 3000-cfm air/HCl/Al₂O₃ stream into three 1000-cfm air/HCl/Al₂O₃ streams.

From the tetrahedron, the three 1-foot-diameter plastic lines extend 10 feet to three closed-top field chambers. Halfway between the tetrahedron and the field chambers, a dilution system is attached that is identical to the variable-flow blower of the control system (fig. 5). The dilution system is connected to the 1-foot-diameter plastic line by a 4-foot epoxy-painted rectangular duct (8 by 11-3/4 inches).

The air/HCl/Al₂O₃ streams leave the three field chambers through 1-foot-diameter plastic lines. The lines extend 10 feet to another tetrahedron configuration. At this point, the air/HCl/Al₂O₃ streams combine into one stream that leaves the tetrahedron through a 2-foot-diameter plastic line that extends 10 feet to a scrubber. The scrubber is a closed-top field chamber with five spray nozzles mounted in the top that mist water into the chamber. The water mist removes the HCl and Al₂O₃ from the stream, so that only air leaves the scrubber and disperses into the environment.

INSECT STUDIES

Honeybees were exposed to concentrations ranging from 4 to 160 parts per million (ppm) of HCl in air over a period of 1 to 4 hours. The response of various groups of bees varied considerably. In initial experiments, many bees died because of the mechanics of transfer and handling. These problems were corrected, and later work produced less control death. Results suggest that bees are not sensitive to expected exhaust concentrations of HCl and/or Al₂O₃. Preliminary data on the effects of HCl on honeybees are available. The behavioral effects of HCl on the honeybee will be studied in the spring of 1978.

A study of corn earworms has been initiated. In preliminary exposures, the larval stages of corn earworms were placed in small plastic containers and exposed to HCl in the air (from 4 to 160 ppm). The high HCl concentrations liquefied the early plastic cages without injury to the larvae. New cages were designed, but the larvae were not injured.

PLANT STUDIES

The plant study concentrated on eight species: citrus, soybeans, tobacco, radishes, morning glories, ivy, wax myrtle, and sunflowers. Citrus and other woody plants are reused after exposure by cutting them back and allowing them to regrow.

CONTENTS

Section	Page	
Preface	iii	1/A5
<u>Measurement of Exhaust Cloud Properties</u>		
CLOUD VOLUME STUDIES R. J. Bendura	1	1/A9
IN SITU EXHAUST CLOUD MEASUREMENTS Dewey Wornom	5	1/A13
MEASUREMENT OF PARTICULATES D Woods	9	1/B3
ICE NUCLEI MEASUREMENTS FROM SOLID ROCKET MOTOR EFFLUENTS Edward E. Hindman, II	13	1/B7
GROUND-BASED MEASUREMENTS OF DM-2 ROCKET EXHAUST EFFLUENTS USING FIXED-FLOW SAMPLERS AND ELECTRETS Michael Susko	27	1/C7
<u>Prediction of Environmental Effects of the Exhaust Cloud</u>		
ACID RAIN: MESOSCALE MODEL Hsiao-ming Hsu	33	1/C13
ACID RAIN: MICROPHYSICAL MODEL A. N. Dingle	65	1/F5
SHUTTLE INADVERTENT WEATHER MODIFICATION EFFECTS G. Lala	83	1/G9
RESPONSE OF SELECTED PLANT AND INSECT SPECIES TO SIMULATED SRM EXHAUST MIXTURES AND TO EXHAUST COMPONENTS FROM SRM FUELS Walter W. Heck	85	1/G11
<u>Baseline Monitoring of the Environment</u>		
ECCOLOGICAL BASELINE STUDIES Dave Vickers	101	2/B1
AIR QUALITY MONITOR AND ACID RAIN NETWORKS Hans Rudolph	117	2/C3

Environmental Impact Statement

ENVIRONMENTAL IMPACT STATEMENT FOR SHUTTLE OPERATIONS AT

VANDENBERG AIR FORCE BASE 125 2/C12

R. C. Wooten

The humidity is usually monitored but not controlled. The plants are much more sensitive to HCl when humidity is high or when the leaves are moist. After a rainstorm or early in the morning while dew is still on the plants, the plants would be much more sensitive.

Plants were not affected by Al_2O_3 . If the plants are dry, the particulates settle on the leaves with no injury. When the plants are moved out of the chambers, the particulates fall off. Adding moisture or wetting plant leaves did not damage plants. Mixtures of HCl plus Al_2O_3 were no more effective in injuring plants than HCl alone.

Two varieties of soybeans and radishes and three of tobacco were used. The radish was one of the most sensitive plants tested; very little effect on citrus was noted, except at high concentrations of HCl.

When considerable injury occurred, a significant growth reduction was found at about 30-percent visual injury. No growth reductions were found without visible injury. Plants recovered after exposure except when injury was severe (about 60 percent).

Figures 6 to 9 and tables I to IV show sample results of exposures of test plants to HCl.

BIBLIOGRAPHY

Heck, W. W.; Knott, W. M.; Stahel, E. P.; Sawyer, A.; Engel, M.; and Shaw, G. G.: Response of Selected Plant and Insect Species to Simulated SRM Exhaust Mixtures and to Exhaust Components From Solid Rocket Fuels. Interim Report to NASA KSC, 1977.

Heck, W. W.; Knott, W. M.; Stahel, E. P.; Sawyer, A.; Engel, M.; and Shaw, G. G.: Response of Selected Plant and Insect Species to Simulated SRM Exhaust Mixtures and to Exhaust Components From Solid Rocket Fuels. JANNAF Working Group on Safety and Environmental Protection (Apr. 1977), pp. 1-19.

Knott, W. M.; Heck, W. W.; Stahel, E. P.; Ambrose, J. T.; Engel, M.; Romanow, L.; and Tyson, J.: Response of Selected Plant and Insect Species to Simulated SRM Exhaust Mixtures and to Exhaust Components From Solid Rocket Fuels. Progress Report. Agricultural Research Service, USDA, and North Carolina State University (Raleigh, N.C.), 1978.

TABLE I.- INJURY TO COMET VARIETY RADISH
FROM EXPOSURE TO HCl^a

Exposure time, min	Percent injury from HCl concentration, ppm, ^b of -			
	0	5	10	20
15	0	1	1	3
30	0	1	3	15
60	0	3	6	52
120	0	3	9	85

^aTwo-leaf average; six plants/value not analyzed.

^b1 ppm \approx 1.5 mg/m³.

TABLE II.- INJURY TO COKER 16 VARIETY
CORN FROM EXPOSURE TO HCl^a

Exposure time, min	Percent injury from HCl concentration, ppm, ^b of -			
	0	10	20	40
15	0	1	1	36
30	0	1	2	67
60	0	1	2	74
120	0	1	2	84

^aThree-leaf average; six plants/value not analyzed.

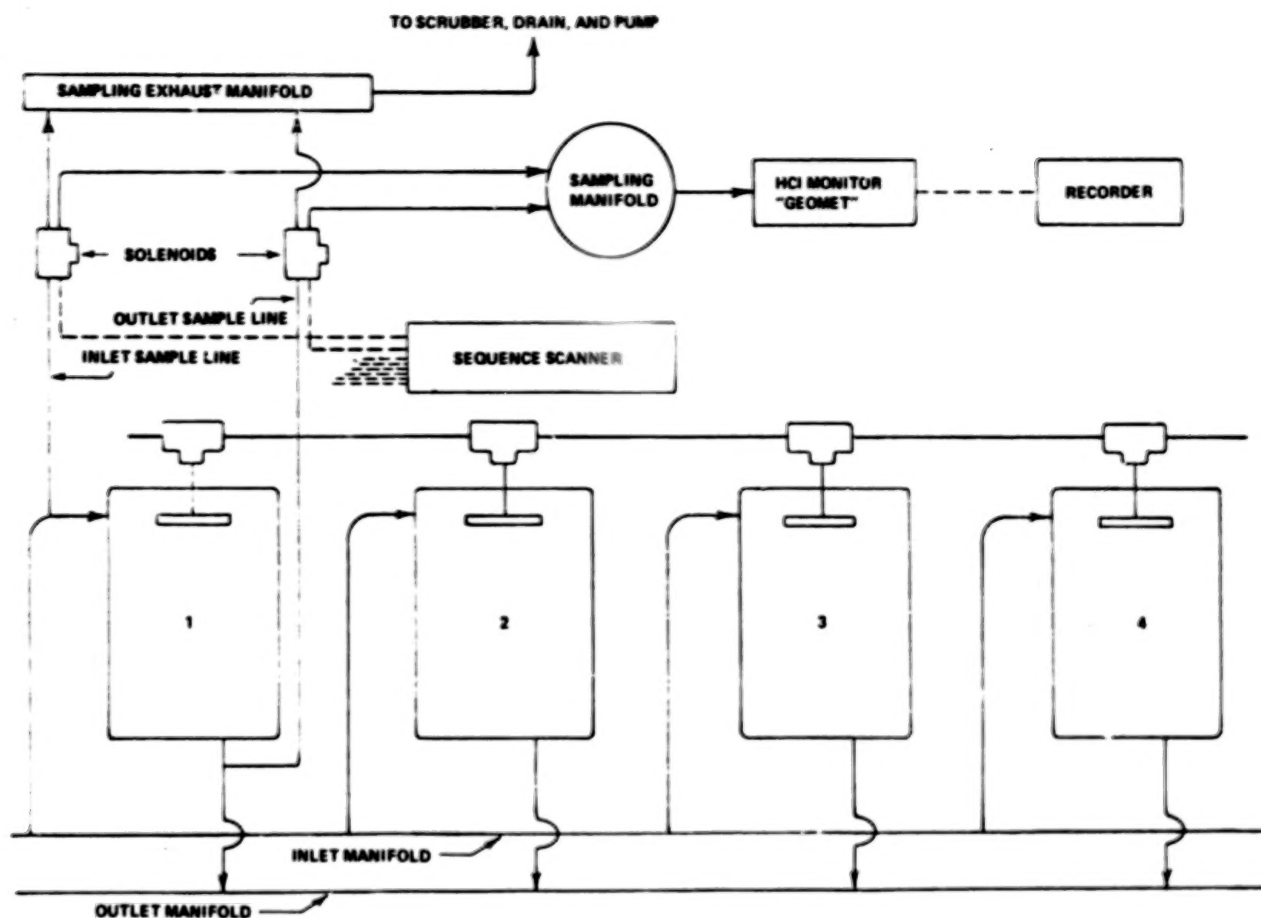
^b1 ppm \approx 1.5 mg/m³.

TABLE III.- INJURY TO TINY TIM VARIETY TOMATO
FROM EXPOSURE TO HCl

Parameter	Value for HCl concentration, ppm, of -			
	0	10	20	40
Injury, percent	0	9	30	69
Control top dry weight (TDW), g	2.98	--	--	--
Change from control TDW, percent	0	1	-24	-53

TABLE IV.- EFFECT ON DARE VARIETY SOYBEAN
OF EXPOSURE TO HCl

Parameter	Value for HCl concentration, ppm, of -			
	0	4	8	16
Control TDW, g				
0 days after exposure	1.31	--	--	--
3 days after exposure	2.22	--	--	--
7 days after exposure	4.20	--	--	--
21 days after exposure	7.96	--	--	--
Change from control TDW, percent				
0 days after exposure	0	1	10	-6
3 days after exposure	0	-6	0	-31
7 days after exposure	0	-2	-11	-43
21 days after exposure	0	12	13	-12



NOTE: 1) ALL SAMPLE LINES ARE 1/4 IN. OUTER DIAMETER TEFLON
 2) SOLID-STATE SCANNER ALLOWS INDEPENDENT OR SEQUENTIAL OPERATION OF
 ARBITRARY NUMBER OF CHAMBERS

Figure 1.- Schematic of sampling system.

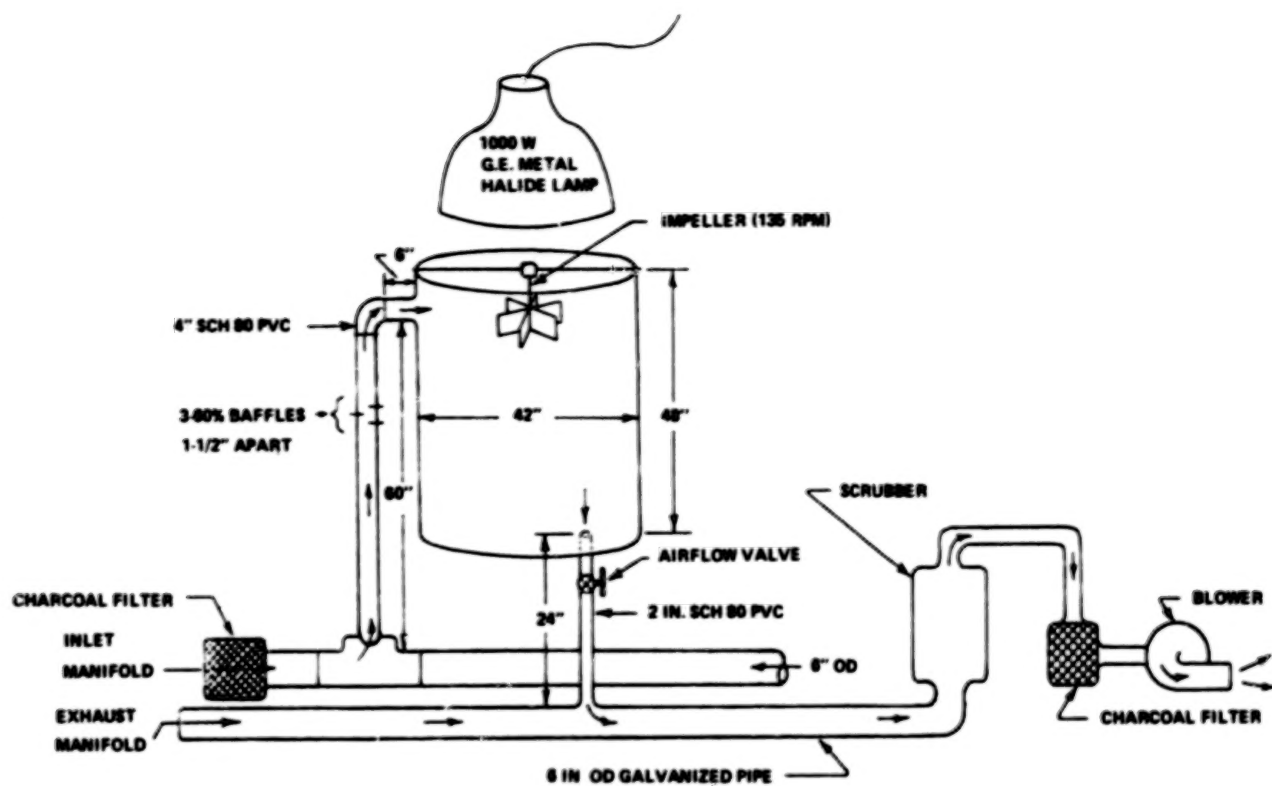


Figure 2.- Schematic of one exposure chamber.

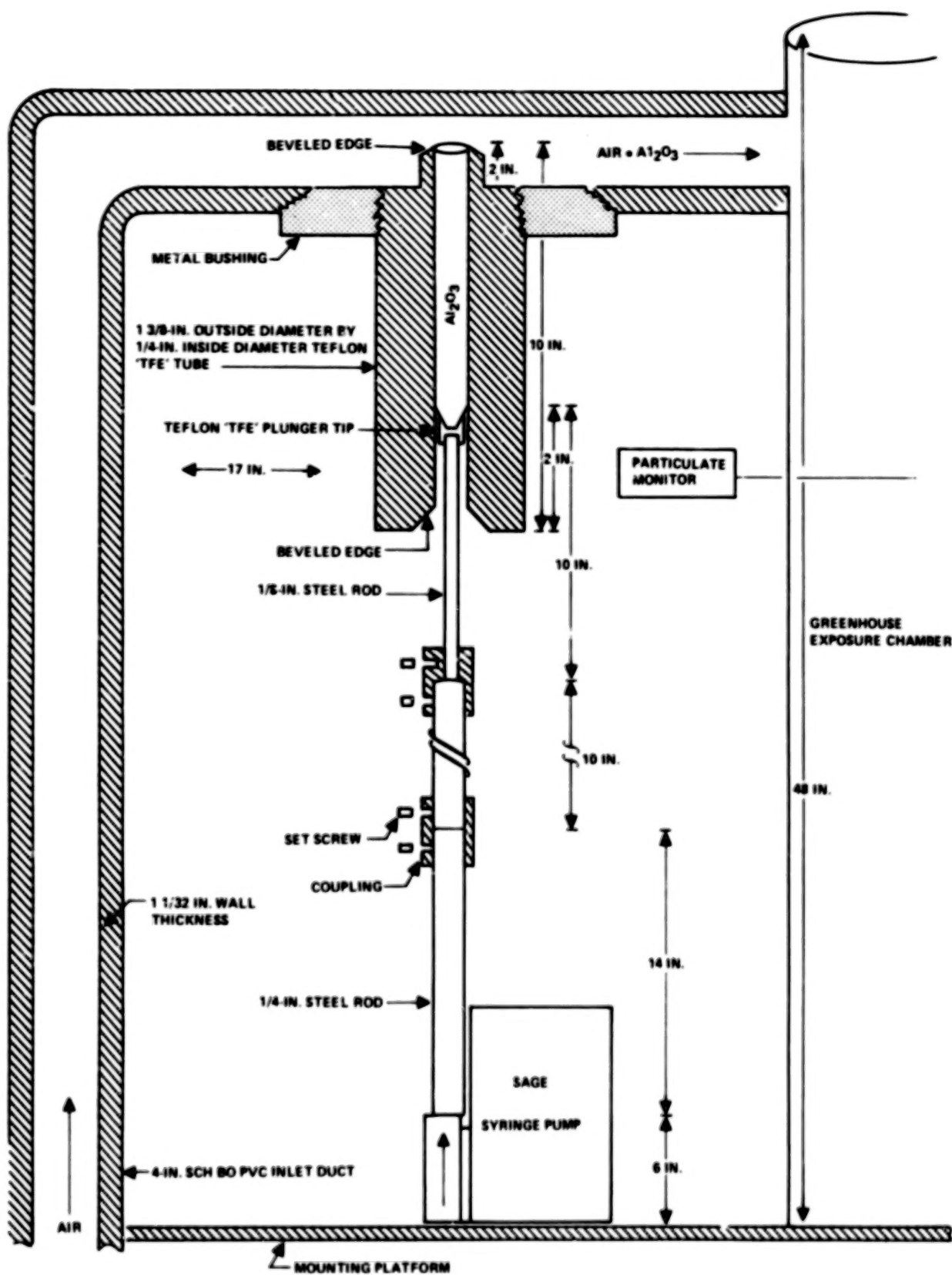


Figure 3.- Schematic of Al_2O_3 particulate exposure system.

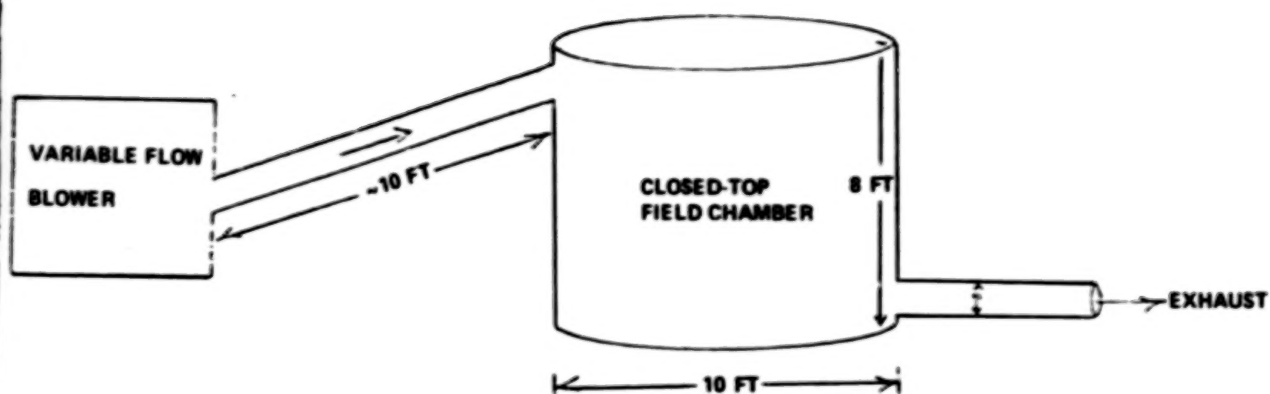
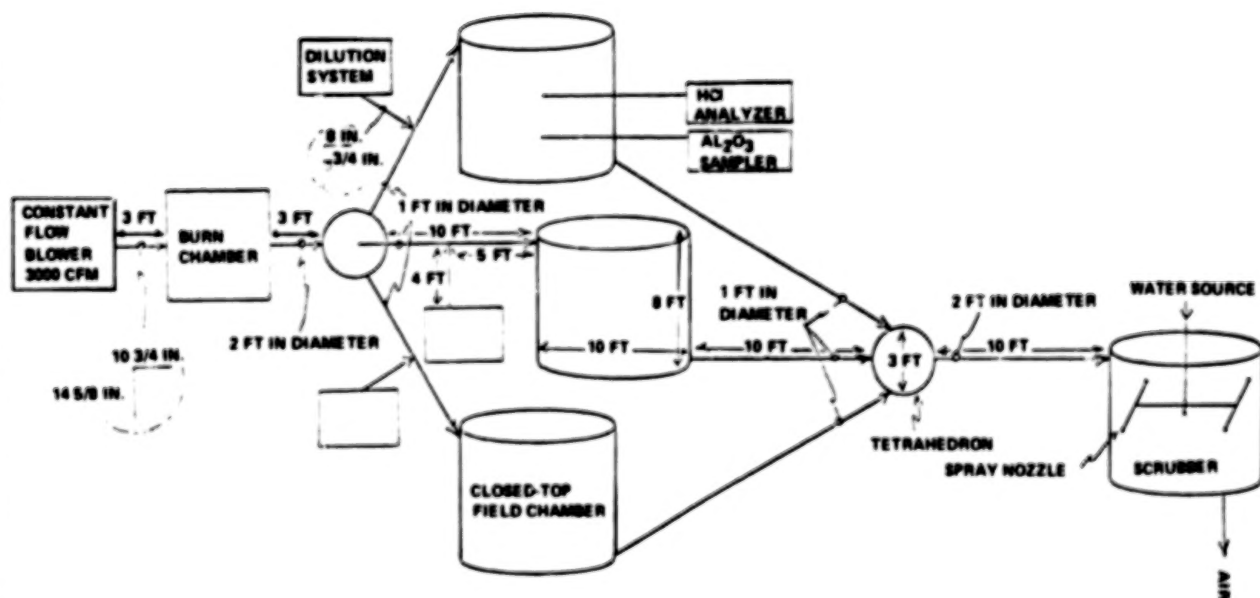


Figure 4.- Schematic of control system.



NOTE: THE ENTIRE SYSTEM SPANS ABOUT 67 FEET

Figure 5.- Schematic of polybutadieneacrylonitrile propellant controlled-burn system.

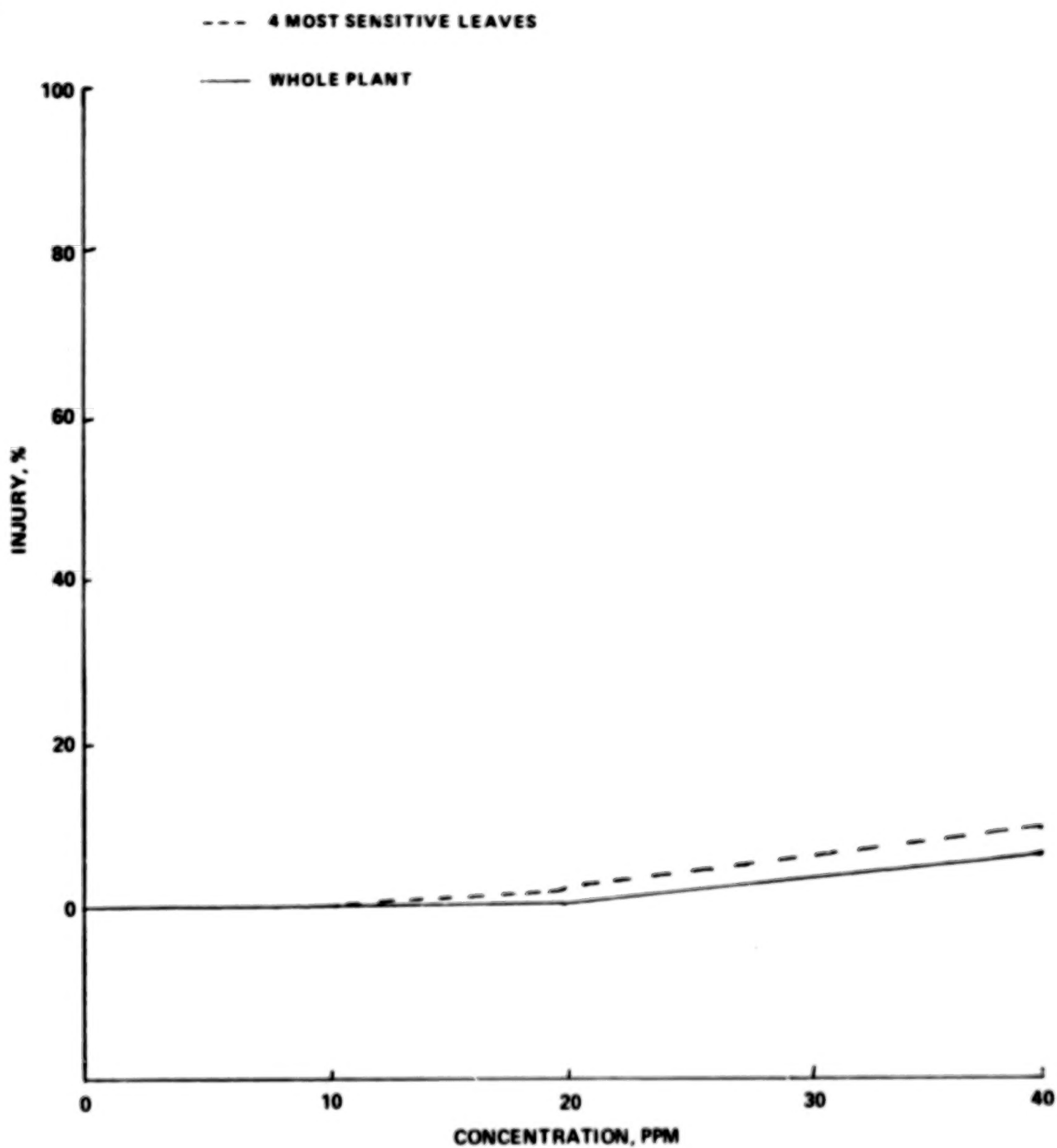


Figure 6.- Morning glory sensitivity screen to HCl.

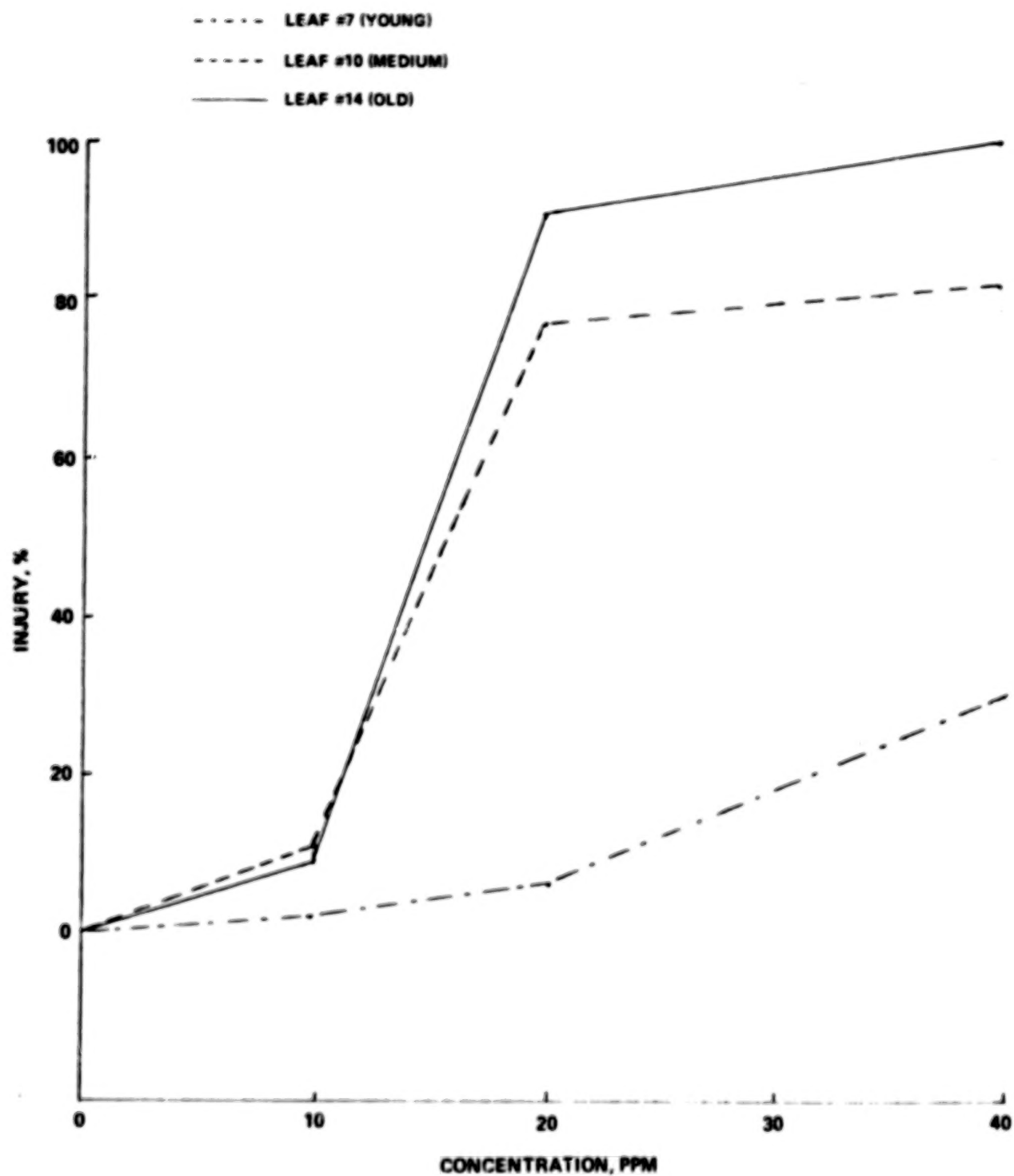


Figure 7.- Ivy sensitivity screen to HCl.

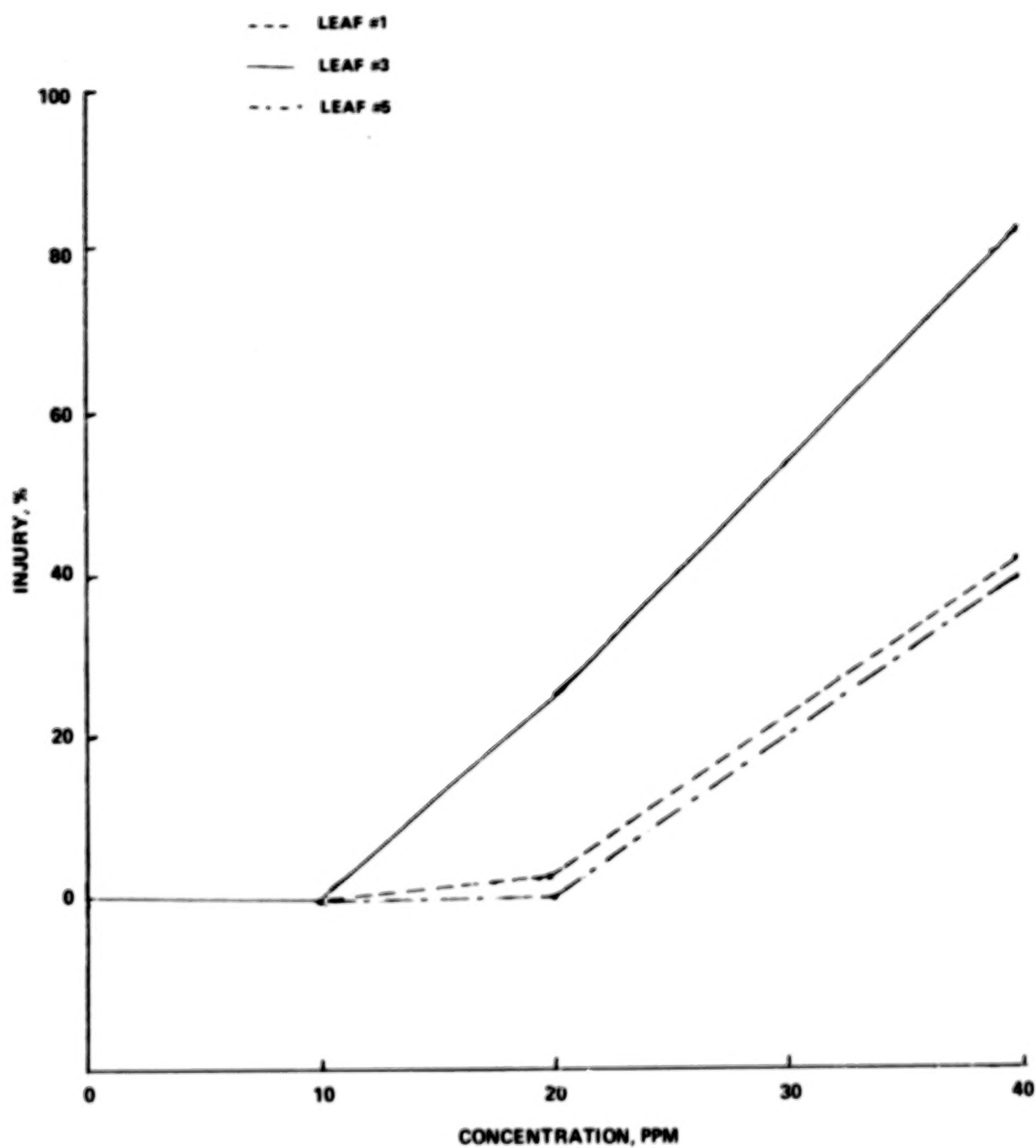


Figure 8.- Corn (Coker 16) sensitivity screen to HCl.

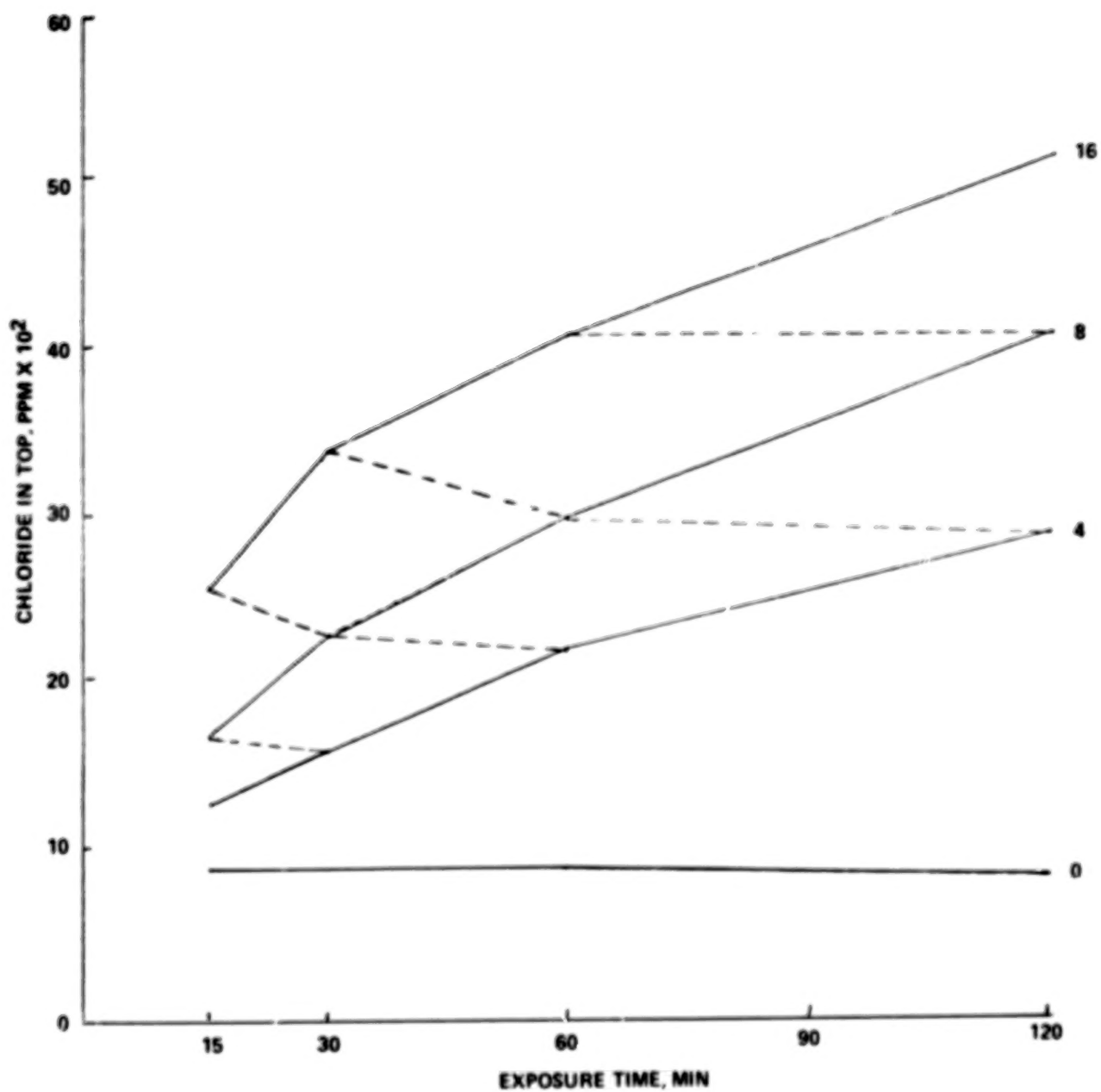


Figure 9.- Soybean chloride accumulation as related to duration of exposure and concentration of HCl.

Blank Page

ECOLOGICAL BASELINE STUDIES

By Dave Vickers*

Five different investigators are working on various aspects of environmental studies of Merritt Island in the NASA John F. Kennedy Space Center (KSC) area. Their primary objective is to document the ecological situation in this area before the initiation of the Space Shuttle launches from KSC. A secondary objective was to make recommendations to NASA around June 1979 on specific types of data collection during the operations phase of the Space Shuttle.

TERRESTRIAL COMMUNITY ANALYSES

The first area of investigation is a terrestrial community analysis, of which Dr. Jack Stout was Principal Investigator. Two major programs of study were to describe and understand plant communities on Merritt Island and to understand the long-term variation in small mammals as indicators of changes in environmental quality. The plant community analysis was complementary with soil studies (completed) and ongoing rainfall and small mammal monitoring programs.

Plant Community Study

The six objectives of the plant community analysis were as follows.

1. To delimit approximately 30 undisturbed stands representative of 10 plant community types as reference points to interpret the upland vegetation complex of Merritt Island and vicinity
2. To develop a quantitative data base on the significant plants of the stands (trees, shrubs, herbs, vines, epiphytes) - Factors studied were the density (number per unit area), the frequency (spatial distribution), the basal area (cross-section area occupied by tree trunks), and the coverage (areal extent of canopy).
3. To reduce data of each stand to a statistical summary
4. To select 10 "reference" stands for continuing study from among the approximately 30 areas delimited in objective 1

*Florida Technological University.

5. To establish a series of permanent line transects in the 10 designated reference stands from which to document future changes or lack of changes in the vegetation

6. To prepare a map of the existing plant communities on KSC property keyed to the master plan

Current accomplishments by Dr. Stout and his staff include the completion of a literature review; the development of sampling methods; the selection of approximately 37 sample areas around KSC, of which 29 areas have been sampled; the completion of a statistical summary of data for 10 areas around KSC; the selection of 10 reference stands; and the installation of permanent transects in each reference stand.

Expected accomplishments for the third year of the program are to complete the quantitative description of upland plant communities of Merritt Island (documentation of all 37 areas and analysis of the data), the establishment of a monitoring program based on 10 reference stands and line transects, and a map of all plant communities of Merritt Island.

Small Mammal Population Study

The second major program in which Dr. Stout was involved was the documentation of small mammal populations. The three major objectives of the small mammal population study were to monitor small mammal species in four different plant communities (flatwoods, hammock, coastal strand or coastal dune, and coastal scrub), to estimate population size of the small mammals at monthly intervals throughout the year, and to document demographic aspects of the population (survival rates, reproductive activity, sex ratios, ectoparasitic burdens, and movements).

The accomplishments to date in the small mammal population study are as follows: (1) the populations of small mammals have been monitored monthly since July 1976, (2) data are routinely entered into a computer file and reduced into summary form at 3-month intervals, and (3) an extensive literature review is in progress to expedite interpretation and publication of the results of the study.

Expected accomplishments in the next contract year are the completion of several publications describing the population dynamics of small mammals of Merritt Island over a 3-year period and the submission of a recommended monitoring program that employs existing study areas to gather baseline data for detecting changes in environmental quality.

Rainfall Study

Florida Technological University (FTU) is supplying technical expertise and manpower for the analysis of rainwater. The objectives of the rainwater

analysis are to monitor the acidity and the concentrations of sodium, potassium, calcium, magnesium, ammonium, sulfate, chloride, nitrate, orthophosphate, fluoride, vanadium, and aluminum.

Rain is collected in two buckets that have movable lids. When a detector plate becomes wet, signaling rain, a current flows and triggers the mechanism that opens the lid to permit collection of rainwater. The water is later brought inside, and the conductivity is measured to determine the total ionic contents. Other parameters, such as the pH factor, are also measured in the laboratory. When the measurements are done, the total acidity of rainfall is determined. The total acidity of the components of rainfall is then separated into weak and strong acids. In addition to total acidity, total ion content in the conductivity measurement and the overall chemical content of water are determined, particularly in relation to acidity.

The computer used for data analysis has three capabilities: data for 18 measurements, evaluative functions, and plotting. Figure 1 is a map of the present sites on Merritt Island for rainfall collection. Collections are made throughout the island. Presently, there are 18 rainfall collectors on the island located in proximity to the study sites wherever possible.

A summary of the results of the precipitation analysis program are as follows.

<u>Dates</u>	<u>No. of samples</u>	<u>Type of study</u>
June 23 to December 28, 1977	278	Spatial variability
November 23 to December 16, 1977	72	Sampling variability
January 1 to February 28, 1978	105	Spatial variability

Six evaluative functions are built into the computer program for handling and analyzing the data on anions and cations.

1. Ratio
2. Neutralizing component
3. Predictive pH
4. Predictive conductivity
5. Sea salt
6. Amount of nitrate contamination

The computer can also generate four types of data dealing with acid characterization of rainfall.

1. Free acidity due to volatile acids
2. Free acidity due to strong acids

3. Free acidity due to dissociated nonvolatile weak acids
4. Acidity due to undissociated weak acids

All the data are then plotted by computer to diminish the amount of manual data handling. The plots generated by the computer are exemplified in figures 2 and 3. Conclusions to date are as follows.

1. The pH of naturally occurring rainfall was quite variable (fig. 2).
2. The amount of free acid showed greater variation than the pH and reflects volume and acidity of sample (fig. 3).
3. Sampling variability of all species ranged from 5 to 20 percent (fig. 4).

Future objectives for the rainfall study include the following.

1. Continued operation of present precipitation network
2. Expansion to 18 different sites
3. Continued improvement in quality of data
4. Routine analysis of rainfall to determine amount of aluminum and vanadium
5. Repetition of sampling variability study during convectional storm activity
6. Expanded utilization of BEST computer (instrument interface and more convenient access to data)

ICHTHYOLOGICAL ANALYSES

The second major area of investigation is the ichthyological analysis, consisting of two studies.

1. Lagoonal fish study (ecological investigations of the marine fishes found in the brackish lagoons around KSC)
2. Molly reproduction study (detailed analysis of reproductive performance in the sailfin molly as an "indicator" for environmental monitoring)

Lagoonal Fish Study

The overall objective of the lagoonal fish study is to understand the basic nature and ecology of the fish fauna in the Indian River lagoon system around KSC. This study complements earlier NASA-supported research

on the fishes in fresh and brackish waters of Merritt Island. Together, these two studies will provide the only comprehensive knowledge available on the fishes of the KSC area.

Component objectives include the following.

1. Inventory the fish species inhabiting the open, brackish waters in the Indian River lagoonal system surrounding Merritt Island and KSC.
2. Monitor the relative abundance of selected fish species at seven permanent study sites in the lagoonal waters by means of a trawling program.
3. Evaluate changes in selected physiochemical parameters of the water in order to evaluate their influence on fish distribution and abundance.
4. Monitor the commercial catch of mullet and sea trout in the lagoonal waters around Merritt Island to evaluate the status and dynamics of the fishery.

Accomplishments to date are as follows.

1. 108 fish species have been documented; habitat, distributional, and other natural history data are available.
2. Bimonthly trawl sampling has occurred at seven permanent study stations since November 1976. Data were stored and analyzed for frequency, biomass, life history, stage composition, importance ranking, and species diversity.
3. Bimonthly analyses of water chemistry at seven permanent study stations were completed. Other data on water parameters from observations throughout the lagoonal system were obtained. Data were stored and analyzed.
4. More than 1700 records of daily catch were gathered from consulting commercial fishermen. Data were stored and computer-analyzed, and graphs of the monthly catch-per-unit-effort were prepared.
5. Ancillary studies (such as cold-caused fish mortality and stingray biology) were conducted.

Third-year projected accomplishments are as follows.

1. To continue faunal analysis, with emphasis on poorly sampled areas and new collecting methods, and to write an annotated faunal list
2. To continue trawl sampling, to refine data analysis, and to subject results to numerical community classification procedures
3. To continue bimonthly and unscheduled water chemistry analyses and to test for correlations between water parameters and fish population characteristics

4. To continue to collect and analyze data from commercial catch censuses and to establish annual trends in catch patterns from graphic analysis
5. To publish the results in scientific journals

Molly Reproduction Study

The overall objective of the molly reproduction study is to understand the details of molly reproduction so that reproductive performance can be used to evaluate subtle changes in environmental quality. Component objectives are as follows.

1. To determine the fecundity, fertility, and size of reproducing females from monthly samples at two study sites
2. To relate reproductive performance to physical, chemical, and biological environmental parameters suspected to be important determinants of reproductive fitness
3. To conduct limited laboratory investigations designed to answer specific questions about molly reproduction

Accomplishments to date include the following.

1. Analysis of reproduction from samples taken monthly since October 1976 at three permanent study sites, computerization and analysis of results, and computation of appropriate descriptive statistics
2. Monthly analysis of water chemistry parameters at three molly reproduction study sites and computerization and analysis of results
3. Design and execution of laboratory experiments on sex ratio, gestation period, growth rates, and food-fecundity relationship

Third-year projected accomplishments are as follows.

1. To continue monthly analyses of field reproduction until December 1978
2. To continue monthly water chemistry analyses until December 1978
3. To refine data analyses and graphic presentations
4. To design and execute appropriate supporting laboratory experiments
5. To publish results in scientific journals

THREATENED AND ENDANGERED SPECIES OF KSC

The third major area of investigation is the study of threatened and endangered species of KSC. Dr. L. M. Ehrhart is Principal Investigator. The number of threatened and endangered species at KSC is relatively large. These programs are aimed at providing KSC with consultation, awareness, and evaluation of matters relating to the Endangered Species Act of 1973.

Bird Studies

Endangered and threatened bird species were studied by means of weekly ground surveys and occasional light aircraft surveys. The American wood stork and the dusky seaside sparrow have been the primary objectives of endangered species surveys. Brown pelicans, southern bald eagles, ospreys, least terns, and the scrub jay were included in the threatened species surveys. Rare species and species of special concern were also included in the surveys.

Marine Turtle Studies

Although the marine turtle is not an endangered species, the KSC beaches are a major nesting ground for the marine turtle; therefore, an extensive study of their population, nesting habits, fertility rates, and hatchling size and vigor has been conducted. The objectives of the marine turtle studies were as follows.

1. To develop an accurate estimate of the size of the population (and its variation from year to year) of adult female marine turtles nesting on KSC beaches (figs. 5 and 6)
2. To develop a thorough understanding of the species composition of the nesting population
3. To develop an understanding of the migratory patterns of sea turtles nesting at KSC
4. To develop an understanding of fertility rates and the normal variation of sea turtle egg clutches at KSC
5. To develop an understanding of developmental rates and hatchling size and vigor at KSC
6. To cooperate with the staff of the Merritt Island National Wildlife Refuge in efforts to propagate sea turtles at KSC

7. To determine the size and species composition of the sea turtle population in the lagoonal waters surrounding KSC

8. To determine the age structure (as estimated by size) of the estuarine turtle population

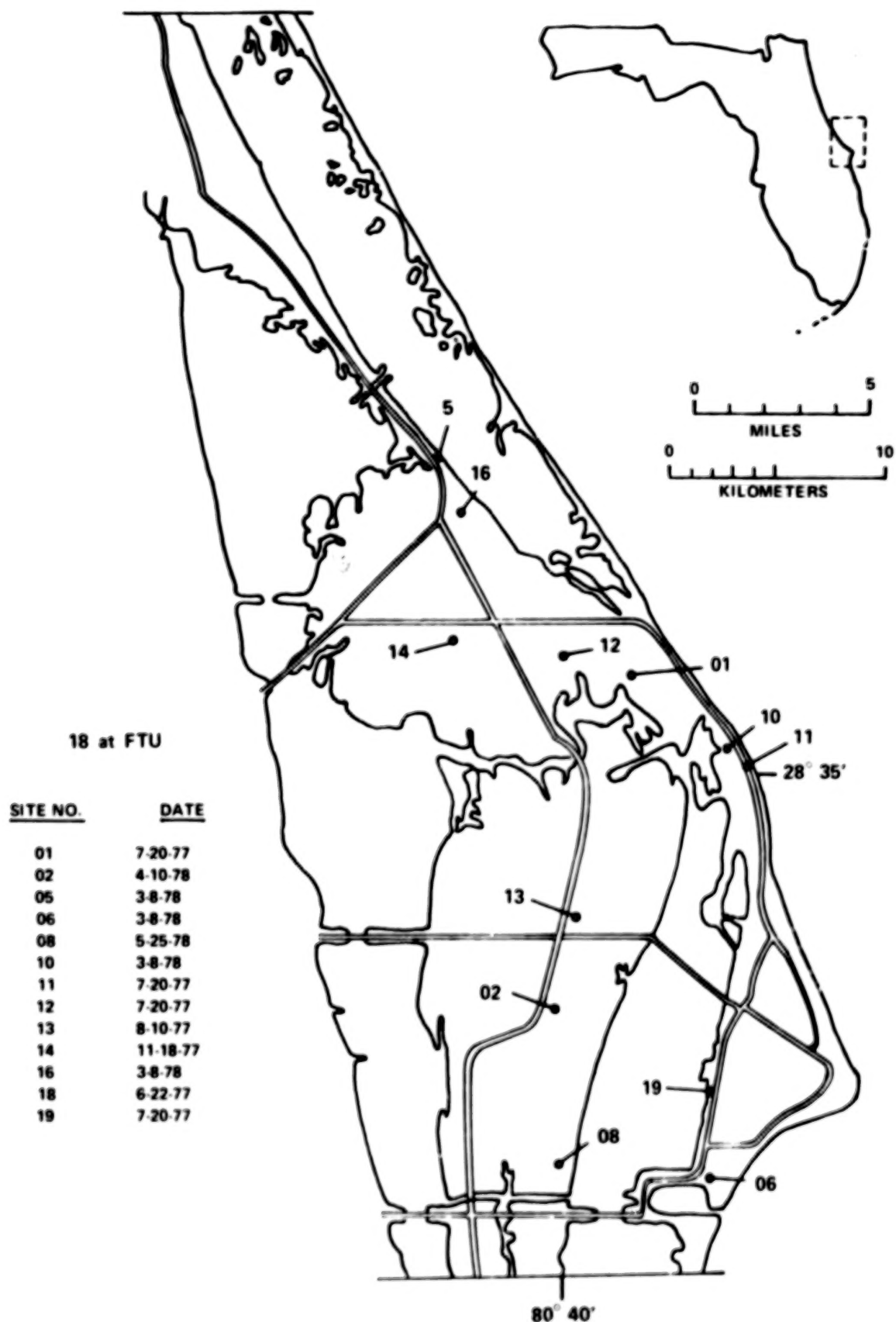
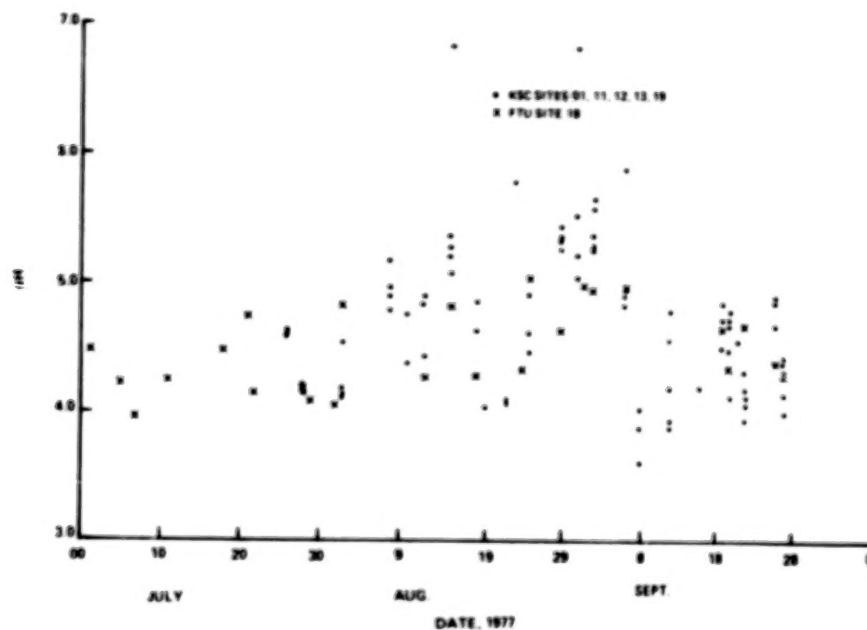
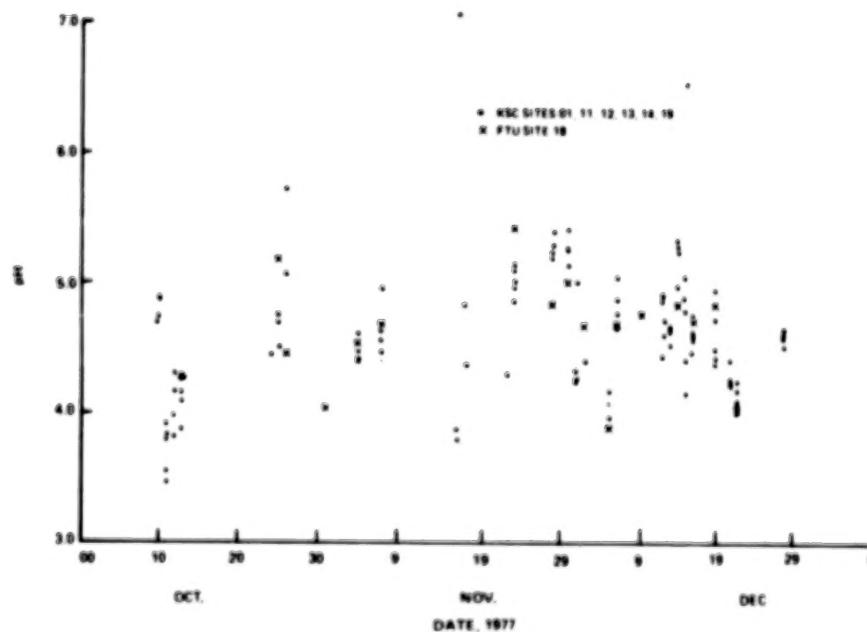


Figure 1.- Location of currently operational precipitation collectors.

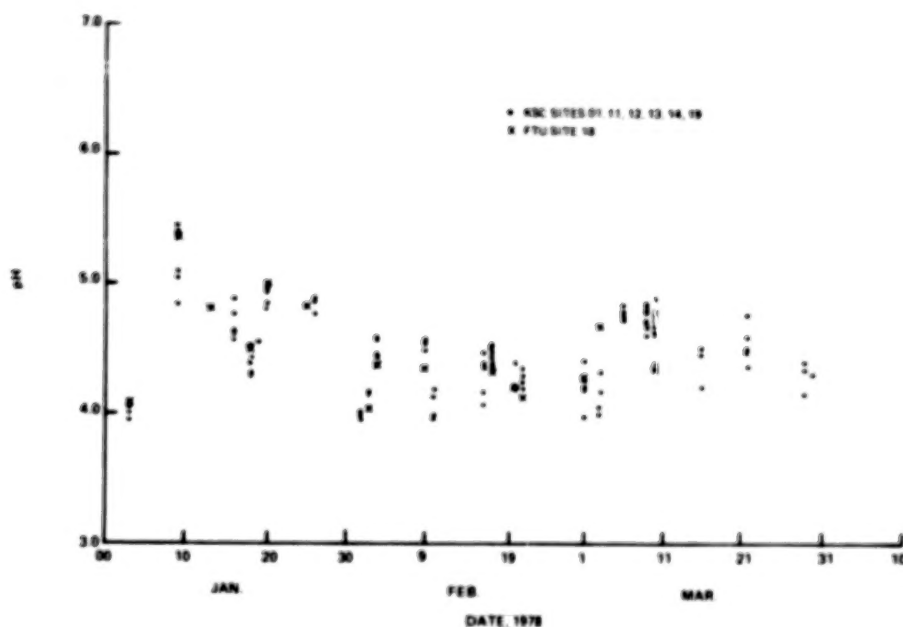


(a) July to September 1977.



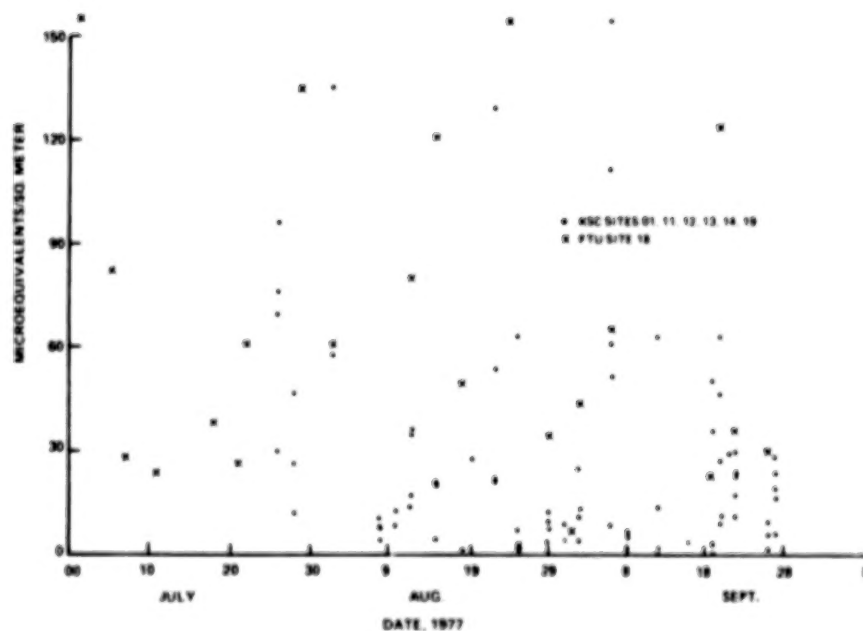
(b) October to December 1977.

Figure 2.- East-central Florida rainfall precipitation pH variation.



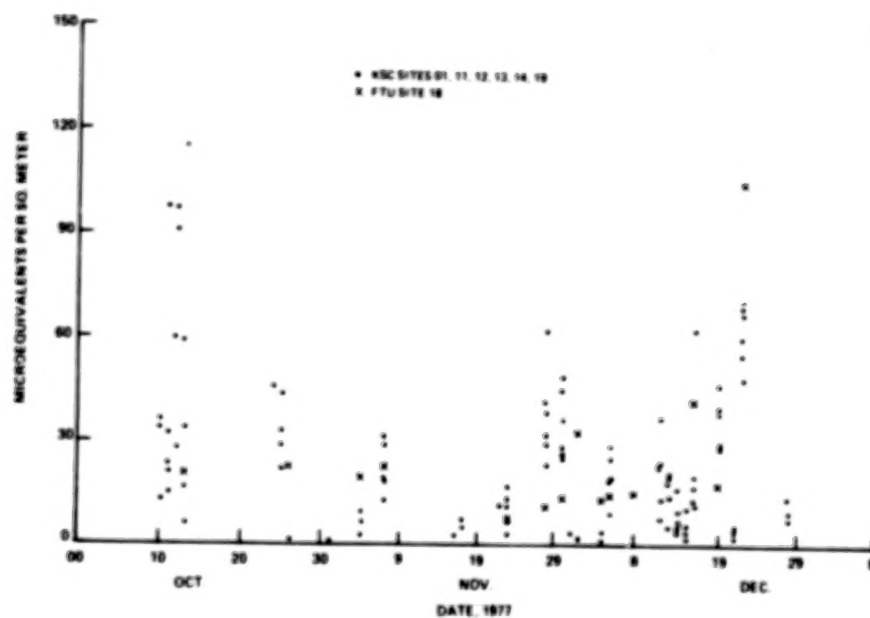
(c) January to March 1978.

Figure 2.- Concluded.

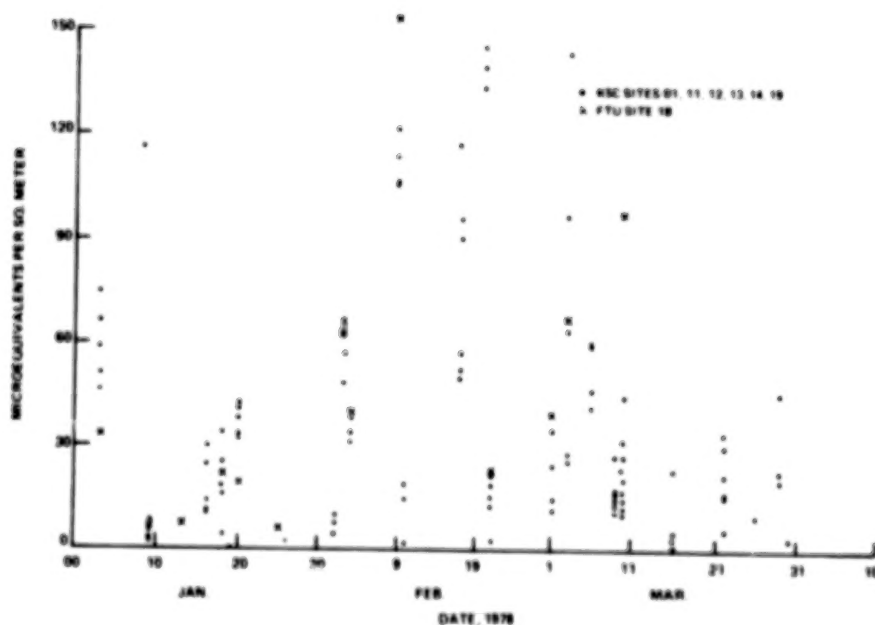


(a) July to September 1977.

Figure 3.- Variation of total free acidity in east-central Florida rainfall precipitation. Free acidity and volume of samples are used to determine the total.



(b) October to December 1977.



(c) January to March 1978.

Figure 3.- Concluded.

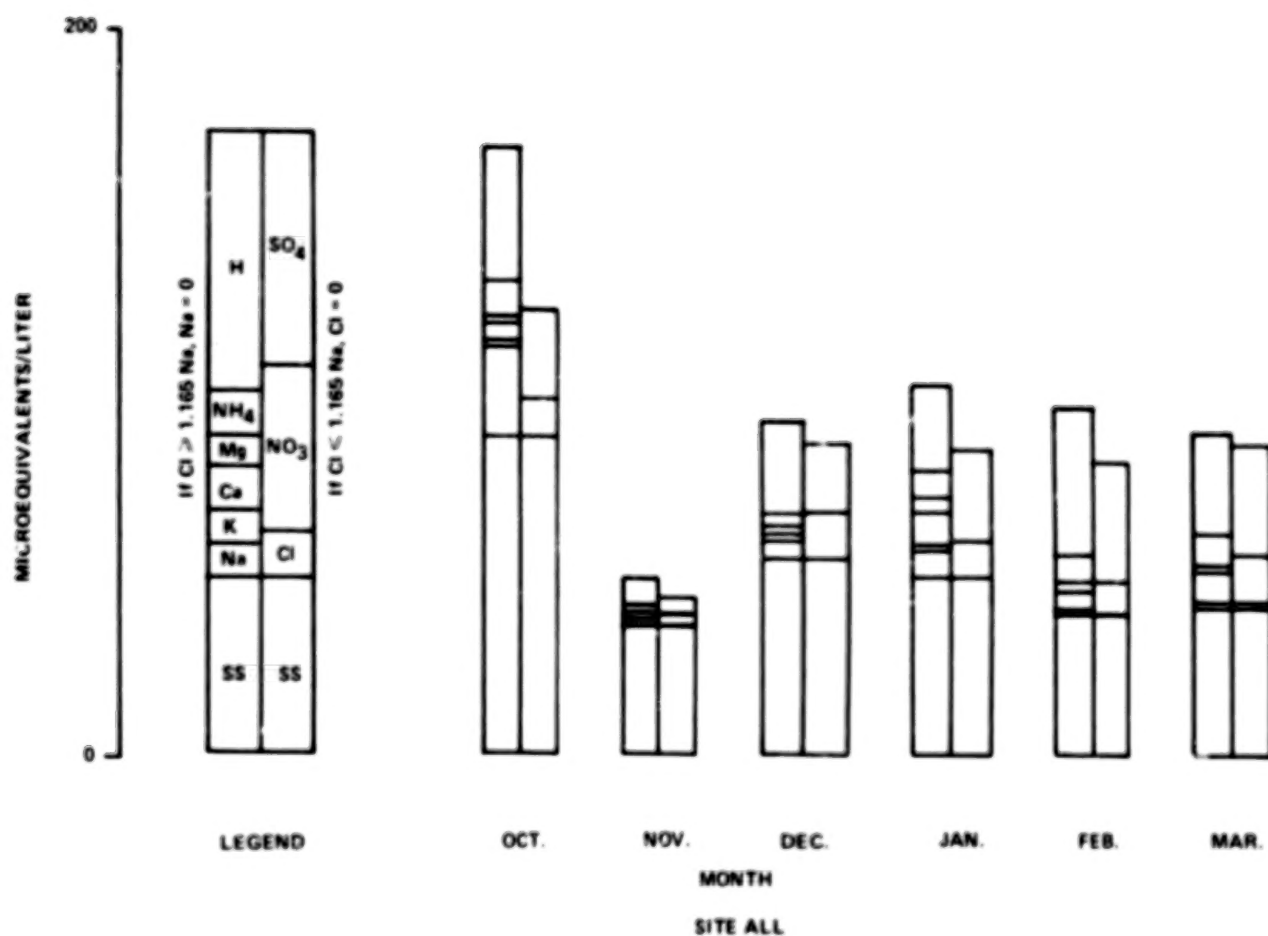


Figure 4.- Variation of monthly volume-weighted average composition of east-central Florida precipitation (all samples).

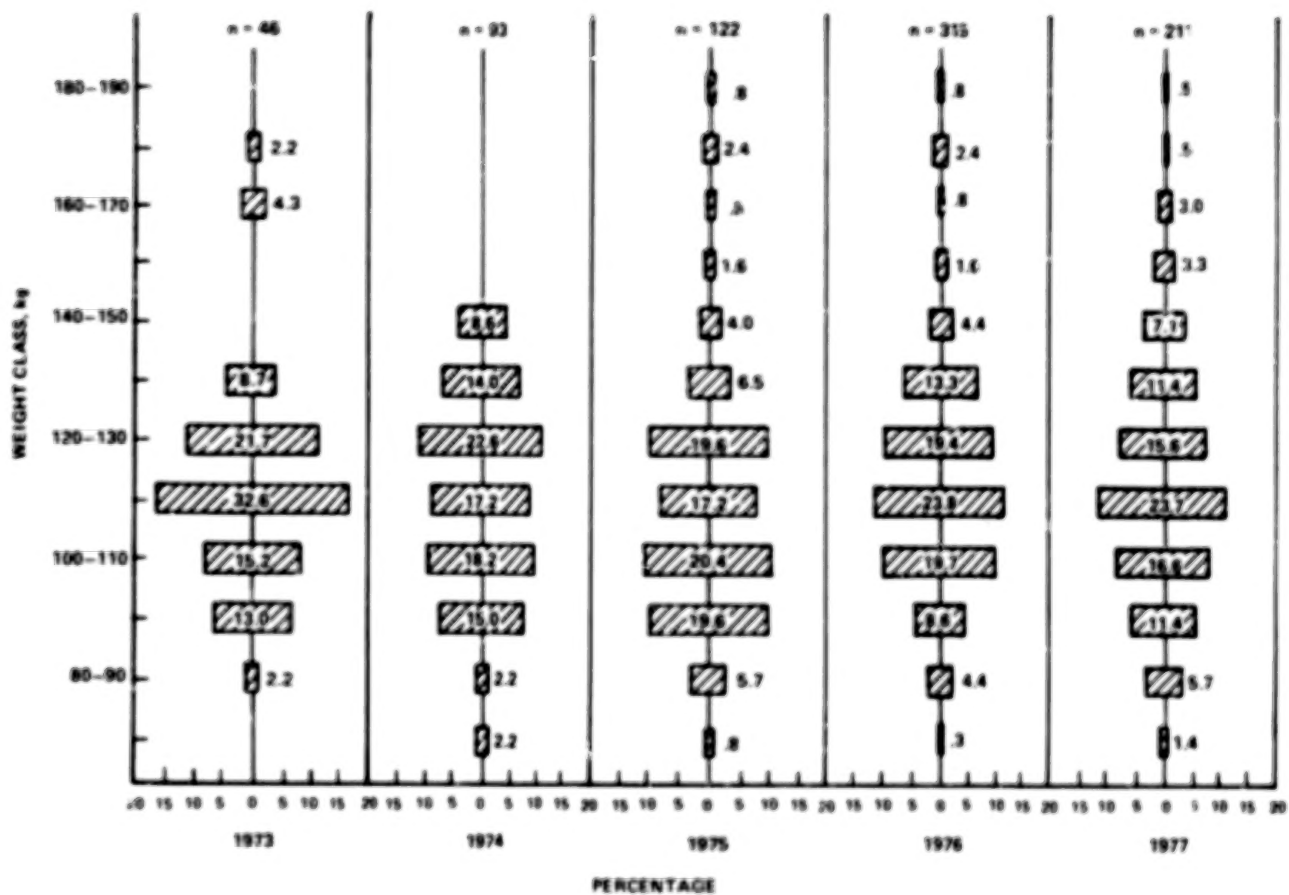


Figure 5.- Weight and class distributions of the populations of female loggerhead turtles nesting at KSC (1973 to 1977).

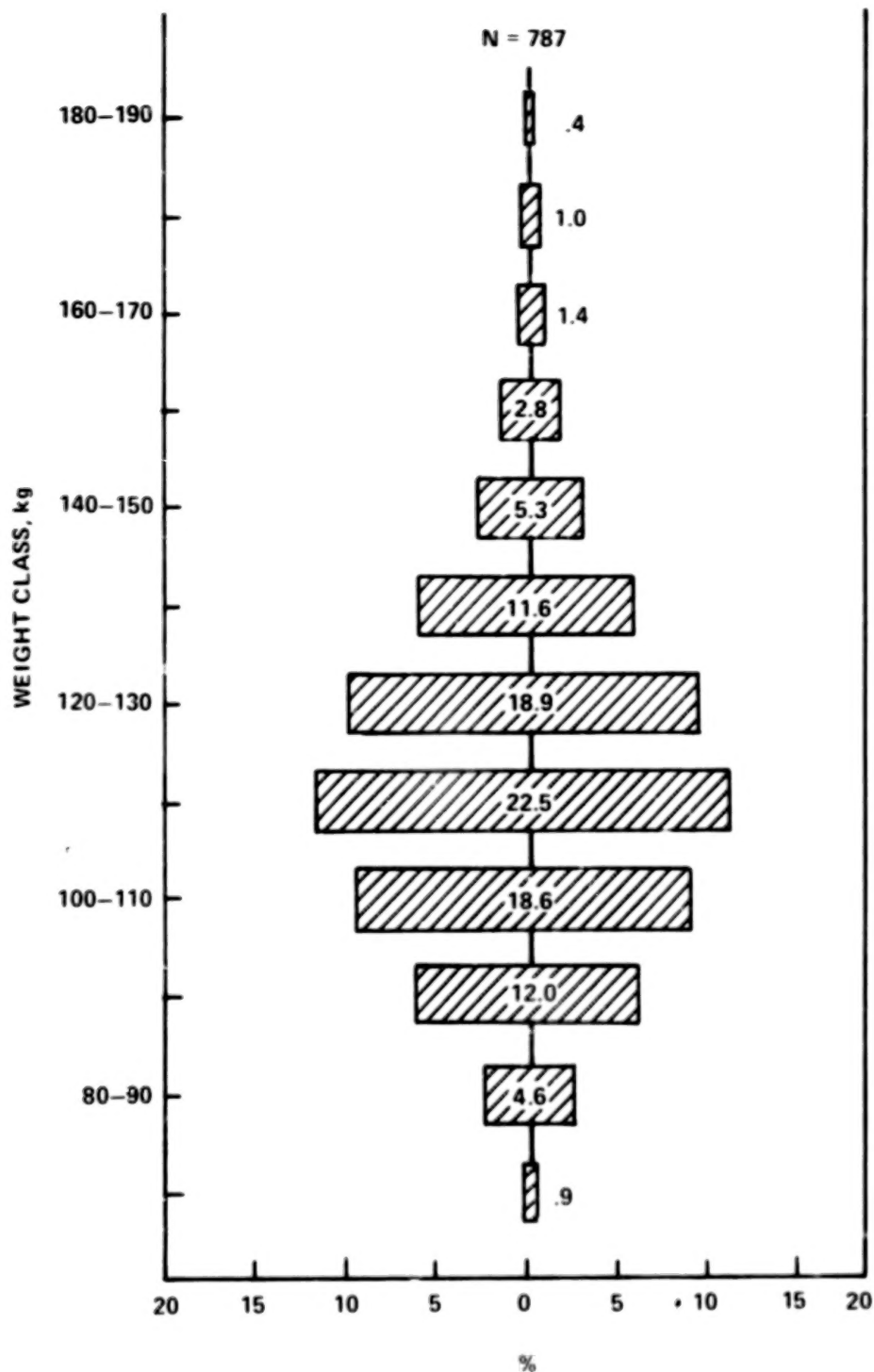


Figure 6.- Five-year mean weight and class distribution of the populations of female loggerhead turtles nesting at KSC (1973 to 1977).

Blank Page

AIR QUALITY MONITOR AND ACID RAIN NETWORKS

By Hans Rudolph*

AIR QUALITY MONITOR PROGRAM

The air quality monitor program consists of two permanent air monitor stations (PAMS's) and four mobile Shuttle pollutant air monitor stations (SPAMS's). The PAMS measures SO_x , NO_x , particulates, CO, O_3 , and nonmethane hydrocarbons. The SPAMS measures O_3 , SO_2 , HCl, and particulates.

Status of PAMS

The second PAMS unit (PAMS 2) is complete and is operating on local with the digital HP-1B system. It will be moved from Launch Complex 39 (LC-39) to Tico Airport (Gate 3) after approval for this site has been obtained. (Siting plans are mapped in fig. 1.) The second PAMS unit is operational in the analog mode and is awaiting memory cards for the digital system. Sample ozone data from PAMS 2 are shown in table I. Sample O_3 data are plotted in figure 2. High values exceeding Environmental Protection Agency (EPA) standards are frequently observed.

Status of SPAMS

Construction of mobile SPAMS units 3, 4, and 5 is still underway. All four units are complete except for O_3 , SO_2 high-volume, and HCl analysis stations. A preliminary selection of sites has been made as follows.

<u>Unit</u>	<u>Site</u>
SPAMS 3	Arthur Dunn Airport, Gate 4
SPAMS 4	TPQ 18, Merritt Island, Gate 2
SPAMS 5	Port Canaveral, Gate 1
SPAMS 6	Florida Technological University (FTU) field laboratory, North Merritt Island, Gate 5

*NASA John F. Kennedy Space Center.

HCl Dosimeters

Hydrogen chloride dosimeters have been developed using Office of Applied Science and Technology funding. A total of 60 geometeorological units has been delivered. Laboratory tests show a sensitivity of 0.4 to 1 ppm-sec, specific for HCl. Use of the units to monitor the ground cloud from the November 1978 Titan launch is planned.

RAIN MONITOR PROGRAM

The NASA John F. Kennedy Space Center (KSC) had six rain collectors operating in July 1976. By November 1976, the number had increased to 7 and by February 1977 to 12 rain collectors. In March 1978, 18 rain collectors were operational. The current problem in the rain monitor program is the collection and analysis of data from all sites.

Data Analysis Software

The software for the rain monitor program includes the following.

1. Logging of rain data on disk files - There is a problem with trying to analyze the data base because the amount of memory required to load the data base and run the computer codes simultaneously is not currently available.
2. A statistics program that runs complete statistical analyses of the data, including mean, average, standard deviation, and confidence level
3. A plotting program to plot any rain parameter against any other parameters, such as the pH value
4. A data summary (due April 1978)
5. Meteorological data comparison - Data will be analyzed against mesoscale and local wind patterns.

Bucket Contamination Study

The bucket contamination study has been completed. Twelve buckets were used (four in the runways, four in the building, and four out in the back yard). These buckets were put out for 7 days. Then, 200 milliliters of water was put in the buckets, and the solution was tested for contamination. The concentrations of impurities did not change very much - they were very small, less than 5 or 10 percent. Basically, then, there was no significant change in a period of 7 days. One contamination problem occurred when the wind blew over an open collector and contaminated the contents. When a collector is not operating, it would be helpful to put an indicator on it to guarantee that the collector is not opened prematurely. It was generally

found that standard deviation of all the samples run on the five collectors 5 meters apart was less than 10 percent of the standard deviation between the elements (which is well within the tolerance expected). Handling quality and the washing seem to be within the 10-percent variation. Dr. Madsen has been using quality control procedures on personnel and on equipment in the hardware by running duplication replicas for every 10 samples.

Summarized data are given in table II for the month of December. The table shows the number of samples collected on selected days of the month.

There is a rainfall measurement system at Cape Canaveral called "tipping buckets." Approximately 18 to 30 of the buckets measure rainfall to hundredths of an inch and send the data back remotely. These buckets are available but are very expensive to operate.

This program is conducted for background regional surveys and is not directly related to the launch. The results of any launch will be seen by the same rain network. If launch results are not seen by that network, one might speculate as to whether there were any real results. However, the network might not provide much data about a Shuttle launch. The KSC has preliminary plans to collect a large number of rain samples over large areas for the first Shuttle launch, but these plans have not yet crystallized.

TABLE I.- SAMPLE OZONE DATA FROM PAMS 2

Sampling date	Time sampled		Range, ppb		Daily av, ppb		Daily time, hr		Wind direction, deg		Over EPA standard		
	d	hr	High	Low	High	Low	High	Low	High	Low	d	hr	percent
Sept. 1977	16	352	48 to 100	10 to 62	73.6 \pm 16.5	34.6 \pm 17.1	14.4 \pm 5.8	8.1 \pm 5.2	130 \pm 112	--	3	12.9	4
Oct. 1977	26	572	33 to 134	5 to 84	68.8 \pm 22.7	36.3 \pm 19.1	13.2 \pm 6.4	11.2 \pm 7.8	119 \pm 99	--	6	22.3	4
Nov. 1977	27.5	605	35 to 70	8 to 54	57.0 \pm 8.5	24.8 \pm 13.3	14.3 \pm 4.8	7.4 \pm 7.5	110 \pm 86	--	0		
Dec. 1977	29.5	649	36 to 115	0 to 58	59.5 \pm 14.8	21.8 \pm 13.1	14.5 \pm 5.6	9.4 \pm 8.6	174 \pm 121	256 \pm 72.4	2	4.3	.66
Jan. 1978	29.5	649	98 to 51	11 to 57	69.2 \pm 12.9	31.9 \pm 12.7	17.6 \pm 4.5	4.6 \pm 4.9	159 \pm 115	242 \pm 94	6	32.3	4.9
Feb. 1978	27.5	605	123 to 58	22 to 58	88.3 \pm 18.6	39.7 \pm 16.6	16.4 \pm 5.2	5.66 \pm 5.1	181 \pm 126	278 \pm 66	16	131	21.7

TABLE II.- RESULTS FROM BEST KSC RAIN COLLECTION NETWORK^a

(a) Basic data

Collection day, Dec. 1977	No. of samples	Sample pH for collector no. -						
		1	11	12	13	14	18	19
1	4			4.27	4.33	4.24		5.01
2	2	4.41					4.68	
5	5			4.08	3.97	4.17	3.90	4.18
6	7	4.70	4.77	4.66	4.72	5.06	4.67	4.88
9	1						4.78	
12	6	4.93	4.91	4.61	4.87	4.44		4.72
13	5	4.53	4.69	4.65	4.53	4.66		
14	7	5.26	5.36	5.20	4.99	5.26	4.86	5.25
15	6	4.16	4.84	6.54	4.79	4.41		5.05
16	7	4.56	4.63	4.76	4.60	4.59	4.72	4.47
19	7	4.50	4.96	4.43	4.73	4.38	4.86	4.72
21	4	4.25		4.27	4.22	4.42		
22	7	4.08	4.10	4.17	4.18	4.25	4.03	4.00
28	6	4.66	4.52	4.59	4.62	4.57		4.58

(b) Statistical data

Parameter	Value for collector no. -						
	1	11	12	13	14	18	19
Monthly total							
vol, ml	3697	5983	5008	6464	5071	5025	8043
Vol weighted							
pH av	4.54	4.71	4.67	4.66	4.65	4.49	4.68
pH deviation . . .	0.34	0.34	0.69	0.31	0.33	0.38	0.39
pH range							
High	5.26	5.36	6.54	4.99	5.26	4.86	5.25
Low	4.08	4.10	4.08	3.97	4.17	3.90	4.00
Amt total H ⁺ . . .	107.3	116.08	107.69	142.28	114.21	161.74	168.47

^aTotal collectors, 7; total samples, 74; collections, 140; ratio of total samples to collections, 52.8 percent.

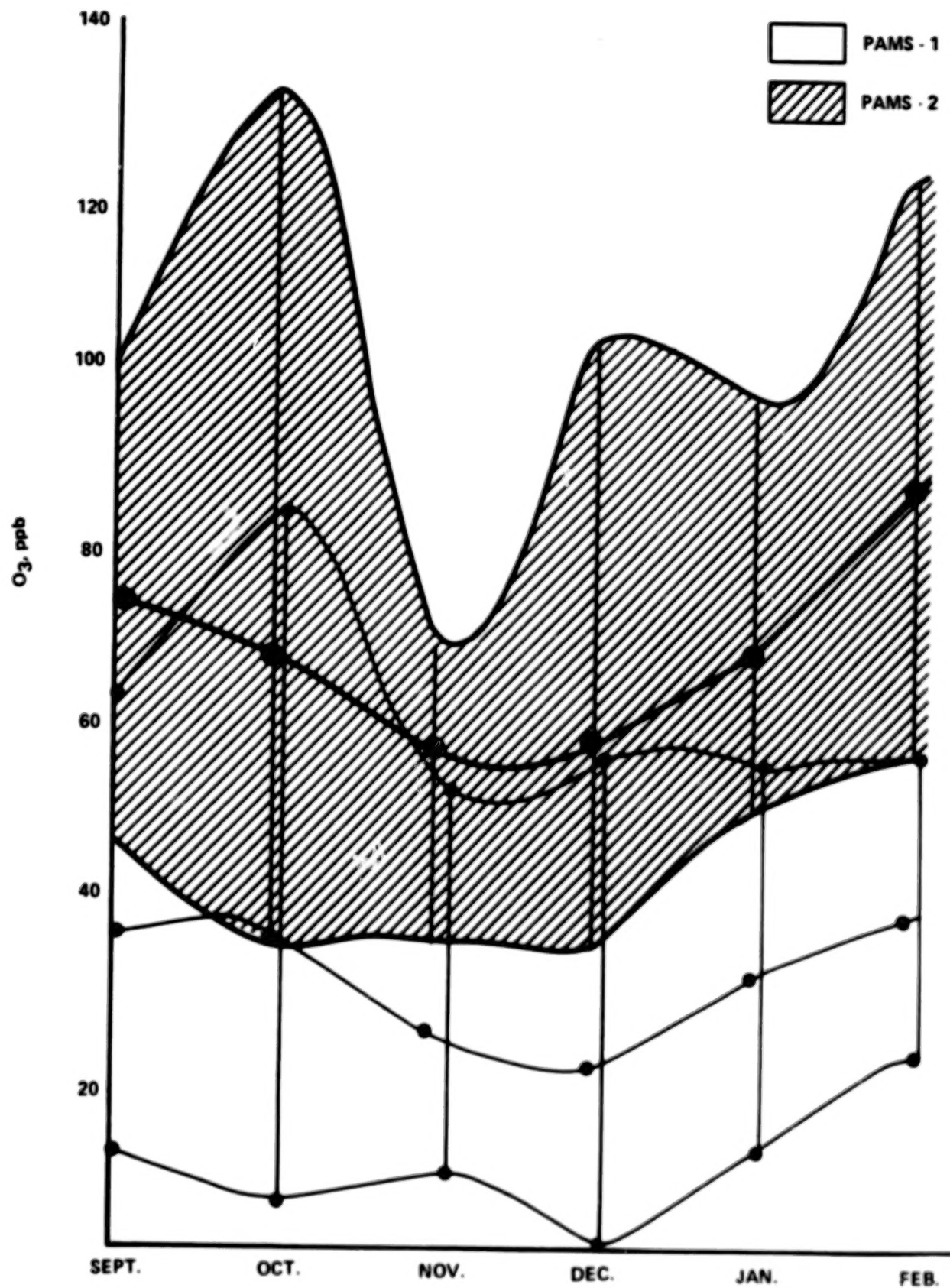


Figure 2.- Ozone concentration data for KSC, September 1977 to March 1978.

Blank Page

ENVIRONMENTAL IMPACT STATEMENT FOR
SHUTTLE OPERATIONS AT VANDENBERG AIR FORCE BASE

By R. C. Wooten*

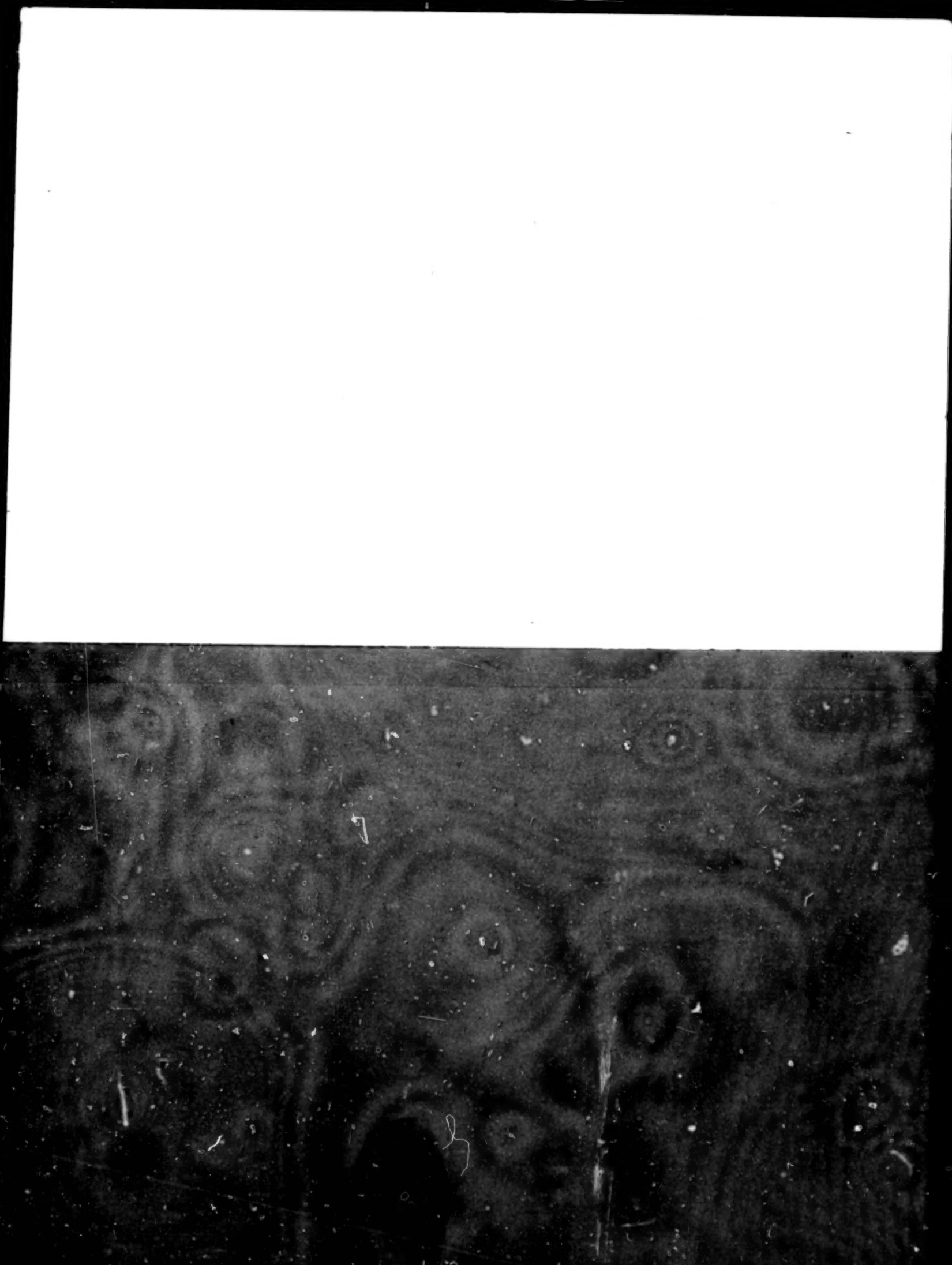
ABSTRACT

Since 1973, site-specific environmental studies of Vandenberg Air Force Base have been in progress. The environmental studies have been filed with the Council on Environmental Quality and have undergone the 30-day waiting period typical of environmental impact statements (EIS's). The U.S. Air Force had a peculiar problem with its impact study because of regulations by which the study had to meet its military construction programs. When the budget for military construction went to Congress, it had to be accompanied by an environmental impact statement. Within the latter EIS, some items deserved more discussion and more data could have been included; but with a strict time schedule, the EIS could not be adjusted. Thus, although the EIS has been completed, some perplexing environmental problems are still being resolved.

In the post-EIS followup, the following activities were considered: the supplements to the EIS, the analysis of the Space Shuttle impact on the U.S. Marines facility at Point Arguello, an update of the socioeconomic baseline, the preservation of cultural and historical resources, an analysis of sonic boom impact on the Channel Islands, the initiation of environmental protection plans with the construction effort, an assessment of air quality, and monitoring of the environment.

*Major, U.S. Air Force Space and Missile Systems Organization.

1. Report No. NASA CP- 2110		2. Government Accession No.		3. Recipient's Catalog No.	
4. Title and Subtitle PROCEEDINGS OF SHUTTLE ENVIRONMENTAL EFFECTS PROGRAM REVIEW				5. Report Date January 1980	
				6. Performing Organization Code	
7. Author(s) Andrew E. Potter, Editor				8. Performing Organization Report No. S-489	
9. Performing Organization Name and Address Lyndon B. Johnson Space Center Houston, Texas 77058				10. Work Unit No. 199-99-00-00-72	
				11. Contract or Grant No.	
				13. Type of Report and Period Covered Conference Publication	
12. Sponsoring Agency Name and Address National Aeronautics and Space Administration Washington, D.C. 20546				14. Sponsoring Agency Code	
15. Supplementary Notes					
16. Abstract Papers from the Shuttle Environmental Effects Program Review held at the NASA John F. Kennedy Space Center on March 21 and 22, 1978, are presented. Measurements of Titan exhaust cloud effluents are documented and compared, mesoscale and microphysical acid rain models are described and a submesoscale model is proposed, various instruments and facilities for measuring ice nuclei and other constituents of solid rocket motor exhaust effluents are discussed, regional air quality monitoring and rain collection systems are described, and the ecological impact of solid rocket motor exhaust effluents is examined. The potential effect of Space Shuttle launches is estimated where data are adequate.					
17. Key Words (Suggested by Author(s)) Air pollution Coastal ecology Exhaust gases Cloud physics Solid rocket Mathematical models propellants				18. Distribution Statement STAR Subject Category: 45 (Environment Pollution)	
19. Security Classif. (of this report) Unclassified		20. Security Classif. (of this page) Unclassified		21. No. of Pages 125	
				22. Price* \$5.50	



END

June 18, 1981